Department of Electrical Engineering and Automation

Design and Implementation of Partial Discharge Measurement Sensors for On-line Condition Assessment of Power Distribution System Components

Muhammad Shafiq

Aalto University

DOCTORAL DISSERTATIONS

Aalto University publication series
DOCTORAL DISSERTATIONS 152/2014

Design and Implementation of Partial Discharge Measurement Sensors for On-line Condition Assessment of Power Distribution System Components

Muhammad Shafiq

A doctoral dissertation completed for the degree of Doctor of Science (Technology) to be defended, with the permission of the Aalto University, School of Electrical Engineering, at a public examination held at the lecture hall S5 of the school on 29 October 2014 at 12:00 noon.

Aalto University
School of Electrical Engineering
Department of Electrical Engineering and Automation
Power Systems and High Voltage Engineering

Supervising professor
Professor Matti Lehtonen

Preliminary examiners
Professor. Mehdi Vakilian, Sharif University of Technology, Iran

Professor Abdel-Maksoud Ibrahim Taalab, Menoufiya University, Egypt

Opponent
Professor Petr Toman, Brno University of Technology, Brno, Czech Republic

Aalto University publication series
DOCTORAL DISSERTATIONS 152/2014

ISBN 978-952-60-5892-4
ISBN 978-952-60-5893-1 (pdf)
ISSN-L 1799-4934
ISSN 1799-4934 (printed)
ISSN 1799-4942 (pdf)
http://urn.fi/URN:ISBN:978-952-60-5893-1

Unigrafia Oy
Helsinki 2014

Finland

441 697
Printed matter

Aalto University

Abstract

Aalto University, P.O. Box 11000, FI-00076 Aalto www.aalto.fi

Author
Muhammad Shafiq

Name of the doctoral dissertation
Design and Implementation of Partial Discharge Measurement Sensors for On-line Condition Assessment of Power Distribution System Components

Publisher School of Electrical Engineering

Unit Department of Electrical Engineering and Automation

Series Aalto University publication series DOCTORAL DISSERTATIONS 152/2014

Field of research Power System and High Voltage Engineering

Manuscript submitted 2 April 2014 **Date of the defence** 29 October 2014

Permission to publish granted (date) 4 July 2014 **Language** English

☐ **Monograph** ☒ **Article dissertation (summary + original articles)**

Abstract

Unplanned interruptions of power supply due to failure of critical components of the distribution network have considerable impact on the modern society. Efficient condition assessment can avoid the loss of critical components by early detection of incoming threats. One of the biggest shortcomings of today's progressing maintenance technology is the lack of low cost instrumentation solutions which are simple in implementation and easily applicable to the network.

In this work partial discharge (PD) measurements have been considered for insulation condition assessment of distribution system components such as overhead covered conductors (CCs) and cables. A high frequency Rogowski coil induction sensor is designed for this purpose. An accurate electrical model of the sensor is necessary for efficient signal processing of the sensed signal and for reliable interpretation of the measured signal. A new method to determine the electrical parameters of Rogowski coil sensor is presented. In-depth analysis of the design stages of Rogowski coil is presented using experimental and simulated environment. Various geometrical designs of Rogowski coil are investigated to analyze the effects of geometrical parameters on high frequency performance of the coil. The guidelines presented regarding geometrical structure are useful when trading off the benefits for better mechanical and electrical design of such sensors.

Location of the detected PD faults is an important task of the diagnostics system in power lines. The conventional techniques of locating PD faults have been known for a single section of a power line. However, these techniques are not suitable for power lines having multi-sections or for branched line networks. In this work, finding the location of PD fault on a power line is recognized as a two stage function; (i) identification of the faulty section, and (ii) location of fault point on the identified section. The direction of arrival (DOA) technique is introduced to identify faulty section whereas fault point location can be determined by conventional techniques. The technique is equally applicable for CC lines or cable networks. The DOA technique is integrated over a cable feeder and an on-line automated condition monitoring and diagnostic scheme is proposed.

Low cost, non-intrusive installation and favorable operating features of Rogowski coil sensor make it suitable for development of an enhanced and automated diagnostic system which can easily be integrated into the distribution network.

Keywords Distribution network, condition assessment, monitoring, diagnostics, partial discharge, induction sensor, ATP-EMTP, distribution automation

ISBN (printed) 978-952-60-5892-4 **ISBN (pdf)** 978-952-60-5893-1

ISSN-L 1799-4934 **ISSN (printed)** 1799-4934 **ISSN (pdf)** 1799-4942

Location of publisher Helsinki **Location of printing** Helsinki **Year** 2014

Pages 224 **urn** http://urn.fi/URN:ISBN:978-952-60-5893-1

Acknowledgements

All praise to The Almighty Allah, merciful, and compassionate, for providing me this opportunity, granting me the capability to complete this PhD dissertation, and all the blessings that have been acknowledged below.

The research work related to this dissertation has been carried out at the Power Systems and High Voltage (HV) Laboratory, Aalto University. Though only my name appears on the cover of this dissertation, a great many people and prestigious organizations have contributed for its successful completion. I want to offer my sincere thanks to all of them.

At the very outset, I would like to express my cordial gratitude to Professor Matti Lehtonen, my esteemed supervisor for, grooming me as potential doctoral student, warm encouragement, and endless cooperation. I have always been greatly benefitted by his continuous support in all kind of matters, thoughtful comments, insightful decisions and guidance, and patience during writing process, truly thank you so much.

I owe my gratitude to current and former members of the Power Systems and HV Laboratory. First of all here, I want to mention Dr. Lauri Kütt without whom I can't imagine to have this work in its current form. I have learned a lot from him, sharing countless ideas and discussions for hours, I really appreciate his sincere and devoted efforts for me. Special thanks to Dr. Petri Hyvönen, Mr. Tatu Nieminen, and Dr. Joni Klüss who have always been ready to understand, analyze, discuss, and suggest, for the realization and execution of my proposed ideas in the HV Laboratory. At the same time, I want to thank Veli-Matti, Jouni Mäkinen, and Ari Haavisto for their anytime help to rectify the problems of the laboratory instruments and computers.

I want to express my deepest sense of gratefulness to all the other members of our working group whom I believe as the roof of this PhD structure. They; Dr. Michael, Dr. Muzamir, Dr. Nagy, Dr. Fattah, Dr. Eero, Farhan Malik, Farhan Mahmood, Merkebu, Mubbashir, Rafi, Sousa and Zoko, have been the integral part of my official and social life. In the same context, I want to extend my gratitude especially to Mr. Amjad, Dr. Hashmi, and Dr. John, for research cooperation, time taking discussions, and chatting any time any topic. I also want to acknowledge the help of Mr. Humayun for language corrections of this thesis time to time. Thank you all for maintaining a friendly, cheerful and ever-memorable atmosphere around us.

I am very grateful to the pre-examiners of this dissertation, Professor Mehdi Vakilian and Professor Abdel-Maksoud Taalab, for their valuable comments and corrections.

I would like to express my sincere appreciation to the financial bodies that have helped me in realizing this work successfully. The financial support from The Islamia University of Bahawalpur, Fortumin Säätiö, Aalto University, and Graduate School of Electrical Energy Engineering, LUT (now DPEEE), are greatly acknowledged which provided me a very suitable atmosphere to proceed smoothly in my research. Again this work was never possible without their contributions.

Most importantly, my immediate family whom this dissertation is dedicated to, has been a constant source of love, concern, support, and strength during all these years. My parents, father Ghulam Mustafa and mother Khadija, receive my veracious gratitude, they have done more than what they could, they have dedicated their lives for us, and provided unconditional love and care. My heart-felt gratitude to my sister closest to me (Tahira) and brothers (Hafeez and Naveed) for their continuous support, advice, and encouragement. The biggest thanks goes to my wife Saba, she has been sticking by my side happily and uncomplaining even when I was irritable and depressed. This journey of several years was not an easy ride, both academically and personally, but her love, sacrifices, and attention made it easier for us. I am deeply thankful to my in-laws especially Mazhar, Mehar, and belated Ambreen (she has left us very recently, we cannot forget her ever, may Allah keep her soul in eternal peace) who have been warmly supportive and caring during this time. I pray To Allah for giving me the strength to plod on during each and every phase of my life.

Muhammad Shafiq

Espoo, September 2014.

List of Publications

This thesis consists of an overview of the following publications which are referred to in the text by their Roman numerals.

I. M. Shafiq, L. Kütt, G. A. Hussain, M.Lehtonen, "Online Condition Monitoring System for Medium Voltage Distribution Networks", 14th International Symposium on Topical Problems in the Field of Electrical and Power Engineering", Pärnu, Estonia, pp. 162-170, 13-18 January, 2014.

II. M. Shafiq, L. Kütt, M. Lehtonen, T. Nieminen and G. M. Hashmi, "Parameters Identification and Modeling of High Frequency Current Transducer for Partial Discharge Measurements", IEEE Sensors Journal, Vol. 13, Issue 3, pp. 1081-1091, 2013.

III. M. Shafiq, M. Lethonen, L. Kütt, G. A. Hussain, M. Hashmi, "Effect of Terminating Resistance on High Frequency Behaviour of Rogowski Coil for Transient Measurements", Journal of Electronics and Electrical Engineering (Elektronika Ir Elektrotechnika) Vol. 19, Issue. 8, pp. 22-28, 2013.

IV. L. Kütt, M. Shafiq, M. Lehtonen, H. Mõlder, and Jaan Järvik, "Air-Core Sensors Operation Modes for Partial Discharge Detection and On-line Diagnostics in Medium Voltage Networks", The Scientific Journal of Riga Technical University - Electrical, Control and Communication Engineering, Vol. 4, Issue 1, pp. 5-12, 2013.

V. M. Shafiq, G. A. Hussain, L. Kütt, M. Lehtonen, "Effect of Geometrical Parameters on High Frequency Performance of Rogowski Coil for Partial Discharge Measurements", Measurement Journal Elsevier, Volume 49, pp. 126-137, 2014.

VI. M. Shafiq, L. Kütt, M. Isa, M. Hashmi, M. Lehtonen, "Directional Calibration of Rogowski Coil for Localization of Partial Discharges in

Smart Distribution Networks", International Review of Electrical Engineering (IREE), Vol. 7. No. 5, pp. 5881-5890, 2012.

VII. M. Shafiq, M. Lehtonen, M. Isa L. Kütt, "Online Partial Discharge Diagnostics in Medium Voltage Branched Cable Networks", IEEE International Conference on Power Engineering, Energy and Electrical Drives (POWERENG 2013), Istanbul, Turkey, pp. 246-251, 13-17 May, 2013.

VIII. M. Shafiq, L. Kütt, F. Mahmood, G. A. Hussain, M. Lehtonen, "An Improved Technique to Determine the Propagation Velocity of Medium Voltage Cables for PD Diagnostics", IEEE International Conference on Environment and Electrical Engineering Wroclaw, Poland, 5-8 May, 2013.

IX. M. Shafiq, G. A. Hussain, M. Lehtonen, P. Hyvönen, N. I. Elkalashy, "Integration of Online Proactive Diagnostic Scheme for Partial Discharges in Distribution Networks", IEEE Transactions on Dielectrics and Electrical Insulation, submitted 7 June, 2013 accepted for publication on 1 July, 2014.

Author's Contribution

Publication I:

Online Condition Monitoring System for Medium Voltage Distribution Networks

Muhammad Shafiq has developed the main idea of the paper. The experimental work, analysis of measurements, paper writing and conference presentation was accomplished by Muhammad Shafiq. Lauri Kütt has contributed in the experimental work and comments. Amjad Hussain has contributed through the comments, discussion, and paper revision. Matti Lehtonen has supervised the work and contributed through comments and discussions.

Publication II:

Parameters Identification and Modeling of High Frequency Current Transducer for Partial Discharge Measurements

Muhammad Shafiq has developed the main idea of the paper. The experimental work, analysis of results, simulation work, and paper writing has been accomplished by Muhammad Shafiq. Lauri Kütt has contributed in the experimental work and through comments and continuous discussions. Matti Lehtonen has supervised the work and contributed to improve the idea and contents of the paper. Tatu Nieminen has contributed in preparing the experimental setups and measurements. Murtaza Hashmi has contributed through comments and discussions during the review (revision) process of the paper.

Publication III:

Effect of Terminating Resistance on High Frequency Behavior of Rogowski Coil for Transient Measurements

The main idea of the paper was developed by Muhammad Shafiq and Matti Lehtonen. Muhammad Shafiq was responsible for the experimental investigation, analysis of the results, signal processing of captured data, simulation, and paper writing. Matti Lehtonen has supervised the work and contributed through the comments and discussions. Lauri Kütt has helped in the experimental work and contributed through

comments, discussions, and paper writing. Amjad Hussain and Murtaza Hashmi have contributed through the comments and discussions.

Publication IV:
Air-Core Sensors Operation Modes for Partial Discharge Detection and On-line Diagnostics in Medium Voltage Networks

This paper is an extension of the work done in Publication II and III. Lauri Kütt was responsible for the main idea of the paper, analysis and writing of the paper. Muhammad Shafiq has contributed in the main idea, analysis of the results, and paper writing. Matti Lehtonen, Heigo Mõlder, and Jaan Järvik have contributed through the comments and discussions.

Publication V:
Effect of Geometrical Parameters on High Frequency Performance of Rogowski Coil for Partial Discharge Measurements

Muhammad Shafiq has developed the main idea and was responsible for experimental work, analysis of the result, and writing of the paper. Amjad Hussain has contributed in the main idea and writing of the paper. Lauri Kütt has contributed in the idea of the paper and improved the organization of the contents. Matti Lehtonen has supervised the work and contributed through comments and discussions.

Publication VI:
Directional Calibration of Rogowski Coil for Localization of Partial Discharges in Smart Distribution Networks

Muhammad Shafiq has explored some interesting features of the induction sensors. Matti Lehtonen has proposed the main idea. Muhammad Shafiq was responsible for the experimental implementation, analysis of the results, and writing of paper. Lauri Kütt has contributed in the experimental work. Muzamir Isa and Murtaza Hashmi have contributed through the comments and discussions. Matti Lehtonen has supervised the work and contributed by comments and discussions.

Publication VII:

Online Partial Discharge Diagnostics in Medium Voltage Branched Cable Networks

The main idea was founded by Muhammad Shafiq together with Matti Lehtonen. Muhammad Shafiq was responsible for the experimental implementation of the idea, measurements, analysis of the results, paper writing, and presentation in the conference. Muzamir Isa and Lauri Kütt has contributed through the comments and discussions. Matti Lehtonen has supervised the work and contributed through comments and discussions.

Publication VIII: An Improved Technique to Determine the Propagation Velocity of Medium Voltage Cables for PD Diagnostics

Muhammad Shafiq has developed the main idea. The experimental work, analysis of the results, paper writing, and conference presentation was done by Muhammad Shafiq. Lauri Kütt has helped in analyzing the results and contributed through comments and discussion. Farhan Mahmood and Amjad Hussain have contributed by suggesting the improvements in the writing and content organization of the paper. Matti Lehtonen has supervised the work and contributed through comments and discussions.

Publication IX:

Integration of Online Proactive Diagnostic Scheme for Partial Discharges in Distribution Network

Muhammad Shafiq has developed the main idea together with N. I. Elkalashy. The experimental work, analysis of the results, and paper writing was accomplished by Muhammad Shafiq. N. I. Elkalashy has contributed by improving the writing of the paper. Amjad Hussain has contributed through analysis of the results and organization of the paper. Matti Lehtonen has supervised the work and contributed through improving the main idea, comments, and discussions. P. Hyvönen has contributed in developing the experimental setups, measurements, and by commenting.

Table of Contents

List of Abbreviations

Abbreviations	Description
ADP	Active differential probe
ATP- EMTP	Alternative transients program- electromagnetic transients program
CC	Covered conductor, used for overhead lines in distribution network
DAS	Data acquisition system
DGA	Dissolved gas analysis
DOA	Direction of arrival
DSO	Digital storage oscilloscope
FAA	Frequency amplitude analysis
FFT	Fast Fourier transform
HFCT	High frequency current transformer
GIS	Gas insulated switchgear
IEC	International electrotechnical commission
IT	Information technology
LCC	Line and cable constant
LV	Low voltage
MV	Medium voltage
PD	Partial discharge
PRA	Phase resolved analysis
QWL	Quarter wave length
RLC	Resistor, inductor and capacitor based circuit connected in a certain configuration
TDA	Time difference of arrival
TDR	Time domain reflectometry
WPV	Wave propagation velocity
XLPE	Cross-linked polyethylene

List of Symbols

Symbols	Description
a	Healthy part of insulation between electrodes
b	Part of insulation in series with the cavity between electrodes
c	Part of cavity or defect inside insulation between electrodes
C	Capacitance per-unit length
C_1	Voltage divider capacitor in PD measuring setup
C_2	Voltage divider capacitor in PD measuring setup
C_c	Self capacitance of Rogowski coil
C_{cable}	Capacitance of cable from Rogowski coil terminals to measuring system
C_{ia}	Capacitance of the portion a, healthy part of insulation of the cable
C_{ib}	Capacitance of the portion b, the part of insulation in series with the cavity of the cable
C_{ic}	Capacitance of the portion c, the defective part i.e. cavity inside insulation
cm	Centimeter
C_p	Capacitance of differential probe
d_i	Internal diameter of Rogowski coil
d_m	Mean diameter of Rogowski coil
d_o	Outer diameter of Rogowski coil
d_{rc}	Core diameter of Rogowski coil
d_w	Wire diameter of Rogowski coil
E_a	Electric field intensity related to applied voltage level V_a
E_{Ba}	Dielectric breakdown strength of insulation, part a
E_c	Electric field intensity across the cavity
E_{Bc}	Dielectric breakdown strength of air filled cavity c
E_{ci}	Electric field intensity across the cavity at PD inception level related to voltage V_{BC}
F/m	Farads per meter
F_1	Feeder 1
f_c	Self resonant frequency of Rogowski coil
f_{oc}	Operating resonant frequency of Rogowski coil system

Symbols	Description
G	Conductance per-unit length
h_c	Thickness of the cavity
h_i	Thickness of insulation
$H(r)$	Total effect of medium and measurement system
$H(r_1)$	Effect of medium
$H(r_2)$	Effect of sensor
$H(r_3)$	Effect of measuring system
H/m	Henrys per meter
$I(x)$	Current of the line at position x
i_1	Current measured by coil sensor at line end 1
i_2	Current measured by coil sensor at line end 2
i_A	Current induced at point A of the line due to partial discharge
i_B	Apparent current at point B of the line due to partial discharge
i_c	Current through self capacitance in Rogowski coil analysis
i_{coil}	Total current induced in the Rogowski coil winding
i_m	Measured current (output current of the sensor)
I_p	Peak value of PD pulse
i_p	Primary current to be measured by the sensors
i_{Rm}	Current through measuring system resistance in Rogowski coil analysis
i_{RT}	Current through terminating resistance in Rogowski coil analysis
J_1	Joint number 1 as a node along feeder F_1
K_c	Calibration factor for Rogowski coil
K_e	Error factor for Rogowski coil
l	Length of the line in general
l_{12}	Length of cable for PD location purpose
l_c	Length of cable for measurement of attenuation constant
L	Inductance per-unit length
L_c	Self inductance of Rogowski coil
M	Mutual inductance
M_c	Mutual inductance of the Rogowski coil
ms	Millisecond
N	Number of turns of the Rogowski coil

Symbols	Description
p	Atmospheric pressure inside the cavity
P_A	The components of A (first) priority, around which coil sensors are installed with their face A toward the components
P_B	The components of B (second) priority and coil sensors are installed so that face B of the coils is towards these components
ps	Picoseconds
$q(t)$	General expression for the electronic charge in terms of current
q_1	Induced charge on the line due to partial discharge
$q_1(t)$	Apparent charge measured at point P_1
$q_2(t)$	Apparent charge measured at point P_2
q_A	Charge induced at point A of the line due to partial discharge
q_B	Apparent charge at point B of the line due to partial discharge
q_o	Actual charge or space charge within cavity transferred during partial discharge
R	Resistance per-unit length
$R_{1,1a}$	The coil sensor representing the $R_{(node1),\ (upstream\ side)(\ phase\ a)}$, and so on for phase b and c
R_{11}	Coil sensor installed at node 1, towards the upstream (left) side of the node 1
rad/m	Radians per meter
R_c	Self resistance of Rogowski coil
RC_1	Rogowski coil 1
RC_2	Rogowski coil 2
R_m	Resistance of measuring system
R_{osc}	Resistance of the oscilloscope
R_T	Terminating resistance
S/m	Siemens per meter
S_1	The sensors installed at the downstream side of the nodes
S_2	The sensors installed at the upstream side of the nodes
t	Time
t_1	Time at which signal is captured by sensor at line end 1
T_1	MV/LV transformer as node 1 on the cable Feeder F_1
T_1F_1	The cable section between the node F_1 and node T_1 and so on for other sections
t_2	Time at which signal is captured by sensor at line end 2

Symbols	Description
t_d	Propagation time difference
T_f	Fall-time of a PD pulse
T_{pc}	Propagation time of pulse on the line
T_r	Rise-time of a typical PD pulse
T_w	Time of pulse width for PD pulse
U_1	Location of PD fault point within line section L_1P_1
U_2	Location of PD fault point within line section P_1P_2
U_3	Location of PD fault point within line section P_2L_2
V	Volt
$V(x)$	Voltage of the line at a position x
$V_1(t)$	Voltage signal recorded by oscilloscope at the terminal of the coil sensor at line end 1
$V_2(t)$	Voltage signal recorded by oscilloscope at the terminal of the coil sensor at line end 2
V_a	Applied voltage from supply, voltage across capacitor C_{ia} in a-b-c model.
V_b	Voltage across capacitor C_{ib} in a-b-c model
V_{Bc}	Breakdown voltage at which the cavity collapses
V_c	Voltage across capacitor C_{ic} in a-b-c model
V_e	Extinction voltage, at which the PD ceases
V_o	Voltage at the output terminals of Rogowski coil
V_{o1}	Voltage output of Rogowski coil 1
V_{o2}	Voltage output of Rogowski coil 2
V_p	Peak value of applied sinusoidal voltage V_a
$V_{rc}(t)$	Voltage induced in the Rogowski coil
$V_{T1,\ 1a}$	Voltage output of the coil sensor representing the $V_{(node1),\ (upstream\ side)(\ phase\ a)}$, and so on for phase b and c, similarly so on for other nodes
υ_d	Drift velocity within the cavity
υ_p	Wave propagation velocity of electromagnetic signal
X_1	The distance of PD fault from the line end 1
Z	Impedance of the line
Z_c	Characteristic impedance of Rogowski coil

Symbols	Description
α	Attenuation coefficient
α_1	The rate of rise of the pulse
α_2	The rate of fall of the pulse
β	Phase constant
γ	Propagation constant
ε_c	Relative permittivity of gas filled cavity
ε_i	Relative permittivity of insulation
ε_o	Permittivity of free space
ζ	Damping coefficient of Rogowski coil
λ	Wavelength of the propagating signal
υ	Frequency of the signal in cycle per second
ω	Frequency of the signal in radians per second
ω_c	Resonant frequency of Rogowski coil (in rad/s)
Ω/m	Ohms per meter

1. Introduction

1.1. Background

Increased dependability and demand of electric power have made the electrical utilities to focus on modernization of power distribution systems. One of the major deriving forces to modernize the current power grid is the demand for improved reliability, efficiency, and safety of power grid. This asks for optimization of capital assets while minimizing the operation and maintenance cost of the network. The networks are always exposed to predictable and non-predictable failures. The probability of occurrence of unpredictable failure event such as natural disaster or sabotage cannot be reduced. However, corrective maintenance techniques can be used for timely identification, isolation, and rectification of the affected or failed component in order to restore the normal operation of the network [1]. On the other hand, predictive failures can be forecasted and hence be avoided by performing preventive maintenance tasks in the form of condition assessment of the power components [2]-[4]. Based on the type of components, nature of operation and effectiveness of condition monitoring results, an optimized maintenance strategy can be implemented to achieve an acceptable trade-off among the value of asset, economic burden of failure, and cost of maintenance strategy [5]-[6].

While designing the condition assessment schemes there are two major concerns; either they should be done on periodic or continuous bases, as shown in Fig. 1.1. Periodic monitoring is a widely used and economical option, however scheduling the monitoring period for components of different age groups (and priority) is very critical. Periodic monitoring is done in both, on-line and off-line operation of the network. The threat of a missing hard event for a component during operation is always there. This kind of monitoring somehow lacks the accurate assessment of component under test due to absence of actual operational environment when the component is off-line [7]. Continuous monitoring, on the contrary, is generally designated as on-line monitoring system [6], [8]-[9]. It is initially expensive due to permanent installation of the measuring system but running cost is low. Constantly surveilled and analyzed data is trended for continuous projection of equipment's health or expected failure [10]-[11]. This kind of monitoring provides updated information of an incipient fault; whether it exists, where it is happening, how far the damage has been done, and how fast it is progressing. The focus of this thesis is on-line condition assessment strategy.

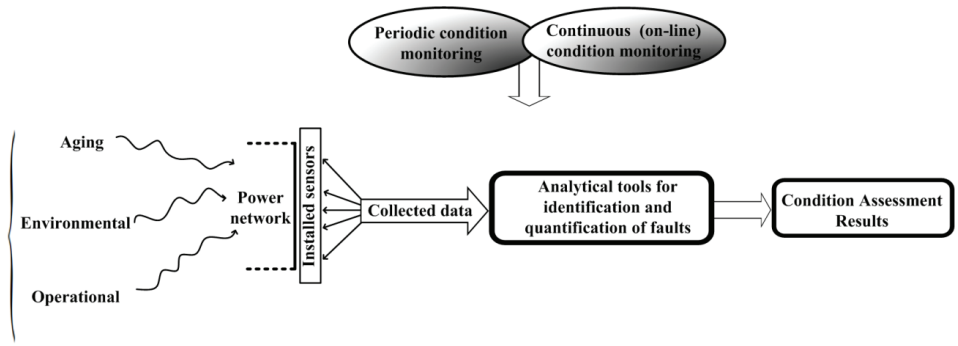

Fig. 1.1. Condition assessment scheme for power components.

Distribution system consists of different types of lines carrying electric power from medium voltage (MV) substation to the consumers via distribution transformers. These lines are underground cables, overhead covered conductor (CC), and bare conductor overhead lines. Switchgear, transformers, and connecting and protection devices are the necessary electrical components used along with these lines. During a survey of Stockholm, out of 1392 total failures, 174 were due to power transformers, cables (including joint and terminations) caused 435 failures, overhead lines, and bus bars were responsible for 36 failures [12] while rest of failures were due to other faults such as disconnectors, circuit breakers, and rectifiers etc. Insulation damage is one of the major causes of failure in these components [13]-[14]. During operation, insulation of electrical components becomes weak due to different stresses like aging, electrical, thermal, mechanical, and environmental stresses. Emission of partial discharge (PD) signals is a clear indication of insulation degradation in the electrical components. Since past 20 years, PD measurement has been widely applied for diagnostics. Efficient diagnostics depends on the performance of PD sensors, techniques of measurement, and frequency of inspection. This asks for simple and economical sensors with effective implementation techniques which can provide measured data making clear recognition pattern for correct assessment of the occurred PD faults, on continuous basis.

1.2. Research Problem Description

Different kind of stresses pose potential threats to the power components which can be detected and corrective plans be executed on 'need to do' basis. Figure 1.1 represents the overall block diagram of condition assessment scheme. One of the biggest shortcomings of today's progressing distribution automation is the lack of low cost instrumentation solutions which are simple in implementation and easily applicable during network being built and system

refurbishment. The major technical element of a condition assessment system is the sensors in order to collect the pre-fault data for early information of upcoming threat to the power components. Flexible physical design, good operational performance, and low cost, enables the sensors to be integrated within the large area of the network which increases the reliability of condition monitoring system to manifolds. The research motivations and problem descriptions of this work is explained as follows.

1.2.1. Design of Sensor for PD Monitoring

In the pre-fault stage, the insulation damage of the power components causes PD events at a certain breakdown voltage level across the component. During PD activity, energy is released, and broadcasted in various forms such as, electromagnetic, acoustic, optical, and chemical. Related to different types of energies transmitted, researchers have been able to develop respective types of sensors [15], which can provide the information of the incipient PD fault. Electromagnetic energy released during PD events can be measured with the help of high frequency voltage or current pulses induced during discharge. In this research, current sensors have been considered. Today there is a variety of current sensing equipment available including shunts, current transformers, Rogowski coils, Hall effect sensors, magneto impedance sensors, and giant magneto resistive sensors. Based on some critical parameters of a sensor such as cost, bandwidth, sensitivity, saturation, linearity, operating temperature, footprints, integratability, flexibility, isolation, and material technology, Rogowski coil has been preferred as a favorite tool for PD current sensing purposes [16].

Each PD event generates low amplitude pulses of extremely short duration having certain wave-shape. For effective PD diagnostics, Rogowski coil sensor should be able to measure these high frequency pulses precisely. For precise or reliable measurements, an accurate model of Rogowski coil is needed. The parameters of Rogowski coil determine the accuracy of the coil model. During design phase, the value of the model parameters are used to calibrate the measured output of Rogowski coil. Therefore, any error in the identified parameters results in an erroneous measurement of the PD signal which means wrong assessment of the fault. In some studies, methods have been presented to calculate the parameters of coil model based on physical geometry of the coil [17]-[18]. It turns out that because of certain limitations, these methods do not provide precise value of the parameters especially for high frequency Rogowski coils. There is a need of an improved method of parameter identification which takes into account the high frequency behavior of the coil and possible effects of the measuring system during operation.

Rogowski coil sensor consists of three essential stages; signal sensing, signal conditioning, and integration. Integrator (last stage) is important to recreate the original signal observed by the coil at its input. Conventional design of integrator consists of active and passive components. The use number of sophisticated components and limitations of amplitude and frequency range of the measured signal due to operational features of components makes the design of integrator complex and expensive [19]-[21]. Obtaining simplicity in the design, better accuracy for wide range of amplitude and frequency of measured signal, and low cost are the challenges during development of integrator for the coil.

1.2.2. On-line PD Diagnostics in the Distribution Network

A distribution network consists of various types of components, such as substation transformers, switchgear, bus-bars, power lines, measurement and protection equipment, MV/LV (low voltage) transformers, and switches. The network topology can be ring or/ and radial. The incoming concept of distributed generation under the umbrella of future smart distribution system is going to make the network topology more complex [22]-[23]. PD faults can occur anywhere along the network in the damaged insulation of an energized electrical component. Considering electromagnetic sensing, it has been noticed that most of the available location techniques are applied on a specific section or component of the network to determine the location of PD source. The propagation characteristics of the PD signals, such as propagation delay (time domain reflectometry or time difference of arrival), and propagation attenuation (frequency amplitude analysis) [24]-[27], are used during implementation of these techniques. These techniques are useful when applied on a single section or component; however due to certain limitations [28]-[30], they alone cannot be used for a multi-section (straight or branched) line network. For a complex topology of the real network having number of sections or components, there is a need for the techniques which can monitor a wider network part. The aim is to present a spatial monitoring system which can be used to identify the faulty section or component of a network as a primary diagnostic task, followed by the location task of the PD source present within the identified section or component.

1.3. Research Contribution

Rogowski coil induction sensor has been used in this research. The design and application aspects of Rogowski coil are exploited for PD monitoring with the help of experimental and simulation platforms as follows:

- Different aspects of the Rogowski coil sensor, such as geometrical design, construction, calibration, and application, are investigated in detail.

- Electrical model of Rogowski coil is presented normally as a second order (resistor-inductor-capacitor) RLC circuit. Basic features of the RLC circuit are investigated in detail in order to analyze the behavior of Rogowski coil which makes the development procedure of Rogowski coil simpler.
- A new methodology to determine the electrical parameters of Rogowski coil is presented.
- To avoid the limitations imposed due to an analogue electronic integrator, digital integration technique has been implemented in the design of the Rogowski coil.
- Directional sensing feature of Rogowski coil has been explored which provides an easy method to determine the direction of arrival (DOA) of PD signals.
- Based on detection of DOA of PD signals along a power line, a technique was developed to identify the faulty line section for both, straight and branched line network topologies.
- Experimentally evaluated DOA technique is integrated over a cable feeder to propose a PD monitoring scheme for distribution network. A novel idea is presented to develop a measurement based algorithm for automated identification of the fault line section or the component in the network.

1.4. Dissertation Outline

The contents of this thesis are a summary and [Publications I-IX]. Brief illustrations of the contents are as follows.

Chapter 2 presents the structure of on-line condition assessment system based on PD measurement. The characteristics of PD signals are described with the help of practically measured PD signals. The important features of PD signals and their application for PD diagnostics are discussed in detail [Publication I, VIII].

Chapter 3 presents the model of a high frequency Rogowski coil for PD measurements. Construction and modeling of the coil prototype are described in detail. A new methodology of identification of model parameters is conferred. Practically developed model of Rogowski coil is simulated in ATP-EMTP software environment, for in-depth analysis and model validation. The role of geometrical parameters of Rogowski coil is experimentally investigated to analyze their effects on performance of coil for high frequency measurements [Publication II-V].

Chapter 4 describes the calibration of Rogowski coil to determine the DOA of PD signals based on detected polarity. The directional sensing is practically implemented for overhead CC lines and cables in the laboratory. For straight lines, the technique is applied for MV

overhead CC line whereas in branched line scenario, MV cables are used. [Publication VI-IX]. The developed technique is integrated over a cable feeder using ATP-EMTP. A methodology of analyzing the signals measured by multiple coil sensors is presented. An algorithm is proposed to develop an expert system for automated identification of the PD faults.

Chapter 5 describes the summary of the all the articles included in this dissertation.

Chapter 6 presents the conclusions of the work and proposes the future work in this field to improve the monitoring and diagnostics capability of condition assessment system.

2. Partial Discharge Signals

2.1. Condition Assessment System Based on Partial Discharge Measurements

This chapter discusses various characteristics of PD pulses for monitoring and diagnostics. Most of the time, either of these terms is used to represent both features of condition assessment of electrical equipment. However in actual sense, the terminology of monitoring refers to obtaining the raw data from the under study equipment with the help of employed sensors whereas diagnostics refers to the analysis of monitored data using certain trends, signatures or calculations, in order to evaluate the state of equipment for maintenance. In this research work, a comprehensive model of the condition assessment system is implemented as presented in Fig. 2.1. Monitoring and diagnostics are two main tasks of the model. PD monitoring system can be divided into three essential elements a) design of sensors, b) measuring system, and c) measurement of the data. The diagnostics basically consists of three elements; d) detection, e) location, and f) quantization. The most suitable order of the elements of condition assessment system is as described in Fig. 2.1.

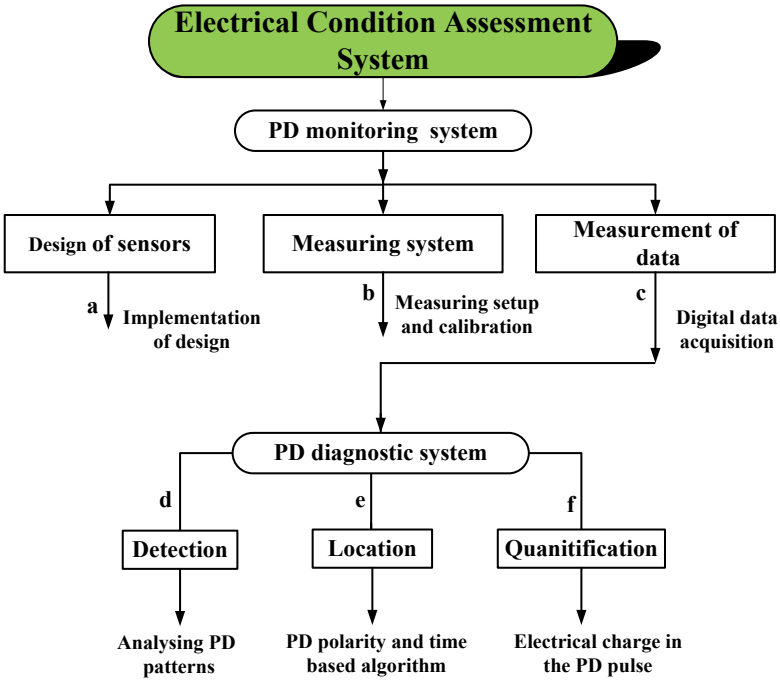

Fig. 2.1. Implementation of condition assessment system for power components.

The organization of the work done for implementation of these elements is as follow. The current transducers are used as monitoring sensors. The design of sensor and measurement of PD signals using induction sensors is described in chapter 3 [Publication II-V]. Detection, location, and quantization of the PD faults are presented later in this chapter. In this chapter, conventional location technique is described. The contribution of this research work to enhance the PD location techniques for distribution lines is presented in chapter 4 [Publication VI-IX].

2.2. Insulation Degradation

A detailed overview of insulation degradation and PD mechanism can be found in [31]-[33]. A solid insulation has a specific electrical breakdown strength (expressed in kV/mm) which depends upon the dielectric properties and thickness of the insulation material [34]. Healthy high-voltage insulation between two electrodes keeps the charges of opposite polarities from passing through the material. During normal operation, the electrical field stress is uniformly distributed across the healthy insulation between the electrodes. However, when this material has some defects (small gaps or cracks filled with some gas), there occurs a non-uniform distribution of electrical stress among the healthy and defective insulation parts. This is due to different dielectric properties of the healthy and defective part of insulation. Depending on the size and type of defect, PD occurs at a certain level of applied voltage. During this activity the charges are able to penetrate through the material with the force provided by the high electric field strength. Some of the most common reasons for the insulation defects are

- Material deterioration due to aging: change in dielectric constant because of chemical effects etc.
- Material deterioration due to environment: thermal effect due to operating temperature and temperature gradient etc.
- Mechanical damage: transportation, installation, storms, earthquake, and other physical stresses etc.
- Operational stress: overvoltage and lightning etc.
- Manufacturing defects: voids and cavities etc.

PD is the process of localized dielectric breakdown of a small portion (voids, cracks, bubbles or inclusions) of a solid or a liquid electrical insulation system which is under high voltage (HV) stress. This discharge partially bridges the phase to ground, or phase to phase insulation. Once the process is triggered, the insulating materials start to deteriorate progressively which eventually leads to an electrical breakdown. Based on difference in location of the gap between the insulation and electrode (phase), PDs are divided into four types, (i) internal discharges, (ii) corona discharges, (iii) surface discharges, and (iv) discharges in

electrical trees [35]- [36]. Internal discharges and treeing (series of internal discharges) are more crucial than surface and corona discharges. When the PD extinguishes, there is an exchange of energy released during PD event in different forms:

- Light energy in the form of electromagnetic radiation.
- Electrical energy in the form of electromagnetic impulses.
- Thermal energy in the form of change in temperature.
- Acoustic energy in the form of noise or sound.
- Chemical energy in the form change of gas pressure of the active oxygen and presence of chemical products such as wax [37].

Analysis of the released energy with the help of a compatible sensor can provide the early information of the ongoing insulation degradation.

2.3. Partial Discharge Mechanism

The operating environment affects the stresses on the components and particularly their dielectric material. Various microscopic effects resulting from dynamic behavior of multiple stresses determine the local physical (aging/degradation) processes [32], [38]. This can cause cracking and ruptures which further develop as cavities or treeing. A cavity and an electrical tree is depicted (see Fig. 2.2) to show a case of internal PDs in an MV cross-linked polyethylene (XLPE) cable. The defect is present inside the XLPE main insulation of the cable which is located between the Aluminum conductor (phase electrode) and cable shielding (ground electrode).

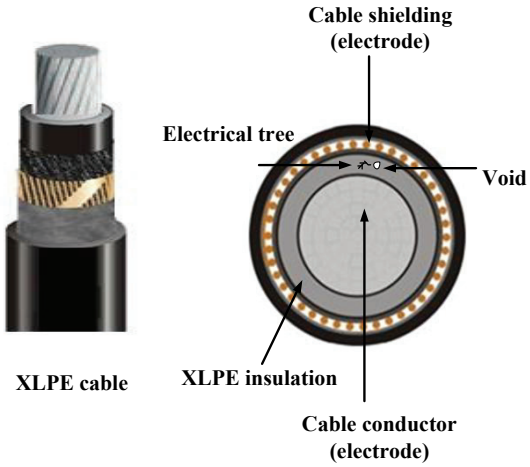

Fig. 2.2. A cavity depicted in the main insulation of a XLPE MV cable.

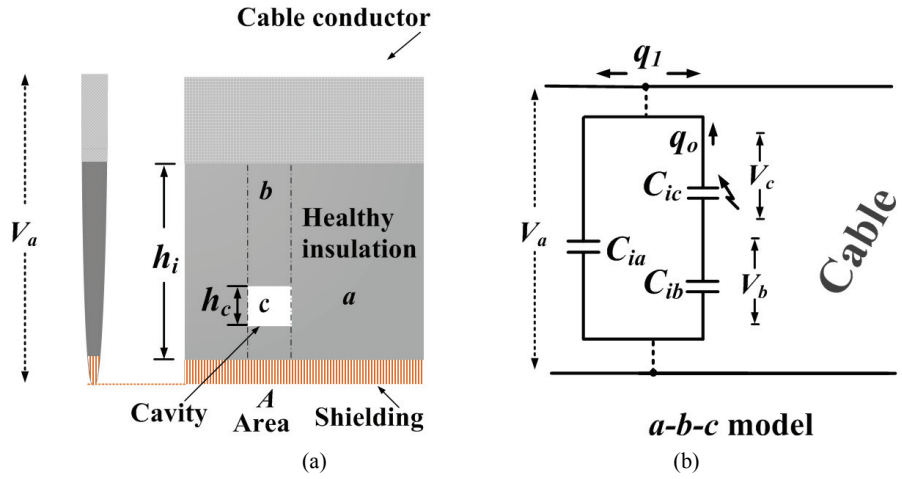

Fig. 2.3. (a) Physical model of the cavity inside insulation (upper half of the cross-sectional view of cable) and (b) electrical a-b-c model of the cavity inside cable insulation.

Considering upper half of the cable's general layout, the physical model of the cavity and its surrounding healthy insulation is shown in Fig. 2.3(a). Assume that the solid insulation of the cable has a thickness h_i while h_c is the thickness disc shaped cavity. The insulation between both electrodes is divided into three portions. Portion *c* represents the cavity of an area *A*, *b* is the portion of healthy insulation under area *A* (apart from the defective site), and *a* is the surrounding portion of rest of the healthy insulation. During normal operation, voltage V_a is applied across the line. The cavity is usually filled with a gas of lower dielectric constant than the surrounding solid insulation. Due to different dielectric constants of the insulation between the electrodes, different capacitances emerge which proportionally divides the voltage applied across the electrodes. To analyze the PD generation, a well known electrical (a-b-c) model of the cavity inside insulation is shown in Fig. 2.3(b). Here C_{ia}, C_{ib}, and C_{ic} are the capacitances and their values depend upon the dimensions and dielectric constants of respective portions *a*, *b* and *c* [39].

Assuming that a disc type cavity is filled with a gas of relative permittivity ε_c, the capacitance of portion *c* is given as [40]

$$C_{ic} = \frac{\varepsilon_o \varepsilon_c A}{h_c} \,. \tag{2.1}$$

The capacitance of portion *b* of relative permitivity ε_i is given as

$$C_{ib} = \frac{\varepsilon_o \varepsilon_i A}{h_i - h_c} \,. \tag{2.2}$$

Similarly, the capacitance C_{ia} can be described for portion *a*. The voltage V_a across C_{ia} is essentially divided across the C_{ib} and C_{ic} which represents the faulty region. The voltage V_c across C_{ic} is of major concern for PD generation and is expressed as

$$V_c = V_a \frac{\varepsilon_i}{1 + \frac{\varepsilon_c}{\varepsilon_i}\left(\frac{h_i}{h_c} - 1\right)} \,. \tag{2.3}$$

The electric field E_a due to V_a is uniformly distributed across the portion *a*. However, due to difference is in electrical permittivity (material ability to permit the electric field) of portion *b* and *c*, there is a non-uniform distribution of the electric field across the portion *c*. Based on *V=Ed*, where *E* is the electric field due to potential *V* across the electrodes at a distance *d*, the electric field E_c across the cavity can be estimated as

$$E_c = E_a\left(\frac{h_i}{h_c}\right)\frac{\varepsilon_i}{1 + \frac{\varepsilon_c}{\varepsilon_i}\left(\frac{h_i}{h_c} - 1\right)} \,. \tag{2.4}$$

If the size of the cavity and relative permittivity is considerably smaller than the solid insulation, as will usually be the case, the E_c will be significantly greater than E_a. For example, suppose that there is a cavity of thickness (h_c) 0.6 mm inside an MV (20 kV) XLPE cable having 6.6 mm thick (h_i) insulation. For ε_c = 1 and ε_i = 2.3 (typical for air and XLPE), the electric field intensity in the cavity is approximately 2 times greater than that of surrounding insulation at a certain applied voltage. The dielectric breakdown strength of material of the solid insulation is E_{Ba} = 21 kV/mm whereas for air-cavity it is E_{Bc} = 3 kV/mm. This (3 kV/mm) value is measured for an ideal air-cavity of 1 mm^3, however for the above described cavity, the voltage V_{Bc} at which the breakdown occurs can be determined in terms of E_{Bc} and dimensional arrangement of the cavity as

$$V_{Bc} = E_{Bc}\left(1 + \frac{\varepsilon_c}{\varepsilon_i}\left(\frac{h_i}{h_c} - 1\right)\right)h_c \,. \tag{2.5}$$

When the voltage across the cavity rises to V_{Bc}, a discharge takes place within the capacitive cavity. Continuing the above example of 0.6 mm air-cavity inside the XLPE insulation of the cable, the discharge should initiate at V_{Bc} = 9.6 kV, calculated from eq. 2.4 and 2.5. As a result of this discharge a PD signal is generated.

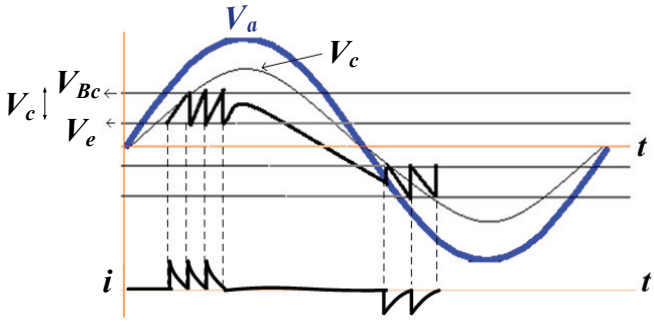

Fig. 2.4. Electrical mechanism of PD activity.

The applied voltage $V_a = V_p$ (sinωt + ϕ) varies periodically and completes its cycle as shown in Fig. 2.4. When the V_a is increased to such a value that the cavity voltage V_c approaches to the breakdown voltage V_{Bc}, cavity collapses and a rapid displacement of charges takes inside the cavity. The displaced charge is termed as space charge. Due to transfer of the charge, the potential difference across the cavity drops to a value V_e (extinction voltage) at which the electric field intensity becomes lower than that of required in order to maintain the discharge. The discharge ceases at this instant and the charge starts to accumulate across the boundaries of the cavity. The voltage V_c starts to build-up due to the increasing value of the applied voltage V_a. Again, the PD collapses at the V_{Bc}, another PD event takes place and this activity goes on repeatedly. The PD activity occurs during both positive and negative cycles of the applied voltage. During PD event the amount of space charge can be expressed as [41]

$$q_o = C_{ic}\left(V_{Bc} - V_e\right), \tag{2.6}$$

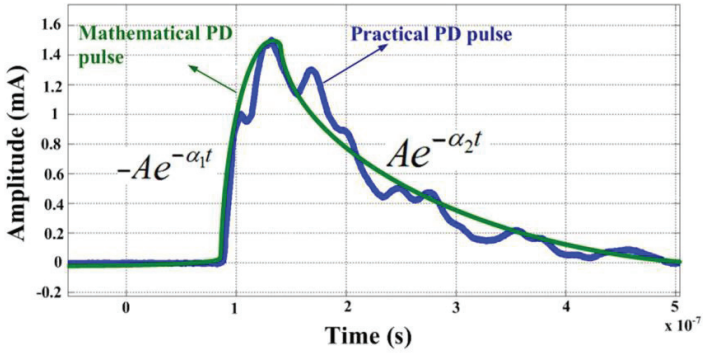

Fig. 2.5. Typical PD pulse in electrical power systems (a) mathematical (ideal) pulse and (b) practically measured typical PD pulse.

where q_o is also called the actual charge which is distributed within the cavity. The PD event occurs in the bulk of the insulation material and therefore, subsequently a proportional charge q_1 is electrostatically induced on the electrode (cable conductor). The induced charge q_1 depends on the location and magnitude of the actual charge q_o. The relationship between actual charge and induced charge can be obtained by using Poisson's equation implemented in [42]-[44].

The discharge event is extremely fast and accomplishes in a very small fraction (having nano to micro second duration) of the period of applied voltage cycle. Respectively, the induced charge is created rapidly during each PD event which results in a high frequency current pulse induced on the electrode. A typical PD pulse is shown in Fig. 2.5. The mathematical model of the pulse can be described as

$$i_{pulse}(t) = A\left(e^{-\alpha_2 t} - e^{-\alpha_1 t}\right), \tag{2.7}$$

where A is the peak value of the pulse, α_1 is the rate of rise-time and α_2 is the rate of fall-time. Rise-time of the pulse is an important parameter of PD activity and also determines the highest frequency components of the PD signal. The typical PD pulse is compared with the practically measured PD pulse. This (practically measured) PD pulse has been injected from a PD calibrator into a line shown in experimental setup given in Fig. 2.6. Comparison of both the pulses shows that practical PD pulse contains high frequency variations which are due line's inherent characteristics. The faster the rise-time, the higher will be the frequency required to capture the PD pulse accurately. The rise-time of PD pulse depends on the drift velocity and the size of the cavity (the path travelled by the discharged avalanche). For a gas-filled cavity, the drift velocity υ_d in cm/sec can be determined theoretically as [45]

$$\upsilon_d = 1.334 \cdot 10^6 + 4.222 \cdot 10^5 \left(\frac{E_{ci}}{p}\right), \tag{2.8}$$

where E_{ci} (kV/cm) is the electric field intensity at PD inception and p is the atmospheric pressure of the cavity. Hence the rise-time (transit time) T_r is calculated as

$$T_r = \frac{h_c}{\upsilon_d}, \tag{2.9}$$

where h_c is the depth of the cavity (void) which is the distance that the charges travel during discharging event. The Equation (2.9) presents an estimation of the rise-time, however also the local factors such as temperature and conductivity of the cavity have an impact [46]. For a cavity of 0.2 cm diameter in two polyethylene films with a void depth of 0.08 mm and 0.12 mm, the rise-time (T_r) of PD pulse is measured as 0.754 ns and 0.991 ns respectively [45]. The fall-

time T_f of the induced PD pulse depends upon the impedance of the cable, propagation characteristics of the medium (cable system) a given pulse must travel through prior to be measured, and the impedance of the measuring system [47]. The PD pulse shown in Fig. 2.5 represents a PD current pulse measured at the terminal of an MV cable. The distortions in the waveform are due to travelling along the line having various electrical parameters and properties of the measuring sensors.

2.4. Detection of Partial Discharge Signals

Phase resolved analysis (PRA) is a well known technique to identify the type (four types mentioned in section 2.2) of a PD defect [35]. This type of analysis is made by taking into account the accumulated PD activity observed during whole cycle of applied voltage. However, PRA is not useful when a single PD pulse is needed to be analyzed for location or quantization purposes. In this work, induction sensors are used to measure the individual pulses during the cycle of operational voltage. Certain features of PD pulses are considered to detect whether measured pulse is a PD pulse or noise. Practical measurements have been used to demonstrate the PD detection.

IEC 60270 (High-Voltage Test Techniques- Partial Discharge Measurements) provides a basic test setup configuration for measurement of PD pulse waveform injected from a PD calibrator into the test circuit. A similar experimental setup has been shown in Fig. 2.6 where a PD voltage pulse is injected from a PD calibrator into a line which resulted in a PD current pulse of 1.5 mA (peak), propagating along the line. The line was matched by its characteristic impedance at the far end and an induction sensor was used for measurement. As the pulse was injected from a commercial calibrator, in a noise free environment, it can be considered as of an ideal kind. The measured PD pulse is shown in Fig. 2.7. A realistic approach is presented next, using an energized setup in order to observe the PDs generated from a real test object. There are various visible parameters of PD signals which can be utilized to investigate the PD activity. The rise-time T_r, fall-time T_f, pulse width T_w, and amplitude I_p are related to a single PD pulse (see Fig. 2.7) whereas phase angle, pulse repetition time, polarity, and wave-shape can be considered more associated with the overall PD activity (group of pulses) during a period of power cycle.

In order to measure a PD signal accurately, the measuring sensor should be designed with compatible sensitivity and bandwidth. Amplitude of the PD pulse refers to estimate the intended sensitivity of the sensor. Similarly, rise-time, fall-time, and pulse width which refer to the frequency contents of a pulse signal, provide intimations for selection of a suitable bandwidth of the sensor. The above mentioned parameters of the PD pulse vary for different types of

insulation in electrical components. Size and type of insulation defect also affects the value of these parameters. Therefore, a specific value of these parameters cannot be stated. Based on practical experiences, the amplitude of PD pulses lie within the range up to few milliamperes while the pulse width ranges between nano seconds to micro seconds. The PD pulse width of the PD pulse shown in Fig. 2.7 is 120 nano seconds.

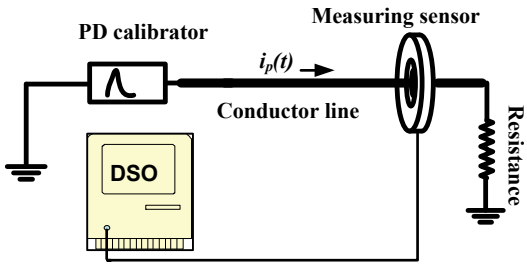

Fig. 2.6. Laboratory setup for measurement of PD pulse from PD calibrator.

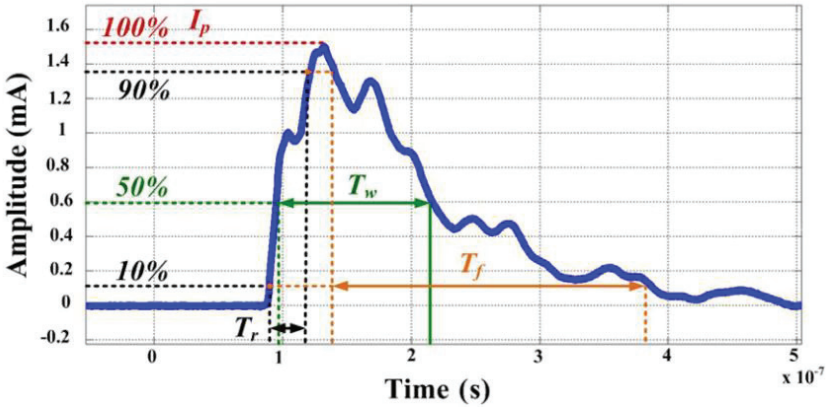

Fig. 2.7. Waveform of the measured (calibrated) PD pulse.

To measure real PDs, a test object shown in Fig. 2.8(a) is energized upto few kV. The experimental arrangements made in the laboratory are shown in Fig. 2.8(b). The test object consists of a plate-plate electrodes assembly inside a cubical solid epoxy resins insulation material. The distance between electrodes is 0.5 cm while there are few air-filled voids within insulation, between the electrodes. The voltage was applied across the test object, from a 0-230V voltage supply (variable) through a 230V/100 kV power transformer. A commercial high current transformer (HFCT) was used to capture the PD signals emitted from the test object at an applied voltage above the breakdown voltage of the PD source. Capacitor C_1 and C_2 make a

voltage divider to measure the applied voltage. PD signals and applied voltage are measured on high sampling rate digital storage oscilloscope (DSO). For detailed analysis, the data is captured for a complete cycle of 20 ms. It should be noted that 20 ms is a long duration as compared to the PD pulse of pulse width in few nano seconds. Therefore, the sampling period is adjusted to 400 ps in order to capture fast PD pulses reliably.

During laboratory measurements such a high sampling rate (small sampling period) can be used for detailed investigation. However this will cause a large amount of data even for a small period of time. For example, it has been observed that sampling frequency of 2.5 GS/s (sampling period 400 ps) requires approximately 70 Mbyte on DSO to store the PD data for 20 ms. The size of the data will be enormous for continuous monitoring, which is an impractical consideration. For real applications, Nyquist sampling frequency should be observed which can be determined by the frequency response of the measuring sensor. For a Rogowski coil sensor of resonant frequency 37.6 MHz (see Chapter 3), a sampling frequency 77 MS/s is suitable enough to capture the measured signals reliably.

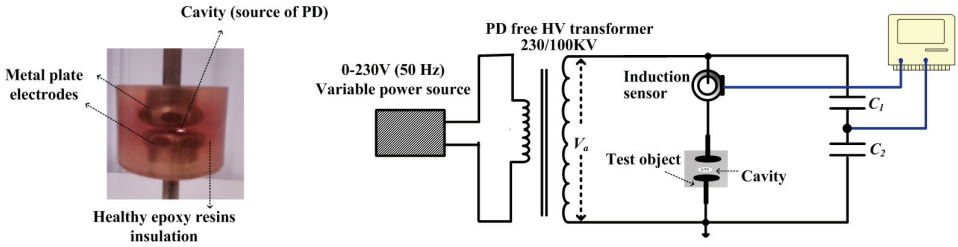

Fig. 2.8. (a) Test PD object and (b) laboratory setup to captured PD signals emitted from the test object.

Figure 2.9(a) shows the PD activity measured along with the applied voltage. PDs were captured at 5.7 kV. A group of PD pulses can be seen during both half-cycles of the applied voltage. Phase angle (θ_1 and θ_2) is the phase location of the PD occurring with respect to the applied voltage. It depends on the location of the cavity. Moreover, it also depends on the shape and geometry of the electrodes and insulation. There are recognized PD patterns, according to which certain PD activity is dominant in a specific region of the supply cycle. In case of corona discharge, the PD pulses can be observed symmetrically around the peaks of the applied voltage. Similarly in case of surface discharges or internal PDs, a group of PD pulses is visible during first and third quadrant of the applied voltage [35]. Looking at the Fig. 2.9(a), it can be seen that a group of PD signals is located in quadrant I and III while quadrant II and IV show some noise. Therefore, the captured signals agree with internal PDs.

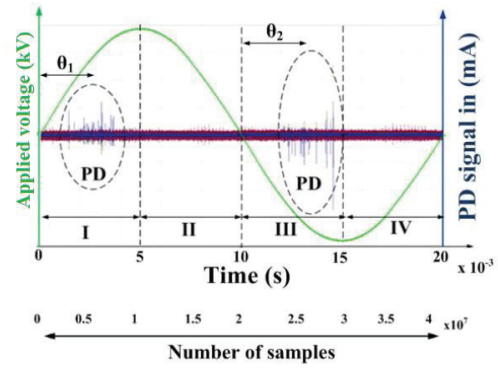

(a)

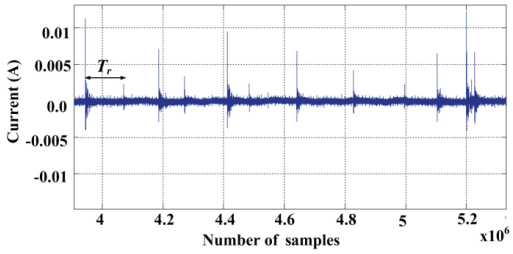

(b)

Fig. 2.9 (a) Phase-resolved analysis of PD activity, and (b) PD pulses during positive half cycle.

Due to the nature of PD process, the cavity charges and discharges take place and generate multiple pulses as can be seen in Fig. 2.9(b). The time interval between the consecutive pulses can be termed as pulse repetition time (T_p). The time T_p mainly depends upon the electric field intensity E_{Bc} (kV/mm) at PD inception and the size of the cavity. It has been observed that time between every two consecutive pulses may not be the same. Similarly, amplitude of each individual pulse does not necessarily present a linear behavior in a power cycle. It can be clearly noticed that, rising towards peaks of applied voltage during positive and negative cycle, the amplitude of PD pulses does not increase or decrease linearly. This is due to partially hysteretic, time-invariant and non-linear nature of PDs which depends on the effect of space charge, availability of seed electrons, and local conditions [46], [48]. However, there is a certain range of this randomness. For example, considering PD activity during positive half cycle, amplitude of captured PD pulses at an applied voltage of 5.7 kV varies between 2-12 mV whereas at increased voltage of 7.1 kV this range is observed to be 4-38 mV. Therefore, overall PD activity exhibits a certain pattern. Figure 2.10(a) shows the signals measured with the help of an induction sensor. An increased PD activity can be clearly observed at higher applied voltage.

The signals captured by the commercial PD diagnostic ICMsystem [49] are shown in Fig. 2.10(b) which describes the similar pattern in the form of the discharge activity.

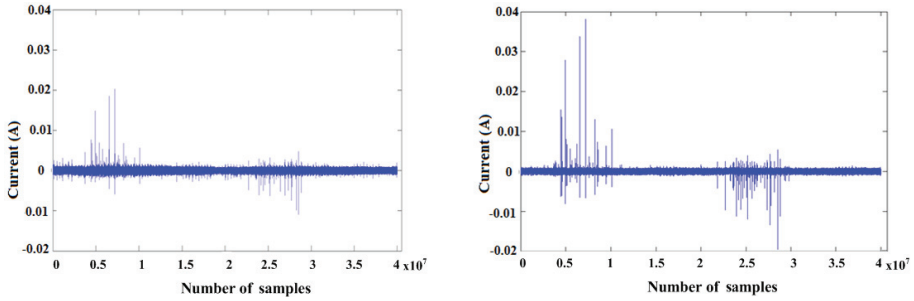

(a)

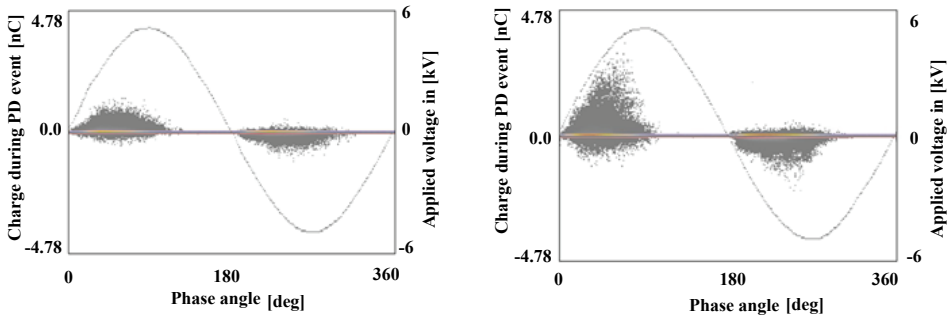

(b)

Fig. 2.10. PD signal captured during two different voltage levels (5.7 kV and 7.1 kV) of supply cycle in the form of (a) PD current pulses and (b) PD charge density.

2.4.1. Polarity

The polarity of the PD pulses is an important factor for diagnostics. The polarity of applied voltage V_a establishes the direction of electric field across the cavity which consequently determines direction of transfer of charge and hence the polarity of the induced PD pulse. Polarity of PD pulses emitted during positive half cycle of applied voltage is positive and vice versa as shown in Fig. 2.11(a) and Fig. 2.11(b) respectively. However, when using induction sensors for measurement, care must be taken for their installation in order to get the true polarity of the originated PDs. It could be identified as a valid indication of the presence of PD activity that all the PD signals in a specific half cycle show the same polarity. This feature of PD signals will be used to determine the location of the PD defect.

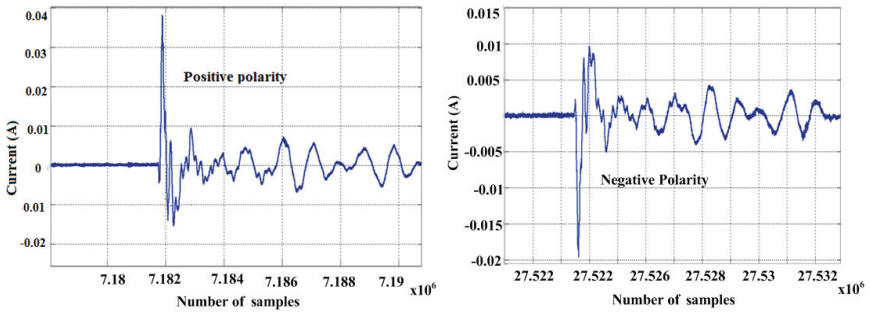

(a) (b)

Fig. 2.11. Polarity of PD signals identification during (a) positive and (b) negative, half cycle of applied voltage.

2.4.2. Waveform

The simulated and practically measured ideal wave-shape of PD pulse was shown in Fig. 2.5, however the wave shape of PD pulse is significantly affected by the properties of the medium through which it travels and the properties of measuring sensors. Considering the case of cables or overhead CC lines, when the induced PD current i_p travels along the line, attenuation, dispersion, reflections and distributed RLC effect of line parameters affects the wave-shape of PD signals [50]-[51]. When an electromagnetic sensor is used to measure a PD pulse, its physical and electrical parameters, and operating characteristics come into play. The sensor measures the PD signal based on its designed sensitivity and bandwidth which affects the measured signal [47]. All the measuring sensors present the measured signal using a digital system. PD signals are high frequency signals and need to be captured using suitable data acquisition system (DAS). The effect of various factors such as noise, amplifier gain and offset, ADC quantization (resolution error), and other error factors, may limit the accuracy of reconstructed measured signal [52]. The block diagram describing the influence of the measurement process is shown in Fig. 2.12. Therefore, the measured signal i_m can be expressed as

$$i_m = i_p K_c H(r) \tag{2.10}$$

where i_p is the primary PD signal, while K_c is the calibration factor and $H(r)$ is the total effect of medium and measurement system, expressed as

$$H(r)=H(r_1) H(r_2) H(r_3), \tag{2.11}$$

where $H(r_1)$, $H(r_2)$ and $H(r_3)$ are the effects of medium, sensor, and measuring system respectively.

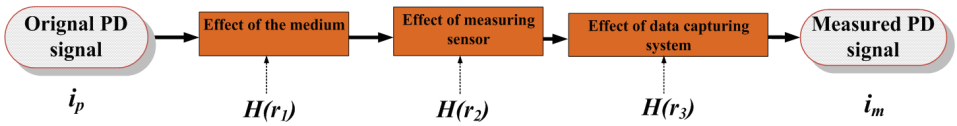

Fig. 2.12. Effect of sensor's measurement system on the captured signal.

Measuring sensors have major impact on the waveform of the captured signals. A sensor is designed for a certain bandwidth and sensitivity, which further depend upon the type of applications, i.e., the components where it has to be applied. During measurement (Fig. 2.8), it was observed that the response of sensor to PD pulses is a specific signature of the waveform. Figure 2.13 and Fig. 2.14 represent two measurements with different signal to noise ratio. All the PD pulses in Fig. 2.13 (greater signal to noise ratio) represent a clear signature as shown in the zoomed view. In case of PDs buried in noise (lower signal to noise ratio), the PD pulses still can be identified with their signature and polarity, whereas noise is seen as a high frequency random variation (see Fig. 2.14). Therefore, any pulse during either positive or negative half-cycle must follow a defined signature to declare it a PD pulse. In case of noisy measurements, useful signals can be extracted with the help of efficient digital de-noising techniques [53]-[54]. The effect of sensor's parameters on the measured signal is described in details in [Publication II-III].

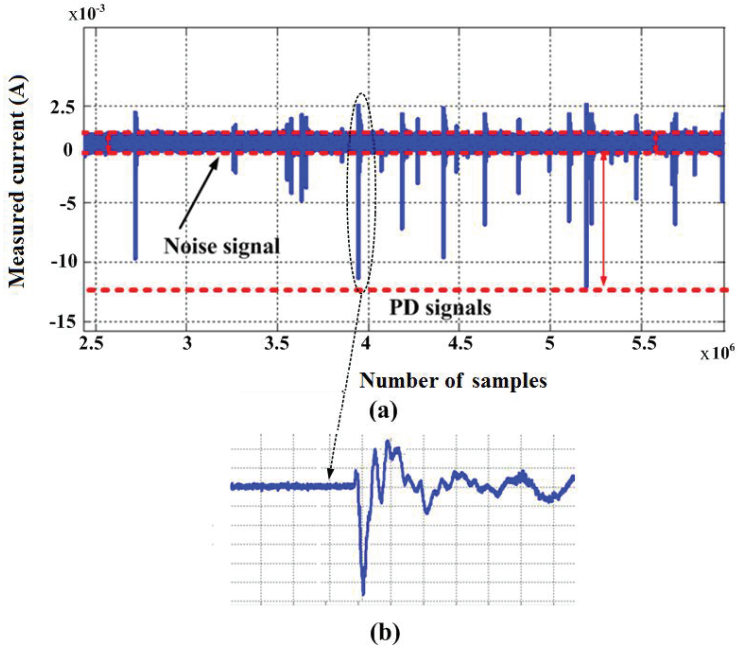

Fig. 2.13. (a) Strong PD signals having low noise and (b) sensor specific signature (waveform) of each measured PD pulse.

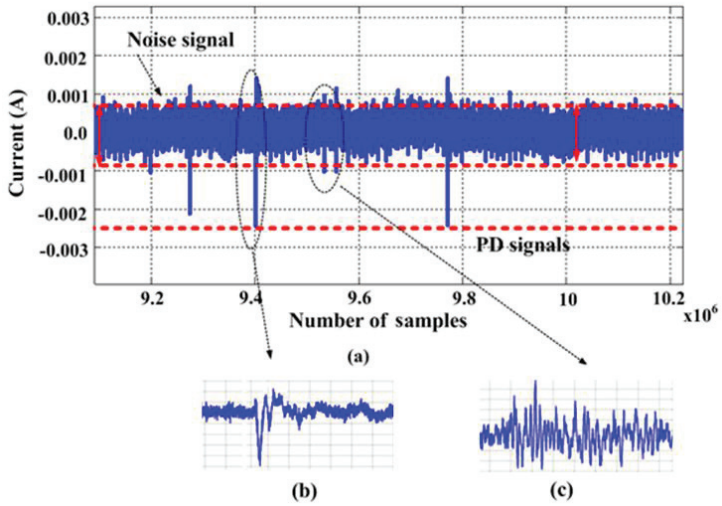

Fig. 2.14. (a) PD signal buried in noise, (b) visible signature of PD signal, and (c) high frequency noise signal presenting no signature.

2.5. Location of PD Defect

Once the pulse is detected as PD signal, it can be used to locate the PD defect on the distribution line. Time difference of arrival (TDA) is a well known technique for location of PD faults on a cable or CC line [25]. A PD pulse generated at the fault point *P* travels towards both sides of the line and can be captured by the sensors at a distance of X_1 and X_2 from the fault point as shown in Fig. 2.15. The time of arrival of PD pulses at the two ends can be expressed by the relation as

$$t_2 = t_1 + t_d\,, \tag{2.12}$$

where t_1 and t_2 are the arrival time of the signals at the respective ends, while t_d is the time difference between the two pulses. Length l_{12} of the given section of the line can be written as

$$X_1 + X_2 = l_{12} \tag{2.13}$$

$$v_p t_1 + v_p t_2 = l_{12} \tag{2.14}$$

where v_p is the wave propagation velocity of the cable. Continuing (2.14), t_2 can be calculated as

$$t_2 = \frac{(l_{12} + v_p t_d)}{2v_p} \tag{2.15}$$

Therefore, the distance of the PD fault is

$$X_2 = v_p t_2 . \tag{2.16}$$

It is important to have accurate value of wave propagation velocity v_p of the cable. [Publication VIII] highlights certain limitations of the methods to determine v_p. A new method is also introduced to find out the v_p of MV cables in [Publication VIII].

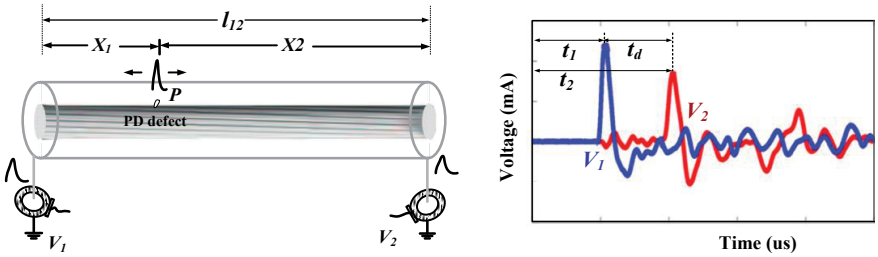

Fig. 2.15. Fault location on a cable section, (a) laboratory setup for measurement of TDA and (b) PD signals measured by sensors at the ends of the cable.

The TDA location technique is employed on a single section of the line of a certain length. For the lines with longer lengths (multi-sections) or branched (multi-ends) topology, TDA technique alone is not sufficient. Chapter 4 [Publication VI-VII] deals with the location function of the diagnostic task in a wider perspective.

2.6. Quantization of PD Defect

2.6.1. Propagation Characteristics of PD Signals

The PD signal induced at the fault point (on cable or CC line) travels away from the discharge site. Therefore, electrical energy travels along the line in the form of electromagnetic wave. The propagation characteristics of the PD waves is determined by taking into account the forward current path, return current path and the insulation between these paths. The insulation or dielectric between the conductors is polarized by the surrounding electromagnetic field. The frequency spectrum of electromagnetic waves consists of a wide range of frequencies up to tens of MHz [55]. The dielectric losses (attenuation) of the line reduce the amplitude of the PD signal as it travels along the line. The components of the PD signals with different frequency propagate through dielectric medium with different phase velocities. This is known as dispersion effect of medium which increases the pulse width and reduces the sharpness of the edges. Both attenuation and dispersion are functions of frequency components of the PD signal, the length of the propagation medium (line), and properties of dielectric material [50]-[51]. In vacuum, the electromagnetic waves travel at the speed of light. However, there is a significant

reduction in the speed of these signals in insulating conductors, depending on the dielectric properties of the medium [56]. All the above mentioned effects have critical importance for accurate diagnostic tasks such as location and quantization of PDs.

In this research, cables and CC lines are used for experimental testing, therefore, PD propagation is discussed in the similar context. In these lines, the arrangement of live conductor, return conductor and dielectric insulation between them, depends upon their specific construction. Figure 2.16(a) represents the cross sectional view of an MV XLPE cable and CC line. Their parameters can be determined depending on the type of line [57]. The insulation between the conductors consists of the main XLPE insulation, conductor screen, and insulation screen. The parameters of the cable take into account its coaxial construction and concentric cylindrical conductors (cable conductor and shielding) [58]. Overhead CC line has different type of construction as shown in Fig. 2.16(a). Ground is used as the return path conductor. The insulation of the conductor and air, determine the total insulation between the conductors. The insulation of the air depends upon the height of the installed CC line. The parameters of transmission line model for CC line can be calculated by considering it a twin-lead line [59].

Propagation time in cable can be expressed as

$$T_{pc} = \frac{l}{v_p}, \tag{2.17}$$

where l is the length of under test cable and v_p is the propagation velocity of the signal through the cable. The observed PD signal has considerably shorter pulse duration (T_{PD}) as compared to its propagation time (T_{pc}). Due to high frequency of the PD signals, the propagation time of PD signals is less than the pulse width of the signals. Therefore, a power line is described as a transmission line. The transmission line theory has been well established for high frequency as well as PD in [58].

When dealing with the propagation of high frequency signals such as PDs, the power lines are represented as transmission line in terms distributed series impedance Z and distributed shunt admittance Y. The impedance Z is expressed as $Z = R + j\omega L$, where R and L are the resistance and inductance per-unit length for both conductor given in Ω/m and H/m respectively. The admittance is expressed as $Y = G + j\omega C$, where G and C is conductance and capacitance between both conductors per-unit length given in S/m and F/m respectively. The distributed parameters of both types of lines are shown with their respective subscripts in Fig. 2.16(b), presenting their electrical models.

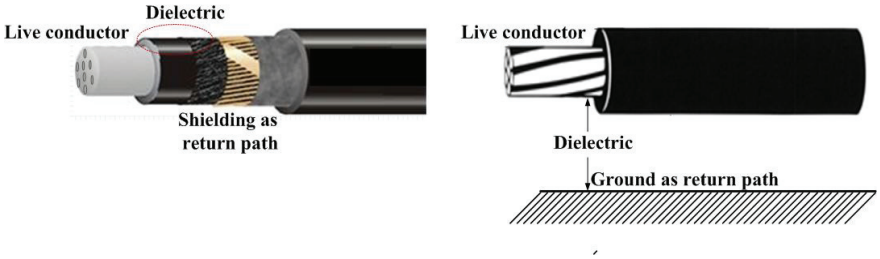

(a)

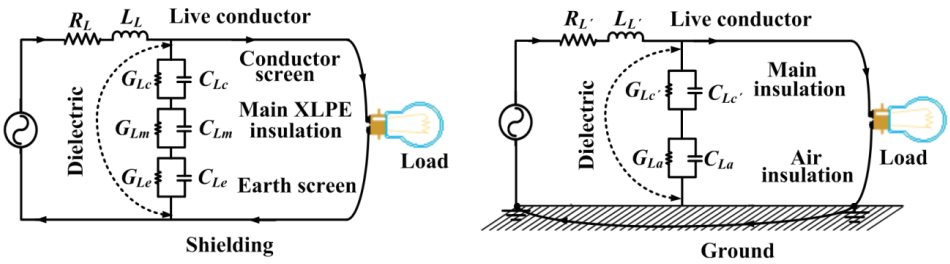

(b)

Fig. 2.16. Model of the power lines, (a) physical model of XLPE cable (left) and CC line (right) and (b) electrical model of XLPE cable (left) and CC line (right).

The relationship of the voltage $V(x)$ between the two conductors of the line, and current $I(x)$ through the conductor at position x is expressed by well known Telegraph equation in the form of differential equation as

$$\frac{\partial V(x)}{\partial x} = -ZI(x),$$
$$\frac{\partial I(x)}{\partial x} = -YV(x). \tag{2.18}$$

The voltage and current derived from above equations is expressed as

$$V(x) = V^{+}(0)\, e^{-\gamma x} + V^{-}(0)\, e^{+\gamma x},$$
$$I(x) = I^{+}(0)\, e^{-\gamma x} - I^{-}(0)\, e^{+\gamma x}, \tag{2.19}$$

where V^{+} and V^{-} are the forward and backward voltage waves respectively, I^{+} and I^{-} are the respective current waves, whereas γ is the propagation constant which is an important parameter to define the effects of line parameters on the propagating signal. Propagation constant is expressed as

$$\gamma = \sqrt{ZY} = \alpha + j\beta, \tag{2.20}$$

where α is the attenuation coefficient in Nepers per meter (NP/m), which describes the losses of the line. There are two main components of α: i) the metal losses due to conductor resistance R and ii) the dielectric losses due conductance G between the conductors. Therefore, α is expressed as

$$\alpha = \sqrt{RG}. \tag{2.21}$$

Attenuation coefficient is highly dependent on frequency components of the travelling signal and dielectric properties of the insulation material. The conductivity and skin-effect mainly contribute for resistive losses. Similarly, dielectric loss greatly depends on loss tangent (tan δ) which quantifies the dissipation of electromagnetic energy of the signal into heat [37].

In the above equation β is the phase constant in radians per meter (rad/m). It describes the change in phase per meter along the propagation path of the signal. As a general definition, β is expressed as

$$\beta = \frac{2\pi}{\lambda} \ rad/m, \tag{2.22}$$

where λ is the wavelength of the propagating signal.

$$\beta = \frac{2\pi\nu}{\lambda\nu} = \frac{\omega}{\upsilon_p}. \tag{2.23}$$

As β describes the change in phase along the line, it mainly depends on the inductance and capacitance of the line and is calculated as

$$\beta = \sqrt{LC}\,. \tag{2.24}$$

A PD pulse signal consists of different frequency components. These components experience different phase change and hence affect the wave-shape of the signal. Attenuation constant and phase constant cause attenuation and dispersion effect on the signal.

Wave propagation velocity υ_p is associated with its electromagnetic field component (in phase with the current) and is an important parameter to determine the location of the PD defects [60]. The velocity of these electromagnetic waves in an unshielded copper conductor is considered to be close to the speed of light (approximately 95-97%), expressed as

$$\upsilon_p = \frac{1}{\sqrt{LC}} = \frac{1}{\sqrt{\varepsilon_o \mu_o}}, \tag{2.25}$$

where ε_o and μ_o is the permittivity and permeability of the vacuum. In case of conductor with insulation, the υ_p depends on its dielectric properties. For example, the υ_p of a typical coaxial cable is about 66% of the velocity of light. The υ_p in a dielectric medium can be calculated as

$$\upsilon_p = \frac{1}{\sqrt{\varepsilon_o \varepsilon_r \mu_o \mu_r}} \tag{2.26}$$

where ε_r and μ_r are the relative permittivity and permeability of the dielectric medium. In case of composite insulation, multiple types of dielectrics are involved. In a XLPE cable construction, the insulation, conductor screen, and insulation screen results in a non-homogeneous dielectric medium. Therefore, effective dielectric constant ε_{reff} is needed for calculation of υ_p which depends on the dielectric constant and thickness of respective type of insulations [56], [61]. [Publication VIII] describes a measurement based method to determine the υ_p for different frequencies.

2.6.2. Proposed Method of Quantization

A comprehensive cable model showing the propagation of an emerged PD signal is given in Fig. 2.17. The dotted line between a-b-c model of PD defect and power line shows a non-galvanic connection from the defective portion of insulation to the line conductor. As a result of PD activity, i_A is the current transient manifested (at point P_A) on the line conductor related to charge q_A induced by the actual charge q_o displaced within the insulation defect. The PD current propagates away from the PD site and can be measured by an induction sensor as i_B (proportional to q_B) at a distance x_2 from the point of origin. The charge q_A can be determined if the attenuation constant of the cable is known

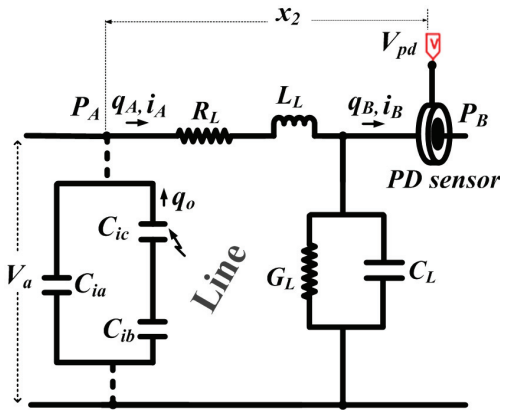

Fig. 2.17. Cable model presenting a cavity inside insulation and PD current propagating toward measuring end.

The approximate value of attenuation constant can be determined by a simple experimental setup as shown in Fig. 2.18. A PD pulse is injected from a pulse calibrator at point P_1. The pulse is measured at point P_1 and P_2. The output of induction sensor is typically measured as voltage signal. The proportional (PD) current is determined as

$$i_1(t) = \frac{V_1(t)}{R_{osc}} \tag{2.27}$$

$$i_2(t) = \frac{V_2(t)}{R_{osc}} \tag{2.28}$$

where R_{osc} is the input resistance of the DSO. A visible change in amplitude (from peak value i_1 to i_2) can be seen due to attenuation as shown in Fig. 2.19. The attenuation constant in this case is expressed as [62], [Publication I].

$$\left|\frac{i_2(t)}{i_1(t)}\right| = e^{-\alpha l_c}. \tag{2.29}$$

The true information of the PD activity can be determined by charge contained in the PD pulse which can be calculated by integrating the current as

$$q\ (t) = \int i\ (t)dt\,. \tag{2.30}$$

Calculation of charge respective $q_1(t)$ and $q_2(t)$ results in

$$\left|\frac{q_2(t)}{q_1(t)}\right| = e^{-\alpha l_c}. \tag{2.31}$$

Therefore, the attenuation constant can be determined as

$$\alpha = \frac{-20\log\left|\frac{q_2(t)}{q_1(t)}\right|}{l_c} \tag{2.32}$$

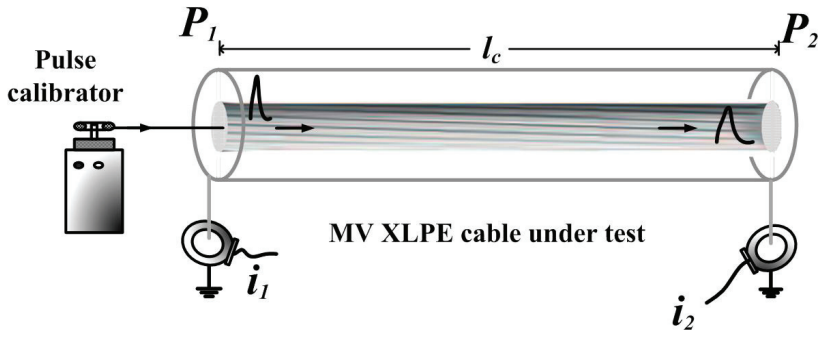

Fig. 2.18. Measurement of PD signals at both ends to determine the attenuation constant.

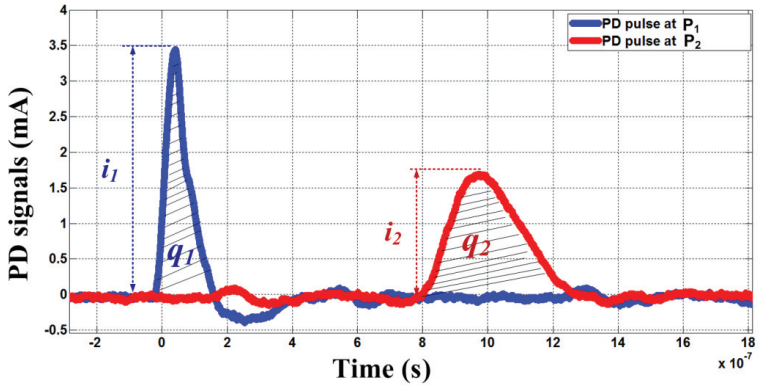

Fig. 2.19. Measured PD voltage at cable end P_1 (blue) and P_2 (red).

Once the attenuation constant for a specific type of cable is found, the induced charge q_A (in Fig. 2.17) at point P_A can be calculated as

$$|q_A(t)| = -|q_B(t)| \frac{1}{\log^{-1}\left[\frac{\alpha\, x_2}{20}\right]}. \tag{2.33}$$

It must be emphasized that the actual charge is not equal to the induced charge. It has been estimated that usually actual charge is few tens of times larger than the induced charge [41]-[43].

3. Design and Modeling of Partial Discharge Measuring Sensor

3.1. Partial Discharge Sensor Technology

The sensor technology is rapidly moving towards electronic, electrical, and digital instrumentation. A measuring sensor transacts a complete measuring function from initial detection to final indication of the measured quantity to study or control the phenomenon under consideration. The initial detection is done by a transducer which is a sensing element and acts as an interface between measured quantity and sensor. Intermediate signal processing of the sensed signal is carried out based on the physical and electrical characteristics of the transducer and the features of the measured signal. Final indication is displayed or recorded with the help of a suitable DAS.

The measurement methodology of PDs is based on the type of the energy exchange which takes place during discharges. There are different phenomena which appear during discharges and give rise to respective detection indicators such as: electromagnetic radiation, sound or noise, thermal radiation, gas pressure, chemical formation, and electromagnetic impulses. Electromagnetic radiation can be in the form of electromagnetic radio frequency waves and optical signals. The energy released is caused due to ionization, excitation and recombination processes during discharge. Radiometric techniques have been implemented using ultra high frequency (UHF) receivers (antennas) having bandwidth in few GHz range [63]-[64]. The ultra violet radiation emitted during PDs can be detected by optical sensors such as photographic recorders, photo-multipliers or image intensifiers, [65]-[66]. During discharges the released energy heats the adjacent insulation material which results in a small and rapid explosion producing sound or noise (acoustic) waves. The amplitude of these waves is proportional to the energy released during discharges. Piezoelectric effect based transducers or other acoustic transducers in combination with amplifiers are the most common methods to perform acoustic measurements in power equipment [67]-[68]. The temperature of the surface of defective site is increased and can be measured by using thermal sensors, however these techniques have not been known to be used for PD measurements [37]. Chemical stresses have a significant contribution in degradation of the dielectric materials and at the same time the discharge process causes chemical changes in the vicinity of the damaged spot [69]. Due to chemical reaction of activated oxygen with the insulation, the internal gas pressure decreases as the discharge occurs. Similarly appearance of by-products such as wax in mass-impregnated cables can be determined to monitor PDs [37]. Dissolved gas analysis (DGA) is one of the most commonly used chemical

methods for PD diagnostics [70]. Similarly, an important class of PD sensors measures the electromagnetic impulses. Due to rapid movement of the charges during discharge event, voltage and current transient appears in the form of electromagnetic waves. These transients can be measured by resistive, capacitive or inductive methods [16], [71]. According to IEC standard 60270, electrical sensors for PD sensing are normally referred as conventional methods whereas non-electrical sensors highlighted above are non-conventional methods [72].

The reliability of PD monitoring or diagnostics depends upon the performance of the sensors applied for measurements. Detailed literature survey of the above mentioned methods of the PD assessment reveals that the suitability of a sensor type leans on the type of application or component under test. The compatibility of the bandwidth of the captured signal and sensors, sensitivity, noise vulnerability, installation of sensors etc are important parameters when selecting a sensor type [73]. Apart from these parameters, structure of the component under test should also be taken into account in order to get effective information from the captured data. The generators, transformers, switchgear, and power lines are the most critical components of an electrical power network. These power components can be divided into two groups:

Group 1: Closed size components, such as power transformers, generators, motors, and switchgear, which have a definite size and are positioned at a specific place.
Group 2: Open size components, such as cables and CC lines, which are distributed along a wider region (few hundred meters up to kilometers).

The scope of PD measuring methods can be determined by their operational attributes. Electrical sensors methods can be employed around the earth straps, cable terminations, and the CC lines. These sensors can sense the high frequency PD current along the power line and then relationship between the captured electromagnetic waves, characteristics of sensors, and propagation characteristics of the line, can be established. When applied to generators, transformers or switchgear, electrical methods can be used to detect the presence of PDs. However, these sensors are not efficient to find the location of the PD defects in these components due to complex and closed size structure. Similarly, non-conventional techniques are not popular for diagnostics in cables or CC lines. Therefore, non-conventional sensors are useful for PDs occurring in the components of Group 1, whereas conventional techniques based on wave propagation characteristics are more useful for cables or CC lines (Group 2) [73], [Publication VI-VII]. This work discusses assessment of PDs in power components of Group 2. Considering the analysis made in [73], reviewed literature and explored features of the induction sensors (presented in this work), the evaluated performance of PD diagnostic methods for critical power components is appraised in Table 3.1. The letters D, L and Q in Table 3.1 are

used for detection, location, and quantization of PD fault in the respective components. The expression D_L_Q (in second column) for electromagnetic wave method qualifies that this method is suitable for detection, location, and quantization purposes in cables/CC lines. Similarly 'D' shows that this method can be used for detection of the PD activity around closed size components (transformers) whereas for location and quantization, they are not feasible. The sign '-' shows that the corresponding method is not suitable for any of the diagnostic task (D, L or Q) for a stated component. The measurement of electromagnetic waves for PD investigation using conventional (electrical) methods have been considered as favorite tool for PD diagnostics in cables and CC lines.

Table 3.1. PD diagnostic methods for power components

PD diagnostic methods	Cables/CC lines	Transformers	GIS	Generators
EM-waves	D_L_Q	D	D	D
Acoustic	D	D_L_Q	D_L_Q	D_L_Q
Chemical	-	D_L_Q	-	-
Optical	-	-	-	-

3.2. High Frequency Current Measuring Sensors

PD current transients generated due to induced charge at the defective site propagate towards both ends of the power line. Several current sensing technologies are available for measurement such as: shunts, current transformers, Rogowski coils, Giant Magneto-resistive sensors, Hall-effect current sensors, and Magneto-impedance sensors. Taking into account economic, physical and operational aspects, costs, sensitivity, bandwidth, dc capability, saturation and hysteresis, linearity, operating temperature, footprint and material technology; the shunts and Rogowski coil are pronounced as preferred sensors [16]. Shunts have additional DC capability, however for PD measurements, this aspect is not an important requirement. Rogowski coils have better bandwidth and the most significant measurement aspect is their non-intrusive installation whereas shunts have to be in a galvanic contact with the line under test.

Rogowski coil based current probes are being used in power electronics and power system applications (metering, protection, monitoring, and control) for measurement of current ranging from few milliamperes to several thousand amperes and with frequency ranging from few hertz to several MHz [74]-[76]. For applications like PD detection and measurement, the design of RC is focused for high frequencies up to few tens of MHz [77]-[78]. Various designs of Rogowski coil have been investigated in this work, however the detailed analysis of the coil having center frequency at 37.6 MHz is presented in [Publications II-III].

3.3. Rogowski Coil as PD Sensor

Thinking of the electromagnetic induction sensing, due to similar construction, Rogowski coil and HFCT are often considered as natural competitors. The conductor carrying current $i_p(t)$ to be measured is considered as the primary winding and the winding with N number of turns is the secondary winding. Following the Faraday's law of electromagnetic induction, the measured output of the sensors coil is the voltage $V(t)$, written as

$$V(t) = -M \frac{di_p(t)}{dt}, \tag{3.1}$$

where M is the mutual inductance between the sensor winding and primary conductor. Having similar construction and working principle, there are still certain differences which determine the specific identity of both (Rogowski coil and HFCT) sensors. Rogowski coil winding is wound over a non-magnetic air core material whereas HFCT usually has a magnetic core. The permeability of magnetic core is more than that of air, consequently the sensitivity of HFCT is higher as compared to that of Rogowski coil. At the same time, due to non-saturable air saturation of magnetic core, Rogowski coil has better linearity in its output as compared to HFCT. Moreover due to characteristics of core materials, Rogowski coil has greater bandwidth than the HFCT. The conventional HFCT have more power consumption due to hysteresis losses while there are no core losses in case of Rogowski coil, which makes it less power consumption sensor. The Rogowski coil is wound by adding (in continuation with the forward winding) a return loop through the center of the core as shown in Fig. 3.1 Return loop provides cancellation of external magnetic field. HFCT do not have the return loop in its construction. These attributes makes the Rogowski coil a preferred sensor for PD applications. Therefore, eq. (3.1) is modified for Rogowski coil (having voltage output $V_{rc}(t)$ and mutual inductance M_c as

$$V_{rc}(t) = -M_c \frac{di_p(t)}{dt}. \tag{3.2}$$

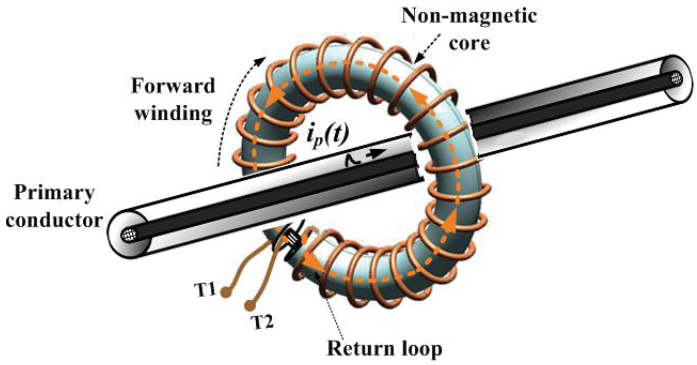

Fig. 3.1. Rogowski coil installed around primary line for measurement of current.

3.4. Modeling of Rogowski Coil for PD Measurements

Several designs of Rogowski coil measuring sensor can be found in the literature. Transforming a transducer into a measuring device, there are several design stages. In all sensors the coil winding element is practically the same (having different dimensions and shapes) as the conventional design described above. However, the remaining design stages, which constitute the signal processing and integrator in order to get the actual primary signal accurately, have different approaches. Few design approaches can be studied in [79]-[82]. In this work, the Rogowski coil measuring system has been organized in three major components: sensing, damping, and integration, as shown in Fig. 3.2. Primary current is detected or sensed by the current sensor which is the wound coil termed as Rogowski coil head. The output of the Rogowski coil head is proportional to the derivative of primary current along with additional signals (in the form of oscillations) introduced by the electrical properties of Rogowski coil head. Damping component minimizes the presence of unintended oscillations. A suitable terminating resistance is selected as damping resistor. The last component is the integrator which is essential to recreate the wave shape of primary current.

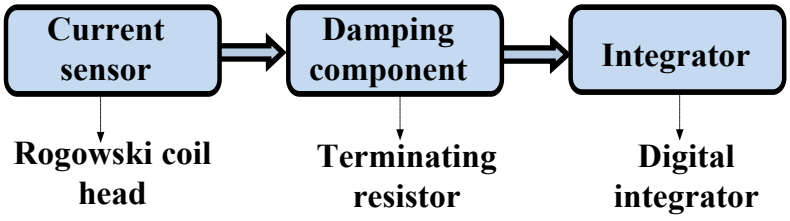

Fig. 3.2. Essential components of Rogowski coil measuring system.

Defining these three components, the Rogowski coil sensor is termed above as 'Rogowski coil measuring system', in order to emphasize that Rogowski coil sensor is not only a wound coil but have other necessary components making it a complete measuring system. The Rogowski coil head can be used for detection of the primary signal while measurement (actual waveform of the signal) requires the design of the Rogowski coil head with the damping and integrating components.

The three components of Rogowski coil measuring system are implemented in four stages (1, 2, 3, and 4) as shown in Fig. 3.3. The design of the hardware of Rogowski coil head as sensing element is the first stage. The second stage begins with the identification of the electrical model of the Rogowski coil. The electrical model and its behavior are analyzed for selection of the suitable terminating (damping) resistance for proper damping of the signal. Third and fourth stage is the implementation of the integrator with the help of DAS. The main purpose of the DAS is to capture the measured data at suitable sampling rate so as to avoid any loss of information of such high frequency current signal. Digital integration technique is used to integrate the sampled signal. Calibration is done by a factor *K*, considering the mutual inductance, and removal of the difference (error) between the expected and measured output. A DSO is normally used as the display with built-in DAS and digital integration tools. The stored data can be transferred to PC for detailed analysis of the measured signal.

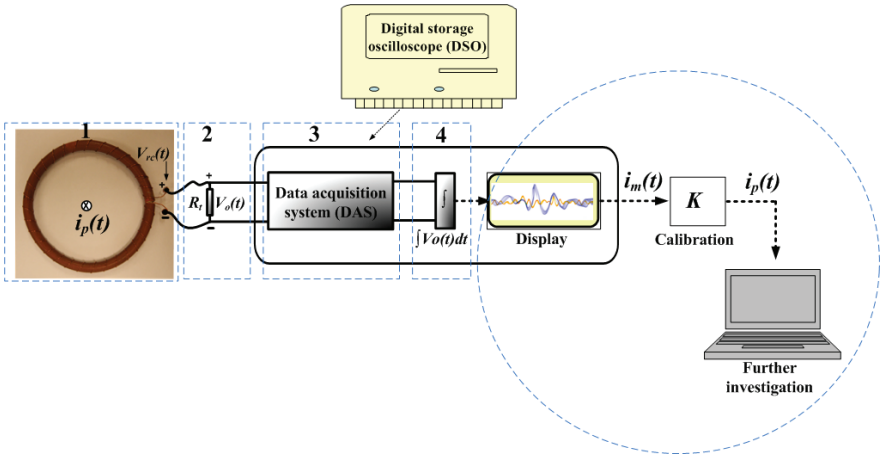

Fig. 3.3. Laboratory implementation of Rogowski coil measuring system.

3.4.1. Geometrical Model of Rogowski Coil Head

The main geometrical parameters of the Rogowski coil are core diameter, internal and external diameters of the coil (which determines the mean diameter of the coil), diameter of the wire used for winding, and the number of turns of the winding. The physical model of the coil prototype designed in this work is shown in Fig. 3.4 whereas the geometrical parameters are stated in Table 3.2.

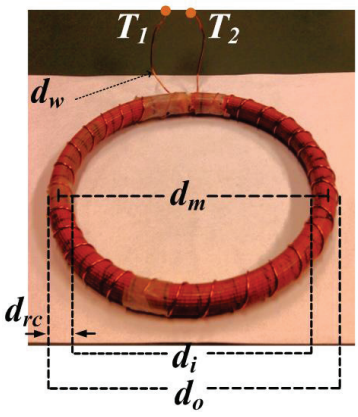

Fig. 3.4. Geometrical model of designed Rogowski coil.

Table 3.2. Geometrical parameters of the designed model of coil.

Model parameter	Symbol	Specification
Number of turns	N	30
Outer diameter of coil	d_o	16.1 cm
Inner diameter of coil	d_i	14.1 cm
Core diameter	d_{rc}	1.9 cm
Mean diameter of coil	d_m	15.1 cm
Diameter of the wire	d_w	0.085 cm

3.4.2. Electrical Model of Rogowski Coil and Damping Component

Every piece of wire has resistance and inductance while every two wires present some capacitance between them. Electrical behavior of this electromagnetic device can be well explained by developing its electrical model. Lumped parameter model is shown in Fig. 3.5 where R_c, L_c, and C_c are structure-based inherent resistance, inductance and capacitance of

Rogowski coil. These parameters direct the electrical behavior of the coil while responding to signals to be measured. The mathematical expressions to calculate these parameters are presented in [16], [18], [83], based on geometrical parameters of the Rogowski coil. However, it turns out that the formulas presented are not very precise when accurate results are needed.

There are various factors which cannot be taken into account while applying mathematical expressions for calculating the electrical parameters of Rogowski coil. Non-uniform turn density, imperfect central position of the return loop, non-uniformity of core or deformation of the circular cross section into oval when bending the flexible coil into closed path, all can cause some geometrical deviations between a manufactured (ideal) and used Rogowski coil. During operation at high frequencies, the phenomena such as skin and proximity effect cause non-uniform distribution of current within the conductor which causes parasitic inductance and capacitance. It is justified to consider these parameters as functions of coil geometry and frequency [17]. Furthermore, the response of a Rogowski coil measuring system also includes the effects of measuring components and devices, as shown in Fig. 3.5. Using simple mathematical formulas (meant for ideal shape of Rogowski coil) can cause miscalculations for determining the inductance and capacitance of Rogowski coil especially for high frequency phenomena. In [Publication II], a measurement based method is presented to determine the coil parameters in an operating environment. These measured parameters are given in Table 3.3.

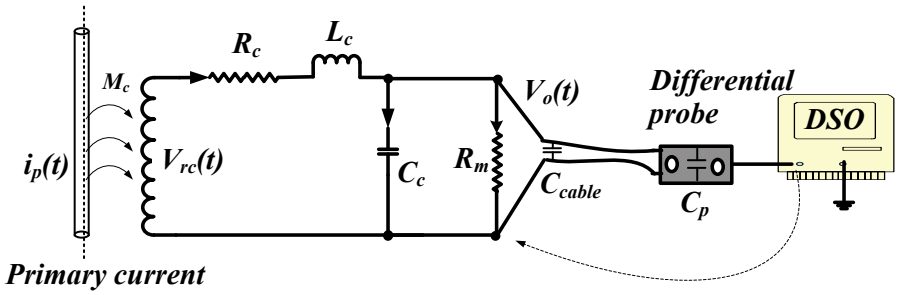

Fig. 3.5. Measurement system using Rogowski coil head.

The output of Rogowski coil is observed by a measuring system having resistance R_m (R_m =1 MΩ, DSO in this case), capacitances C_{cab} and C_p of coil cable, and differential probe, respectively. The voltage $V_{rc}(t)$ is induced in the Rogowski coil while $V_o(t)$ is the voltage collected at the terminals of the Rogowski coil measuring system, expressed as

$$V_o(s) = \frac{\frac{1}{L_c C_{cs}}}{s^2 + \frac{1}{L_c C_{cs}}(\frac{L_c}{R_m} + R_c C_{cs})s + \frac{1}{L_c C_{cs}}(\frac{R_c}{R_m} + 1)} V_{rc}(s), \tag{3.3}$$

where $V_{rc}(s) \xrightarrow{L^{-1}} V_{rc}(t) = -M_c \frac{di_p(t)}{dt}$ and C_{cs} is the overall capacitance of the measuring system as calculated in Table 3.3.

Table 3.3. Electrical parameters of the designed model of the Rogowski coil.

Parameter	Symbol	Value of the parameter
Self-resistance of coil	R_c	0.71 Ω
Self-inductance of coil	L_c	1.19 μH
Self-capacitance of coil	C_c	5.16 pF
Probe capacitance	C_p	2.42 pF
Capacitance of coil cable	C_{cab}	7.1 pF
Capacitance of coil system	$C_{cs}=C_c+C_p+C_{cab}$	16.46 pF
Mutual inductance	M_c	125.4 nH
Self resonant frequency of coil	f_c	64.6 MHz
Operating resonant frequency of coil system	f_{oc}	37.6 MHz

The sensitivity and resonant frequency are the key performance factors of a Rogowski coil. The sensitivity can be determined by eq. (3.3) and the resonant frequency f_{oc} of the coil system can be expressed as

$$f_c = \frac{1}{2\pi\sqrt{L_c C_{cs}}}. \tag{3.4}$$

The response of Rogowski coil measuring system was analyzed by experimentally described in [Publication II-III]. The setup was based on the measurement of a PD pulse injected from a PD calibrator into a primary conductor as shown in Fig. 3.6. The captured response of Rogowski coil was presented in time and frequency domain (see Fig. 3.7). The PD current pulse shown in red color in Fig. 3.7(a) is measured by a commercial HFCT. The HFCT is used as a reference measuring sensor. The oscillating signal (blue color) in Fig. 3.7(a) is the output of the Rogowski coil in time domain. The signal shown in Fig. 3.7(b) is obtained by fast

Fourier transform (FFT) (showing operating resonant frequency of coil system 37.6 MHz) of the captured signal. The oscillating response is due to 2nd order RLC parameters of the Rogowski coil. Based on circuit analysis theory [84]-[85], the oscillatory response of the Rogowski coil can be expressed in terms of forced and natural response as presented in [Publication III]

$$V_o(t) = V_{rc}(t) + V_{rc}(t) \cdot e^{-\xi\omega_c t} \cdot \sin(\omega_c \sqrt{1-\xi^2}\, t), \tag{3.5}$$

where ξ and ω_c are the damping coefficient and resonant frequency (in rad/s) of Rogowski coil, respectively. Damping coefficient ξ depends on all the four parameters of the Rogowski coil (L_c,C_c, R_c, and R_m). As derived in [Publication III], ξ can be expressed as

$$\xi = \frac{1}{2\omega_c\, L_c\, C_{cs}} \left(\frac{L_c}{R_m} + R_c C_{cs} \right). \tag{3.6}$$

Here L_c, C_{cs}, and R_c are fixed for a certain geometrical design of coil, however measuring resistance R_m can be varied by an additional terminating resistance R_T across the terminals of the Rogowski coil. This modifies the expression for ζ presented in eq. (3.6) as

$$\xi = \frac{1}{2\,\omega_c\, L_c\, C_{cs}} \left(\frac{L_c}{(R_T \| R_m)} + R_c C_{cs} \right). \tag{3.7}$$

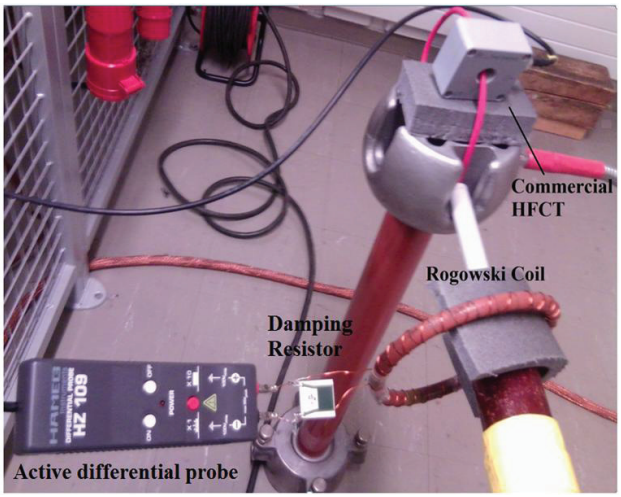

Fig. 3.6. Laboratory setup for measurement of PD signal with commercial HFCT and designed Rogowski coil.

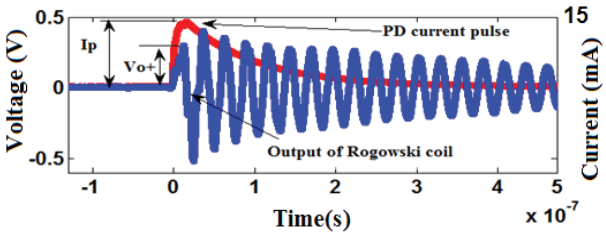

(a)

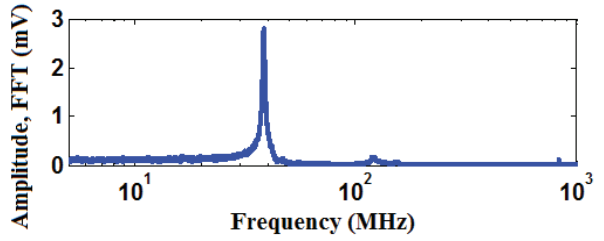

(b)

Fig. 3.7. Measured response of Rogowski coil, (a) time domain plot and (b) frequency domain plot.

The output of Rogowski coil is critically damped if $\zeta = 1$ In order to get such response of the coil, the required value of R_T is derived as

$$R_T = \frac{L_c}{2\xi\omega_c L_c C_{cs} - R_c C_{cs}}. \tag{3.8}$$

It should be noted that R_T is expected to be considerably smaller than R_m, therefore,

$$R_T \| R_m \approx R_T.$$

Based on the parameters described in Table 3.3, it turns out that for equivalent circuit of the coil shown in Fig. 3.5 (including a parallel resistance R_T with R_m), the suitable value of terminating resistance in terms of characteristics impedance of the coil Z_c is

$$R_T = \frac{Z_c}{2} = 175\ \Omega \tag{3.9}$$

where $Z_c = \frac{1}{\omega_c C_{cs}}$. (3.10)

Effect of Terminating Resistance

The effect of R_T has been analyzed in detail in [Publications III]. During practical investigation, different values of R_T were connected to observe the behavior of $V_o(t)$. A route locus map is presented in [Publication II], to quantify the effect of variation in R_T on the

location of complex poles. The oscillations in the $V_o(t)$ are due to charging and discharging of the coil inductance and capacitance, in the presence of high resistance (R_m=1 MΩ) at the terminals. The behavior of the different currents through RLC components (shown in Fig. 3.8) of the coil was analyzed. The current i_{coil} is the current through series parameters R_c or L_C, the total current induced in Rogowski coil winding. Furthermore, i_c, i_{RT}, and i_{Rm} are explained in Fig. 3.8. It is known that

$R_T << R_m$,

therefore,

$i_{RT} >> i_{Rm}$,

which results in

$$i_{coil} \cong i_c + i_{RT} . \quad (3.11)$$

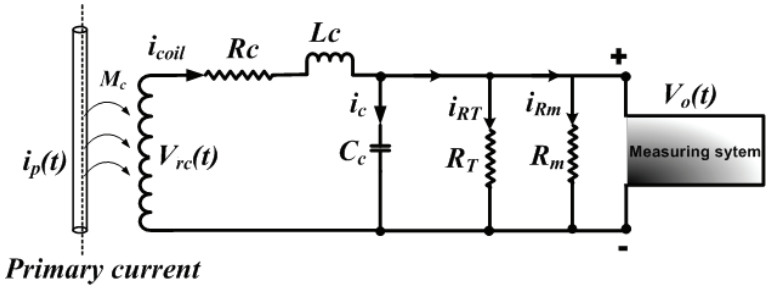

Fig. 3.8. Rogowski coil model representing current distribution in various components of coil.

Analyzing the Effect of Terminating Resistance Using Simulated Model of Rogowski Coil

It is not possible to measure the current through non-physical RLC components. Therefore, simulated model is used for this purpose. The Rogowski coil is simulated in ATP-EMTP environment as shown in Fig. 3.9. In the simulation model, experimentally measured PD pulse is used as primary current. The block B1 is the PD source injecting the PD pulse into the line. Block B2 represents the current sensing by Faraday's law of electromagnetic induction. Block B3 represents the model of Rogowski coil head, using measured parameters given in Table 3.3. The details can be found in [Publications III]. For certain values of R_T, the measured currents are shown in Fig. 3.10. Each plot in Fig. 3.10 shows the above mentioned three currents (i_{coil}, i_c, and i_{RT}). It can be observed that when R_T is decreased, $i_{RT}(t)$ increases and $i_c(t)$ starts to decrease. This reduces the capacitance current which results in minimized amplitude of the oscillations due charging and discharging of C_c and L_c. The coil can be seen as behaving more like an RL or inductive circuit. This results in decreased oscillations in the output current and hence in the output voltage.

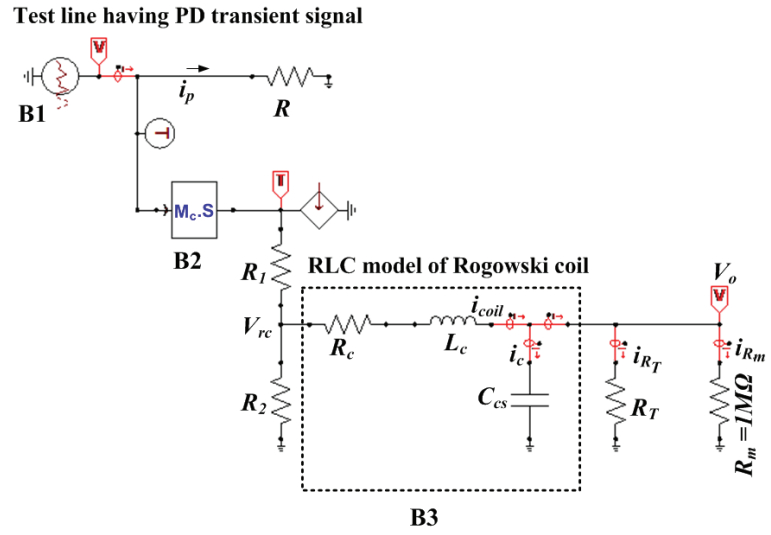

Fig. 3.9. Simulated model of Rogowski coil using ATP-EMTP.

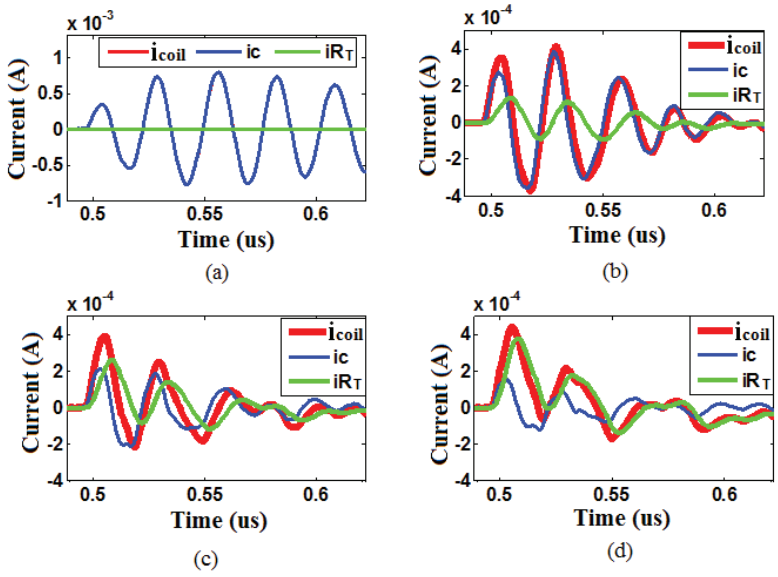

Fig. 3.10. Each plot represents the current i_{coil}, i_c, and i_{RT} through the components of L_c, C_c, and R_T of Rogowski coil respectively for different value of R_T as; (a) R_T= 1MΩ > Z_c (in this plot i_{coil} and and i_c are equal currents), (b) R_T=Z_c , (c) R_T=Z_c/2 and (d) $R_T \leq Z_c/2$.

3.4.3. Integrator

The conventional means of performing integration of the output of Rogowski coil are by an electrical or electronic integrator, and self-integration [19], [83]. In this work numerical

integration is used after the coil output voltage is digitized. Numerical integration can be expressed as

$$i_o(t) = -K_c \int V_o(t)dt, \tag{3.12}$$

where $K_c = 1/M_c$ is called mutual inductance factor. An error constant K_e is used to fine-tune the output of the coil sensor by removing the error between obtained output i_o and expected output i_p. The error factor is determined as

$$K_e = \frac{i_o}{i_p}, \tag{3.13}$$

therefore, the final output becomes

$$i_p(t) = -(K_c\ K_e)\int V_o(t)dt, \tag{3.14}$$

where $K = K_c\ K_e$ is the calibration factor of the Rogowski coil measuring system.

There is a broad family of numerical algorithms to compute the definite integral. A method known as trapezoidal rule which in general is considered as having faster convergence in particular cases of rougher signals is chosen in this work. This is calculated as [86]

$$i_p(N) = K\left[i_p(N-1) + \frac{1}{2f_s}[V_o(N-1) + V_o(N)] \quad N > 0 \right], \tag{3.15}$$

where f_s is sampling frequency and N is the order number of sample. In laboratory setup, the DSO is used for digital integration. In the simulated model for implementation of the digital integrator, the model shown in Fig. 3.9 is modified by adding a built-in block B4 as integrator in Fig. 3.11. The step wise output of each individual component of the Rogowski coil measuring system is shown in Fig. 3.12. The signal shown in Fig. 3.12(a) is the output captured at the terminal of Rogowski coil head. The signal shown in Fig. 3.12(b) is captured across the damping component and Fig. 3.12(c) represents the integrated signal as final outcome. The designed model of the Rogowski coil measuring sensor is compared with the output of simulated model and that of HFCT in Fig. 3.13. The comparable performance of the designed coil validates it for high frequency PD measurements. The Rogowski coil has also been used for the measurement of real PD signals (see [Publication II]) in the laboratory. The simulation model analyzing all the development stages of the Rogowski coil from a transducer to a measuring device has been presented in [87].

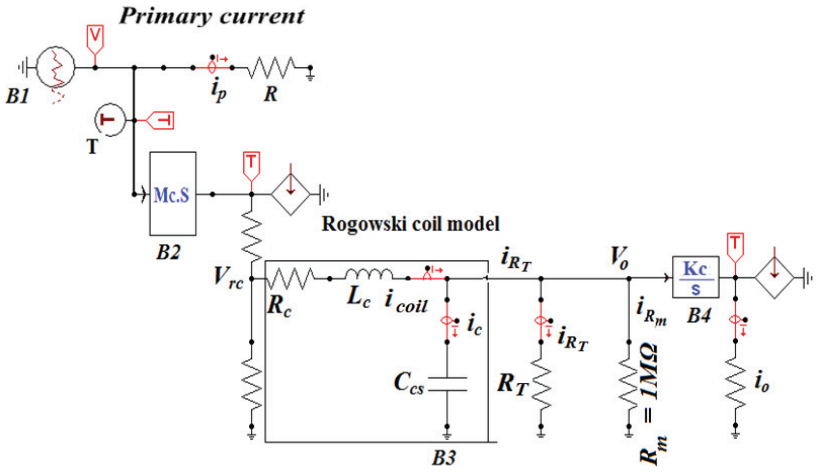

Fig. 3.11. Simulated model of Rogowski coil with damping and integrating components.

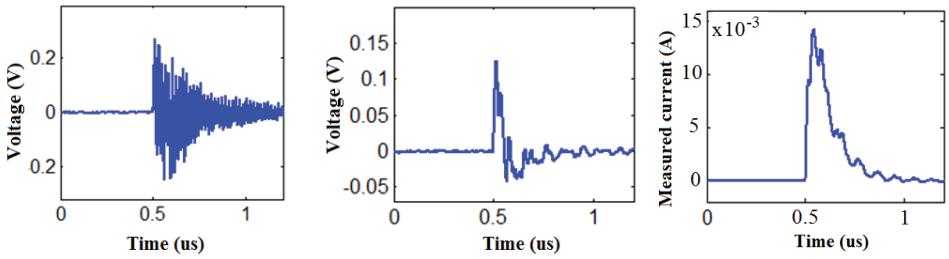

(a) (b) (c)

Fig. 3.12. The stage wise shape of the signal captured at, (a) the output of Rogowski coil head, (b) the output of the damping (terminating) resistor, and (c) the output of integrator.

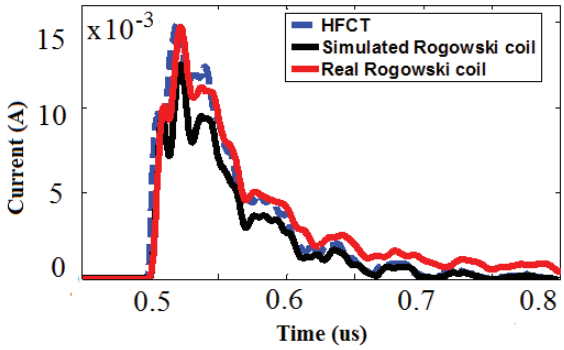

Fig. 3.13. Validation of the performance of designed model of the coil with simulated model of the coil and commercial HFCT.

3. 5. Influence of Resonance on the Performance of Rogowski Coil for Partial Discharge Measurements

Measurement of pulse phenomena is a complex task. A pulse contains signal components in a wide range of frequency. The reliability of the measurement depends on how accurately the different frequency components of a signal are measured. Resonance in induction sensors is an important phenomenon to determine the frequency characteristics and bandwidth of the sensor. The coil sensor can operate in different modes of resonance. It is important to identify the suitable mode of operation to achieve better sensitivity and bandwidth. Sensitivity can be defined as the output voltage induced at the terminals of Rogowski coil due to change in primary current at a specific frequency. Bandwidth is the frequency range over which the sensor provides relatively high sensitivity. The [Publication II-III] (summarized previously in this chapter) includes analysis of various aspects of coil's captured signals in time domain. This section presents the analysis of operating modes in frequency domain regarding coil's sensitivity and bandwidth.

Practical measurements have confirmed that the PD pulse shown in Fig. 3.13 is identical to the pattern of actual PD waveform. The reference PD waveform is measured by an 80 MHz (bandwidth) commercial HFCT while the Rogowski coil is designed for a resonant frequency of 37.6 MHz which reliably measures the reference PD pulse [Publication II]. In [Publication IV], a Rogowski coil with a resonant frequency of 37.6 MHz is analyzed to study its frequency response under different scenarios of damping and integration and is discussed as follow.

Common to RLC circuit of the coil, its transfer function is a second order function which can have significant oscillations in its response to high frequency transient pulse, provided that the sensor loading is light (for example 1 MΩ resistance of DSO). This operation of coil is termed as under-damped mode. The magnitude transfer plot of the coil is shown in Fig. 3.14. The effect of differentiation is clearly visible in this plot. As the frequency increases, the transfer rate also becomes higher. The rate of change of 20 dB/dec reflects that the amplitude transfer will increase 10 times when frequency is increased by 10 times. The resonance clearly occurs at frequency 30 MHz, where the magnitude transfer will see a sharper and significant increase. For frequencies above the resonant point, the magnitude transfer will decrease with rate of –20 dB/dec, presenting a filter for the higher frequency components. Figure 3.15 shows the Phase transfer plot describing the phase shift of 90 degrees for the lower frequency range (below resonant frequency), as a result of the differentiation. This will be turned by 180 degrees at the resonant frequency, effect caused by 2 poles in the same location, with every pole providing total of 90 degrees phase shift [Publication IV].

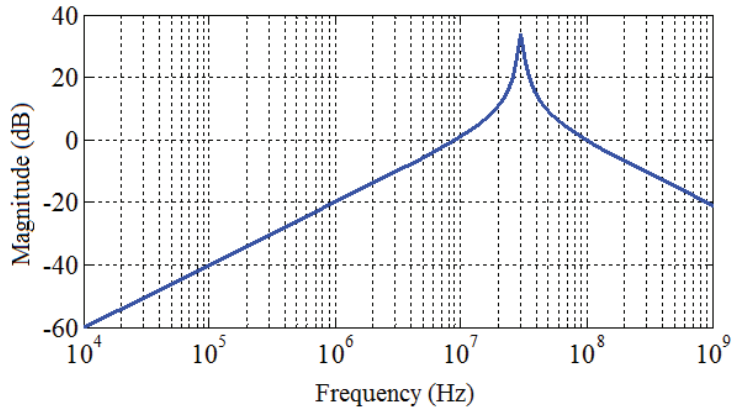

Fig. 3.14. Magnitude transfer plot for Rogowski coil loaded with high-impedance (1 MΩ), with resonant frequency of 30 MHz.

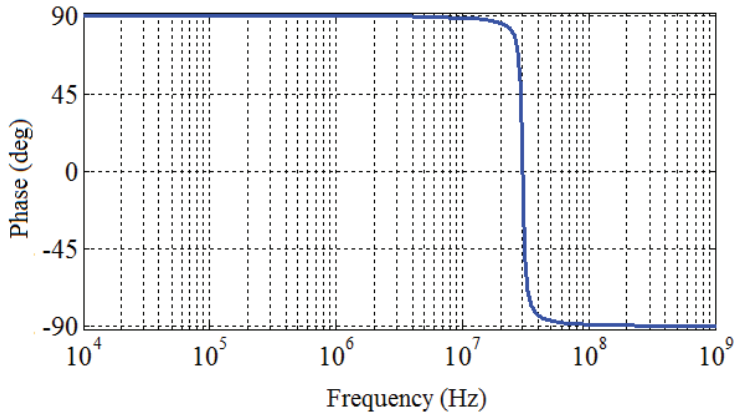

Fig. 3.15. Phase transfer plot for Rogowski coil head loaded with high-impedance (1 MΩ), with resonant frequency of 30 MHz.

Considering the loading of the coil by different terminating resistances R_T, which offer a certain extent of damping, the resonant operation of Rogowski coil can be divided into three modes: under-damped, critically-damped, and over-damped. The presented (Fig. 3.14 and Fig. 3.15) response of the coil describes the under-damped mode without loading ($R_T \cong \infty$). The comparison of the magnitude transfer function of the three resonant damped modes is made in Fig. 3.16. The plot has been normalized so that the damped mode provides highest transfer rate of 1(0 dB). The sharp increase of oscillations at 37.6 MHz is critically-damped. The over damped response provides lower transfer rate than the other modes.

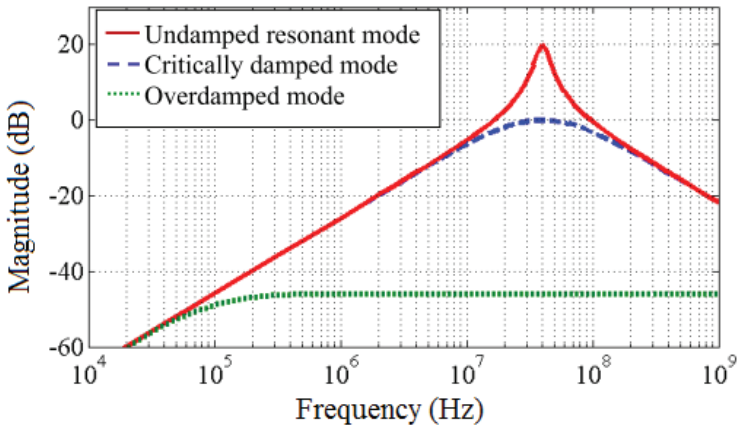

Fig. 3.16. Comparison of resonant modes of coil's operation with damping resistor**.**

The absolute sensitivity of the sensor can be described better by integration of the resonant modes. In damped-resonant modes, the output voltage of the sensor increases linearly with the frequency of the components, whereas the damped and integrated output (see Fig. 3.17) is rather independent of the frequency of the particular frequency components. The time domain plots of the damped and integrated outputs are shown in Fig. 3.18. It can be seen that critically-damped integrated output matches best with the waveform of the original signal. It is concluded that resonant mode is not suitable for accurate measurement, since it emphasizes the frequency components near resonant point and the oscillations are even present in the integrated signal. The over-damped mode provides a better high frequency response especially during rising edge of the transient pulse. However, due to limited low-frequency response, the trailing edge of the waveform is not measured accordingly. It is more feasible to use the coil in critically-damped mode. It has been identified that the resonant frequency determines the bandwidth of the coil sensor. The response of the coil in critically damped integrated mode is constant up to resonant point, whereas after the resonant point the transfer rate drops at -40 dB/dec which means drop in output as 100 times per frequency increase 10 times. Different approaches to analyze the frequency response of coil sensors have also been studied in [88].

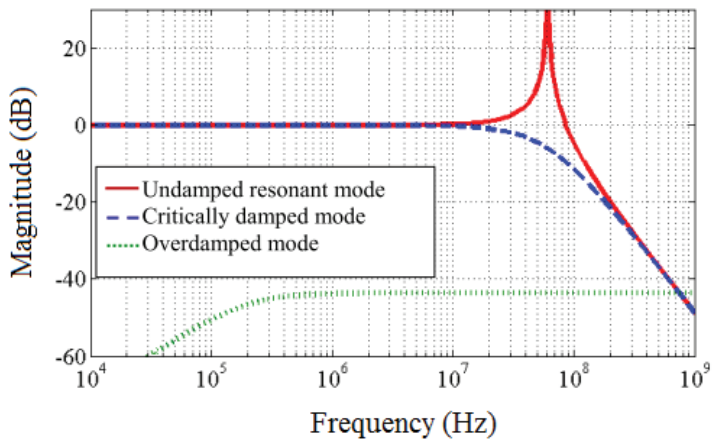

Fig. 3.17. Comparison of resonant modes of coil's operation with damping resistor and integrator**.**

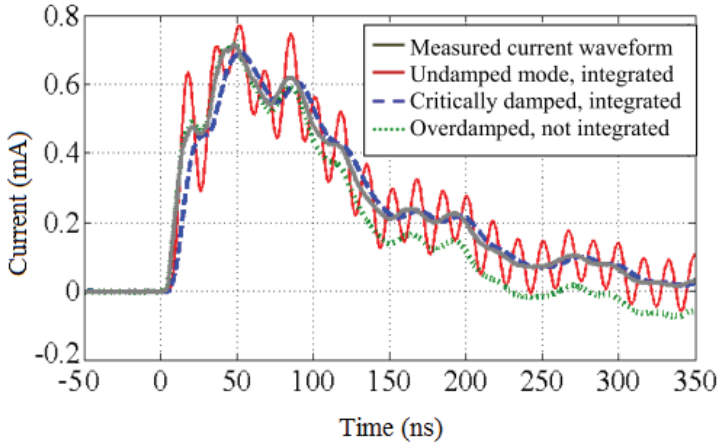

Fig. 3.18. Comparison of measurement performance of Rogowski coil in different modes of operation.

3.6. Significance of Geometrical Parameters of Rogowski Coil to Predict its Electrical Response

For real applications, there are different designs of Rogowski coil sensors with respect to geometrical dimensions and electrical performance [89]. The variation in size (dimensions) directly affects the key performance parameters of the coil i.e., sensitivity and bandwidth. Resonant frequency (center frequency) is taken as the main component of bandwidth as explained previously. In this work, various geometrical designs are investigated for measurement of PD signal and their performance is compared in terms of sensitivity and resonant frequency [Publication V]. As the sensing part of this device is the coil winding therefore, Rogowski coil head (without damping and integration) is used for this analysis.

The variation in parameters (see Table 3.4) such as core diameter d_{rc}, coil diameter d_m,

diameter of the copper wire d_w used for winding, number of turns N, and type of the return loop (return conductor and return winding), has been experimentally investigated. The symbols are labeled in (Fig. 3.4) to represents respective geometrical parameters. The coil *A* is taken as the reference coil whereas the test coils (*B*, *C*, *D*, *E*, and *F*) are having the parameters different from coil *A*. Each test coil has been analyzed to determine the effect of variation in a specific parameter as described in Table 3.4. Based on experimental analysis, the percentage variation in a geometrical dimension and its effect on sensitivity and resonant frequency is quantified in Table 3.5.

Table 3.4. Different design of Rogowski coil with respect to geometrical parameters

Coil type	d_o (mm)	d_i (mm)	d_{rc} (mm)	d_m (mm)	d_w (mm)	N	Parameter variation
A	155.0	131.0	12.0	143.0	0.85	30	Reference coil
B	160.0	126.0	17.0	143.0	0.85	30	Core diameter
C	107.6	83.6	12.0	95.6	0.85	30	Coil diameter
D	155.0	131.0	12.0	143.0	0.85	60	Number of turns
E	155.0	131.0	12.0	143.0	0.65	30	Wire diameter
F	155.0	131.0	12.0	143.0	0.85	60	Return winding

Table 3.5. Analysis of the effects of changes in geometry of the Rogowski coil

Name of parameter	Change in parameter	Sensitivity	Resonant frequency
Core diameter *(d_{rc})*	41% ↑	100% ↑	16% ↓
Coil diameter *(d_m)*	97 % ↓	100% ↑	13% ↑
Wire diameter *(d_w)*	20 % ↓	≈ 0 %	≈ 0 %
Number of turns *(N)*	100% ↑	100 % ↑	33% ↓
Type of winding R.L	R.W	≈ 0 %	26 % ↓

* R.L - return loop, R.W- return winding

The presented analysis provides a quantified assessment of the behavior of the Rogowski coil for any change in its parameters. For certain application, if required is the change of a specific dimension of the coil, the expected change in sensitivity and frequency response can be compensated by introducing a proportional change in some other parameters. Similarly, the alteration in design can be made for required performance of the coil.

3.7. Discussion

Reliable condition monitoring of power system components depends upon accurate measurement of the fault indicating signals. Therefore, performance of the measuring equipment plays a key role to execute predictive maintenance plan in order to avoid incoming PD menace. Suitable design of sensor reduces the risk or ambiguity which may arise during personal assessment of the measured signal. The different type of power components like: CC lines, cables, transformers, generators, motors, and switchgear, emit PD signals in different range of amplitude and frequencies. Therefore, the same design of a Rogowski coil with respect to most important performance indices i.e., sensitivity and bandwidth, cannot be used for all types of PD applications. A coil with inappropriate bandwidth will attenuate the significant portion of a PD pulse having frequency contents above or below the bandwidth of that coil. Similarly, a coil with lower resonant frequency will result in a measured pulse with slower rate of change and greater pulse width. To illustrate the fact, Table 3.6 and Table 3.7 present two different designs of coils to measure the same PD pulse. Figure 3.19(a) shows the resonant frequency of both coils while the measured output of both coils is given in Fig. 3.19(b). Slower response of coil 2 can cause inaccuracies. Therefore, further calculation (area of the pulse) to obtain the amount of apparent charge for estimation of the PD intensity will not be reliable. Hence the design of a Rogowski coil should be determined based on its specific applications, keeping in mind the estimated frequency range of PD signals.

Table 3.6: Parameters of Coil 1

Symbol	Specification
d_o	155 mm
d_i	131 mm
d_{rc}	143 mm
d_w	0.85 mm
N	30

Table 3.7: Parameters of Coil 2

Symbol	Specification
d_o	155 mm
d_i	131 mm
d_{rc}	143 mm
d_w	0.85 mm
N	60

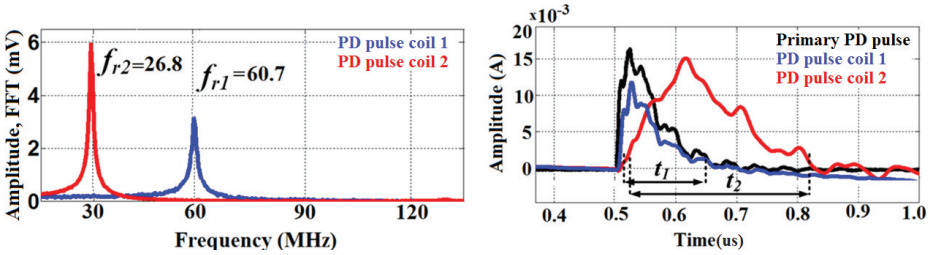

(a) (b)

Fig. 3.19. . Comparative performance of different designs of coils for PD measurement. (a) Frequency response of the coils and (b) measured signal by the coils.

In real cases the measurement of a PD pulse in the form of a typical wave shape is an optimistic expectation. Such criterion is essential to follow while designing the coil where calibrated PD pulse is used. A proper pulsed wave shape is most likely in the case, too, if the line through which PD signal is propagating, is properly terminated i.e., by using a terminating impedance equal to the characteristics impedance of the line. For real applications this is possible when making off-line PD investigation by disconnecting the line from the network for proper termination. However, in on-line applications such condition may not exist. Therefore, a realistic approach is needed for assessment of the PD activity. Electrical model of power lines is represented by RLC (distributed or lumped) parameters. Due to mutual effects of the line's RLC model, the oscillations are superimposed on the propagating PD signals. In this case, the PD signal will most likely be measured as an oscillatory waveform. As elaborated in Chapter 2, the rise-time of a measured PD signal is characterized by the properties of PD defect whereas fall-time can significantly be affected by the properties of the line through which the signals is propagating. Therefore, the closest approach is to consider the first peak of the measured signal. The corresponding peak value can proportionally provide the apparent charge to estimate the PD intensity. Consequently, the induced charge can be obtained if the attenuation constant of the line and location of the PD fault from the measuring sensor are known.

4. On-line Condition Assessment of Distribution network

4.1. Power Distribution Network

The factors such as: enhanced asset management, improved power quality, reduced interruptions, and advances in technology (digital and wireless) make a way for smart solutions in the modern power grids. The presence of PDs in an electrical equipment is the confirmation of its insulation degradation. Location and extent of PDs determines the expected remaining life of the insulation. This leads to carry out corrective actions timely. Achieving the above goals means a leap towards the predictive maintenance and self-healing networks. This is one of the objectives of smart distribution networks. This chapter presents a comprehensive technique for PD location in a distribution network.

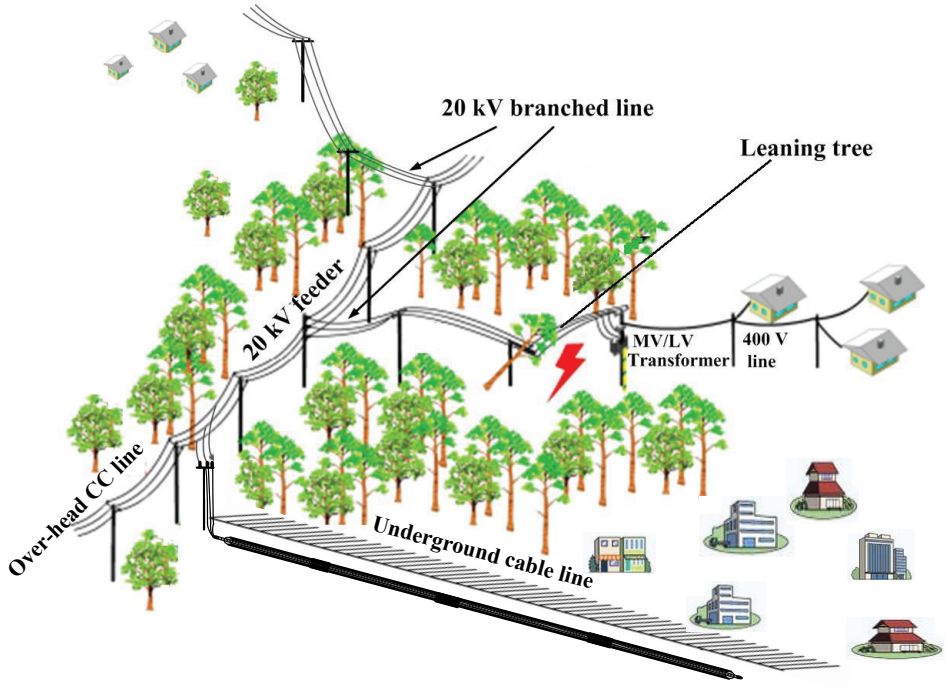

Fig. 4.1. MV network representing CC lines and cables for distribution network.

A distribution system is the final stage in the delivery of electricity to the consumers. The industrial or commercial consumers generally are connected to the primary substation

(HV/MV transformer) at distribution voltage (MV) level. The residential consumers are connected to the secondary substations (MV/LV transformers) at LV level. The feeders emanating from primary substation can be underground cables, overhead bare conductors, overhead CC lines, or combination of these. The topological configurations of the feeders are different in different regions of the world. A practical network feeder may consist of single or branched line network. Considering the example of the United States, three phase main feeders carry power from primary substation to secondary substations, and are typically 13-24 km in length. Three phase and single phase primary laterals (branches) are tapped from the main feeders and these branches can extend several kilometers from the feeder. Primary system normally tends to be overhead when possible and underground when required. Similarly, typical urban underground cable network in UK has a number of branches tapped from the main cable feeder [90].

Figure 4.1 represents a 20 kV distribution network supplying the power by using CC lines with the probability of trees falling on the line causing PDs [41]. The transition between the overhead line and underground cable can be seen in the figure. Leaning trees are no more a threat for underground cable, however, the cables have their own PD causes [91]-[92].

4.2. PD Location Techniques

Power components in a distribution network are located in a wide geographical region. In large substations, voltage is transformed down to MV level (1 kV…36 kV) and a number of feeders (typically 10-30) are connected to the bus bar [93]. As mentioned above, an outgoing feeder is usually not a single cable, but divided into a number of sections and branches of cables that are interconnected through ring main units (RMUs). These cables contain a number of joints, terminations, cables of different lengths and impedances. The cables are connected in straight and branched topologies. PD faults can be located anywhere (bus bar connections, switching components, transformers, cables, CC lines, joints, and terminations) within the network.

The most frequently used PD fault location techniques such as time-domain reflectometry (TDR) [24], time of arrival analysis (TOA) [25], and frequency-amplitude analysis (FAA) [27], are most often applied on a single section of the line or cable. These techniques are useful for single section of CC line or cable, however due to certain limitations described in [Publication VII], they are not suitable for multi-section or branched cable or CC line networks. In this study, the section is referred to a line of specific length or a branch of line in distribution network. Basic challenges of PD investigation in branched line networks have been described in [30], still there is a lack of research work for location diagnostics in such type

of network topologies. In this work, a new and simple two-stage location technique is proposed for branched cable networks. The first stage is to detect the presence of PD activity around and to identify the section or branch of the line containing the PD fault. This stage is based on direction of arrival (DOA) detection technique. The same PD pulse starting from discharge location propagating to different branches is detected by directionally calibrated induction sensors (Rogowski coil or HFCT). Consequently the comparison of the signals captured by sensors identifies the faulty section. The second stage is to determine the fault location on the identified section using one of the above mentioned conventional (TDR, TOA or FAA) techniques. The second stage of this technique has already been well studied, therefore, the focus of the presented work is in the first stage.

The DOA technique has been developed in three stages. The first stage is the directional calibration of Rogowski coil sensor, presented in [Publication VI]. The second stage (presented in [Publications VI-VII]) is the identification of the faulty section in single route line and branched route line, using directionally calibrated sensors. The DOA based identification works in the similar manner in CC lines and cables. Therefore, one type of line is considered to describe the identification task for one type of route. The MV CC line is considered for single route line [Publication VI] whereas MV cable is used for branched route line [Publication VII]. The integration of the DOA technique over a cable feeder is proposed as the third stage in [Publication IX]. In this chapter, the proposed integration scheme is enhanced using ATP-EMTP simulation environment. Based on simulation results, intelligent algorithm is proposed for automated PD fault identification in the network.

4.2.1. Directional Calibration of Rogowski Coil

The directional calibration of Rogowski coil is made by using the polarity of measured PD signals in order to determine its DOA. The PD pulse provides the information of ongoing PD activity. Based on the waveshape, area of the pulse estimates the apprent charge, and peak of the signal determines its polarity. Accuracy of the charge estimation depends upon how accurately the wave shape is measured and the sensor is calibrated. According to IEC 60270, in general, the first peak value of the captured PD signal can be assumed to be proportional to the apparent charge and polarity of the PD pulse [72]. Therefore, the first peak can be used for both charge estimation and identifying the polarity. This alternative provides an option to use the Rogowski coil in its basic form i.e., Rogowski coil head without damping and integration. In this form the response of Rogowski coil to a PD pulse will be similar to as shown in Fig. 3.12(a) and is sufficient for PD location purpose as polarity of signal is the only requirement for DOA technique. The purpose of using the coil in its basic form is to save additional components or

processing such as termination, integration, and calibration of the coil. However, considering the practical scenario where the installation of such sensor system is itself have a comparable economic burden therefore Rogowski coil along with its accessories (additional compnents) can be used as a better trade-off. It should be kept in mind that coil calibration and directional calibration are different tasks as stated previously.

4.2.2. Polarity Based Assessment of DOA of PD Signal

As mentioned in Fig. 2.11 (Chapter 2), positive and negative polarity PD pulses are emitted during positive and negative half cycle of the applied voltage respectively. In addition to the operating principal (Faraday's law of electromagnetic induction), the output polarity of Rogowski coil depends on the direction of arrival of signal, its polarity, and connection of output terminal of the coil with the oscilloscope as shown in Fig. 4.2.

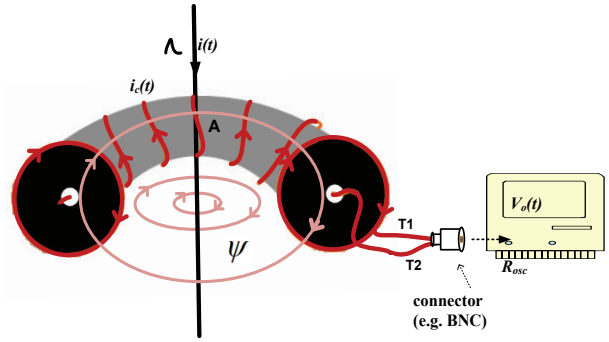

Fig. 4.2. Operation of Rogowski coil to represent the direction of primary current, face of coil, and connection of the terminals.

The experimental description of directional calibration is described in [Publication VI]. The important aspects of calibration are briefly described as follow

- In Fig. 4.3 there are two possible locations of PD fault, either within the section Q_1Q or Q_2Q, whereas Q is the location of the coil.
- Considering the geometry of the coil, the face illustrating a clock-wise progression of the coil winding, is designated as face *A* of the coil whereas the opposite face showing an anti-clock wise progression of the coil winding and is designated as face *B*.
- The starting and return end of the winding conductor is designated as terminal T_1 and T_2 respectively, as shown in Fig. 4.2.
- PD arriving through face *A* of coil is measured as positive pulse, and vice versa (see Fig. 4.4).

- If the polarity of the PD pulses measured during positive cycle of the applied voltage is positive, the direction of arrival of the PD signals is through face *A* of the coil. Therefore, PD source lies within section Q_1Q of the line as shown in Fig. 4.3.
- If the polarity of the PD pulses measured during positive cycle of the applied voltage is negative, the direction of arrival of the PD signals is through face *B* of the coil. Therefore, PD source lies within section Q_2Q of the line as shown in Fig. 4.3.
- In the above, the polarity of measured PD signals is analyzed for positive pulses emitting during positive half cycle of the applied voltage. The analysis is equally valid for negative pulses appeared during negative half cycle.

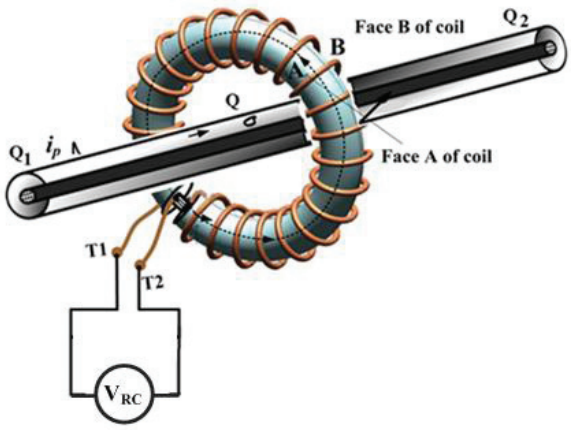

Fig. 4.3. Calibration of Rogowski coil to detect DOA of PD signals.

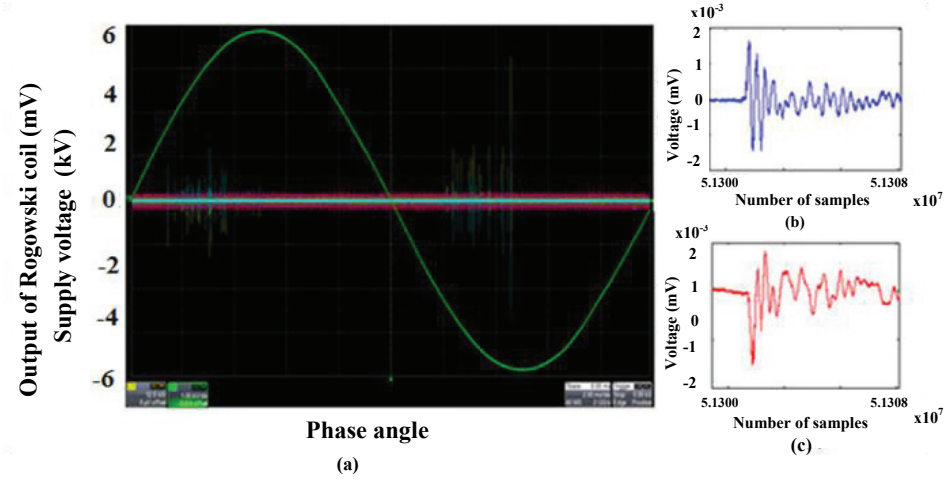

Fig. 4.4. On-line PD signal captured at energized CC line during directional calibration of Rogowski coil. (a) The PDs captured during one power cycle, (b) pulse captured for PD source along the section QQ_1, and (c) pulse captured for PD source along the section QQ_2.

4.2.3. ATP-EMTP Model of Rogowski Coil

The ATP-EMTP is a digital simulation software for analysis of transient phenomena in electrical power systems. This program provides models for large number of power components which can provide accurate response over a wide frequency range. High frequency geometrical model of Rogowski coil, identification of its electrical parameters, and model validation in ATP-EMTP are presented in [Publication II-III]. In continuation to the previous work done by the authors, this section modifies the simulated model of Rogowski coil as directionally calibrated sensor to identify the DOA of a pulse.

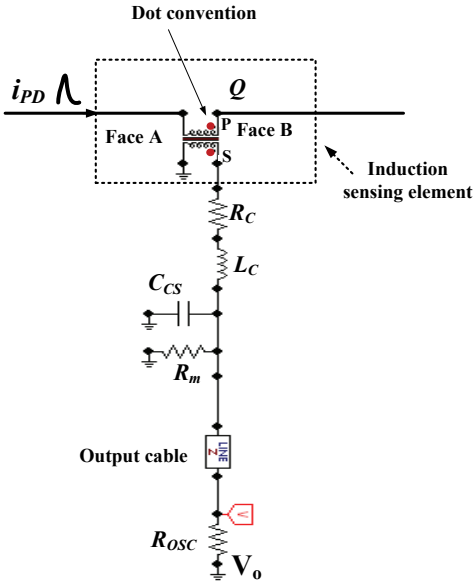

Fig. 4.5. Simulated model of Rogowski coil for DOA identification.

The practical measurement scenario shown in Fig. 4.3 has been simulated by the model in Fig. 4.5. Inductive sensing element is obtained with the help of single phase transformer. The current carrying line is the primary whereas coil head is the secondary winding of the transformer. Based on measurements, magnetization relation is established as linear due to non-saturable core of the Rogowski coil. The dot convention is used to define the relative polarity of the transformer's winding. Positive pulse entering through the dot-end of primary winding induces positive polarity voltage at the dot end of secondary winding and vice versa. Terminal *A* and *B* of the transformer represent face *A* and face *B* of the Rogowski coil respectively. The components R_c= 0.7 Ω, L_c = 1.19 µH, and C_{cs} = 16.45 pF, are the measured parameters as given

in Table 3.3. The output voltage V_o of the coil is measured using a high sampling rate (2 GS/s) DSO with R_{osc} = 1 MΩ being the input resistance of oscilloscope. The CC line is modeled as given in [41]. The simulated model has been validated for assessment of DOA as described in previous section.

4.3. Identification of the Faulty Line Section

The use of CC lines is increasing due to their improved reliability as compared to cables and bare conductors. In normal conditions, relative to cable, the failure density of bare conductor lines is 4.92 times/100 km/year, whereas in CC lines the failures leading to customer outages occur only 0.3 times / 100km / year [94]. However, in forest areas during harsh weather conditions (storms and heavy snow), the ratio of faults in CC lines can be increased. The Fig. 4.6 represents a threatening situation for CC lines. Permanent installation of the induction sensor along the CC lines (across the susceptible area) at specific intervals can help for early detection the PD faults due to leaning trees. The use of single sensors can identify direction of the location of the fault with respect to the location of the sensor. Two sensors can be used to split a specific length of the line into three different sections as illustrated in Fig. 4.7. Continuing the same scheme, three sensors can divide a certain part of the CC line network into four sections and so on. Therefore, *m-1* number of sensors is required to monitor the line in *m* sections. The pair of sensors around the defective section will identify the faulty section using DOA technique.

Fig. 4.6. A tree is falling on the CC lines passing through forests [95].

Experimental setup described in [Publication VI] and [Publication IX] (shown in Fig. 4.7) represents the models for the implementation of DOA technique to identify the faulty section in CC line. The scenario of this measurement demonstrating the directional installation of the coils and three sections as possible locations of the fault is illustrated in Fig. 4.8. The schematic of simulated model is depicted in Fig. 4.9. A 20 m long MV CC line is used as a single route line. Three cases were considered to evaluate the performance of installed coils for DOA identification for three different locations of PD source as follows:

I. At L_1U_1= 3 m, at location U_1.
II. At L_1U_2 = 12 m, at location U_2.
III. At L_1U_3 = 17 m, at location U_3.

The small length of the CC line used in this experiment is due to limitation of the laboratory implementation. In real cases, the forest area through which the CC line is passing could be of several kilometers. In this model, the CC line is divided into three sections (L_1P_1, P_1P_2, and P_2L_2) by using two coils RC_1 and RC_2, located at points P_1 and P_2. The data of practically captured PD pulse is imported to the PD source block in Fig. 4.9. The PD source block is connected at three different fault point locations U_1, U_2, and U_3, considering single fault at a time. The PD signals captured by RC_1 and RC_2 for fault case are shown in Fig. 4.10. Based on the installed face directions of Rogowski coils, faults are identified as follows:

I. Positive polarity detected by both RC_1 and RC_2 shows the DOA of PD current pulse through face A of both coils. This identifies the presence of a PD fault in section L_1P_1, i.e., U_1 in this case.
II. Negative polarity detected by RC_1 and positive polarity detected by RC_2 identifies the presence of a PD fault within section P_1P_2, i.e., U_2 in this case.
III. Negative polarity detected by both the coils identifies the presence of a PD fault along section P_2L_2, i.e., U_3 in this case.

The knowledge developed from the above three observations defines the rules to interpret the output of a pair of Rogowski coils in response to the PD activity progressing in the surroundings. The presented work is done for single phase line. In case of three phase line, sensors are needed to install around each phase as described in [96].

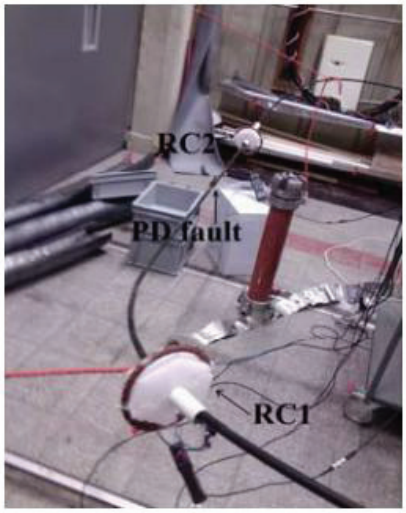

Fig. 4.7. The Rogowski coil installed on a CC line to evaluate the performance of DOA technique.

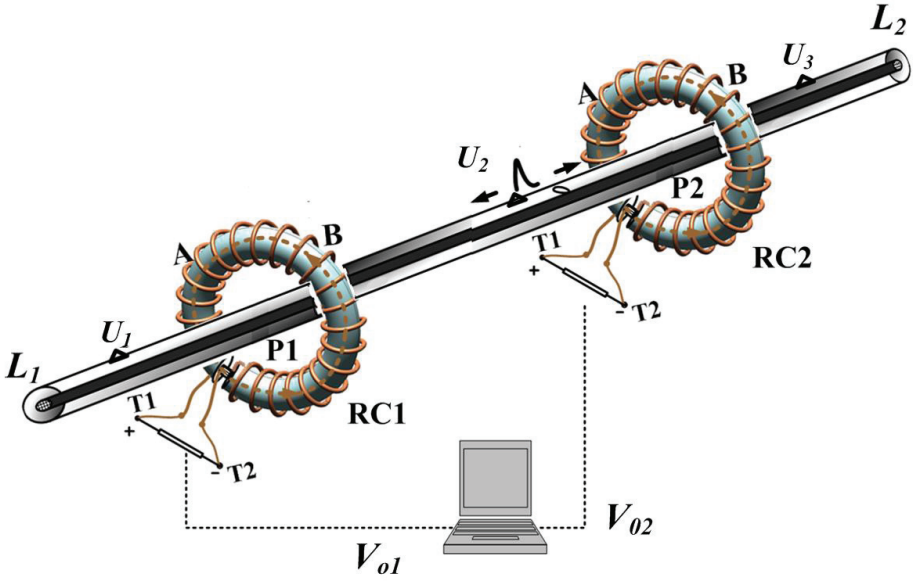

Fig. 4.8. Installation scenario of a pair of Rogowski coils to identify the faulty section on a CC line.

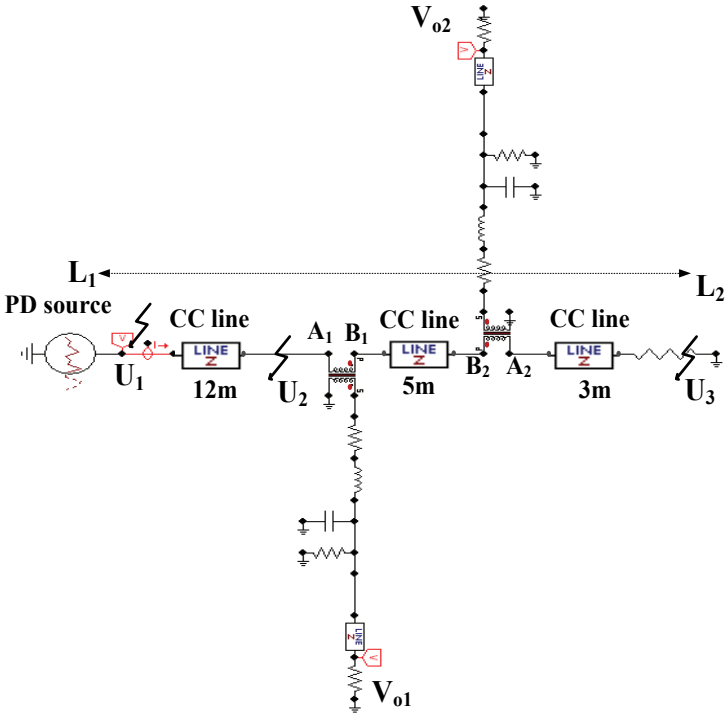

Fig. 4.9. Simulation of faulty section identification task on a CC line using DOA technique.

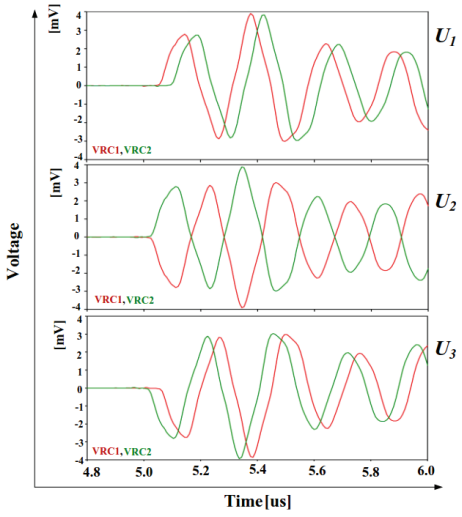

Fig. 4.10. Signals measured by both sensors for three different locations U_1, U_2, and U_3 of PD source (considering single source at a time).

During measurements, Rogowski coil is installed around the primary current line which means no electrical connection between the coil circuit and the primary current. The coil inductively measures the current without affecting the primary current. In the presented model, the primary side of current transformer is connected in series with the line carrying primary current. The arrangement works well as long as the coil circuit does not provide any disturbance to the primary current. However, if any reflections occur within the coil circuit, they may conduct to the primary side via N: 1 winding ratio. This phenomenon may affect the characteristics of PD signal. Therefore, an improved model is developed in Fig. 4.11. The TACS block senses the current of the primary line and eliminates the possibility of conducting any reflections from secondary side towards the primary side. Additional advantage of using such a model is to provide simplest topology of connections for the measurements while using three phase primary lines. Measurement operation of both kinds of installation is same and therefore can be used alternatively.

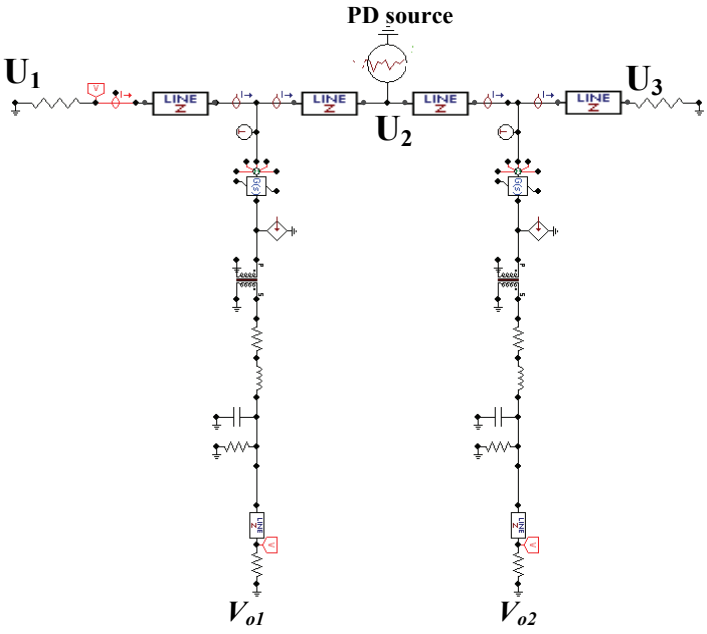

Fig. 4.11. Improved installation model of Rogowski coil.

4.4. Practical and Simulated Installation of Rogowski Coil in MV Cables

The proposed DOA technique can equally be applicable for cable networks. Due to different construction of CC lines and cables, the installation of Rogowski coil to sense the (magnetic field of) PD current in CC lines and cables is shown in Fig. 4.12 and Fig. 4.13 respectively. The CC line system consists of two separate conductors (covered conductors and grounds) therefore the coil is installed around the CC line. The cable consists of two coaxial conductors i.e., the main inner conductor and the coaxial shielding. The PD current travelling through the main conductor returns through the shielding which results in cancellation of the magnetic field and hence the total magnetic field due to PD current around the cable becomes zero. Therefore, the coil cannot be installed around the cable to sense the magnetic field of PD current. The possible location to measure PD current in cables is the joints and terminals where the main conductor and shielding are separated for further connections with the cable or incoming devices. Figure 4.13 shows a cable terminal. The Rogowski coil can be installed around either the main conductor or earth strap. However, the installation of Rogowski coil around the latter is preferred [97].

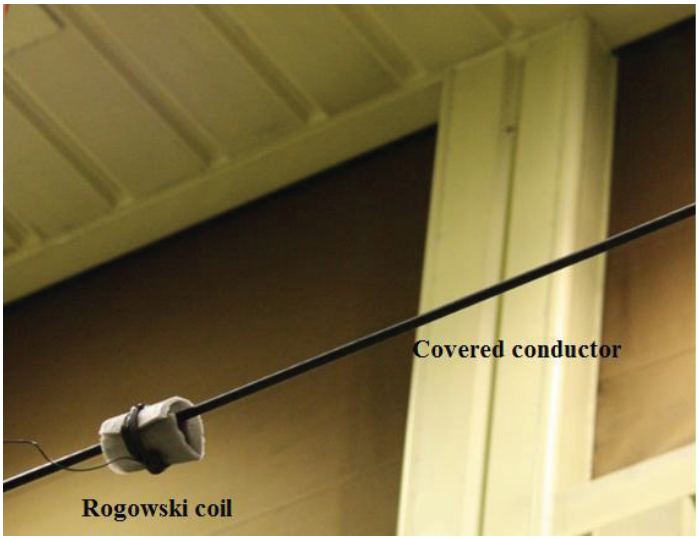

Fig. 4.12. Installation of Rogowski coil on an MV CC line for measurement of PDs.

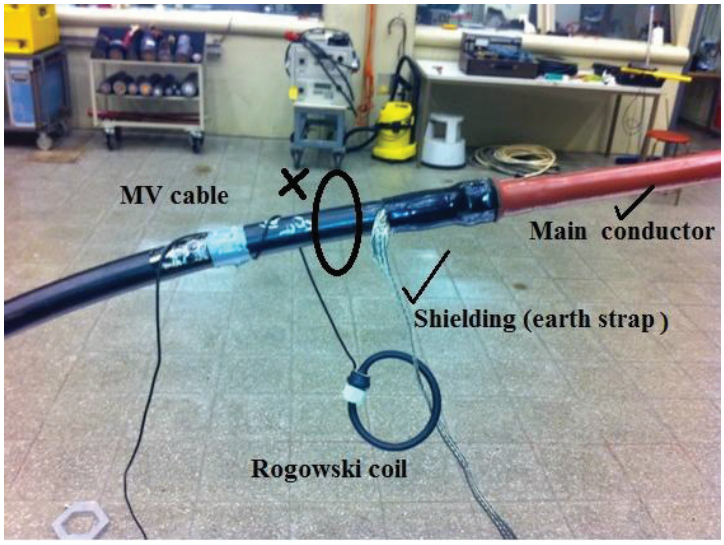

Fig. 4.13. Installation of Rogowski coil on an MV cable for measurement of PDs.

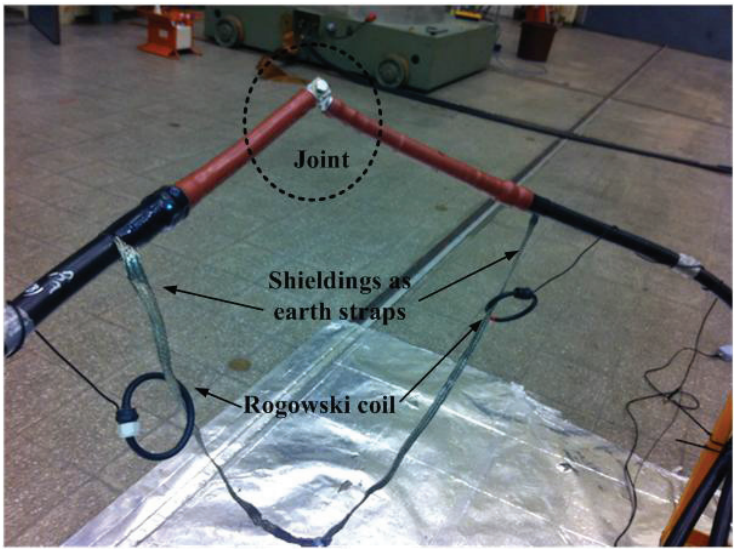

Fig. 4.14. Laboratory installation of Rogowski coil on a straight joint (around earth straps) MV cable for measurement of PDs.

The basic idea of connections of MV cables is presented in Fig. 4.14. The conductors and the shielding conductors which act as earth straps, are connected to each other. The coil sensors can be installed as depicted. A similar arrangement is made to represent a T-branched joint using MV cables in [Publication VII]. The detailed description of the direction of flow of PD current and methodology of identifying the faulty cable branch using DOA technique (in case of

branched joint) is presented in [Publication VII]. A typical (three phase) MV cross bond joint is shown in Fig. 4.15. The shielding of each phase of cable is connected to that of the other cable in a crossed pattern [98]. The cross-bonding link-box is usually available in underground cable systems. It is possible to use inductive sensors without any interference and therefore to have impact on the cable system. In case of cross-bonding, the DOA of the PD current can be evaluated accordingly. The flow of PD current in cross bonded joint is shown in Fig. 4.16 [99].

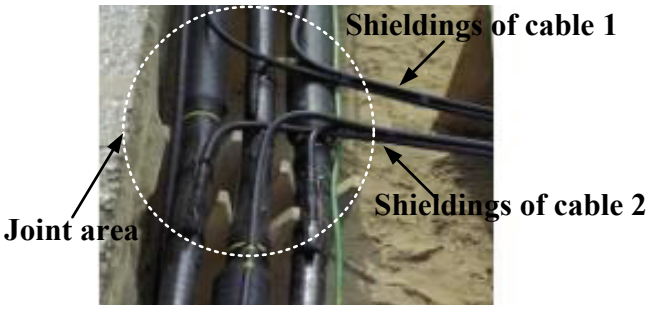

Fig. 4.15. A typical cross-bond joint in MV cable system [98].

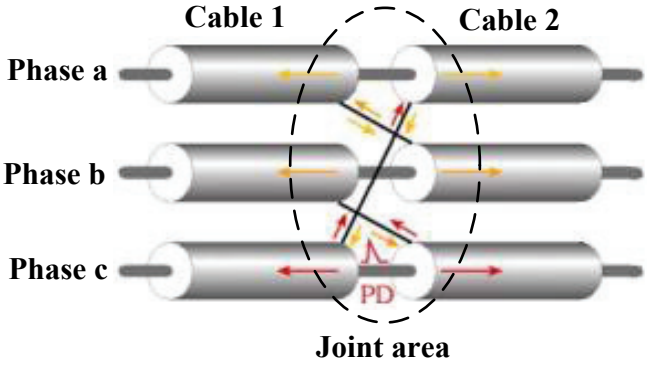

Fig. 4.16. Propagation of PD signal in the cross-bond joint [99].

Underground cable installation in distribution network is becoming increasingly popular especially in the urban areas. Visual inspection during faulty or fault initiation situation is not possible. Therefore, accurate diagnostic methods are needed to localize the PD faults in order to avoid excessive loss of time and revenue. Remaining of this chapter mainly deals with the integration of DOA technique over an MV cable feeder. Experimental implementation of DOA technique for a single phase MV cable is presented in [Publication VII]. The ATP-EMTP simulation environment considering three phase cable is briefly discussed further in this section. The next sections of this chapter present the layout of integrated scenario over a cable feeder, and the simulation results.

A primary feeder is generally connected to a number of MV/LV transformers which can be ground-mounted (underground cable feeder) or pole-mounted (overhead feeder) or a combination of both. Distribution transformers are tapped from the feeder by using T-joints. Instead of specifying and selecting individual components required for a T-joint, the required components are frequently available in an integrated package known as a ring main unit. The induction sensors can be installed on the terminations of the cables connected to T-joints. In the simulation, the MV cable is represented by a three phase integrated line and cable constant (LCC) object using enclosing pipe type in ATP-EMTP. The LCC objects in ATPDraw are based on the line constants, cable constants or cable parameters. LCC based cable simulation can be achieved by using different model such as Bergeron or Clark, PI, JMarti, Noda and Semlyen. It has been found that JMarti model has been preferred due to its better performance [101]-[102]. Due to high frequency of PD signals, cables' inherent R-L-C parameters, and mutual coupling, various effects are emerged in the form of added oscillations, amplitude variation, pulse width variation, and mutually induced PD signals from the neighboring conductors (in case of three phase cable system). However these factors do not have a considerable impact on the polarity of the PD signals. Polarity of the PD signals mainly depends upon the polarity of the applied voltage. Therefore, polarity based fault identification methodology is adopted as a diagnostic solution. The focus of this work is to present the sensor installation scheme and comparison of the polarity of the PD signals captured by the installed sensors in order to proceed for location diagnostics. Therefore, comparative accuracy of the cable models has not been analyzed in this work and JMarti model is used due to its better frequency-dependent performance in high frequency applications [102]. This enables the ATPDraw to perform an ATP run process to create an electrical model of the cable. Each cable section has different length depending upon the distance between consecutive nodes. The transformers are connected symbolically in this model as shown in Fig. 4.17. During operation, the PD activity can occur within the transformers, connecting accessories, joints, or the cable sections.

Another practical aspect of the three phase MV cable system is the cross-bonded construction of the cable joint where the shielding conductor of each cable is connected to that of its next cable (phase). In the presented scheme of sensor installation, the sensors are installed around the shielding earth straps. The direction of PD current and hence the captured polarity for the cable conductor and cable shielding is opposite to each other. In-depth analysis of this fact has been experimentally presented in [Publication VII]. In order to simplify the simulation circuit and polarity comparison (Fig. 4.17), the PD signals propagating along the conductors have been considered to implement the DOA technique. Therefore, shielding straps and cross bonded-joints are not considered in this simulation work.

The described simulation is focused on the study of PD transients from the PD source. Due to high frequency design of the coil, the coil filters out the lower frequency signals. Therefore, operating supply voltage (50 Hz) has not been considered in this simulation. The MV/LV load point is termed as node T_1. The location of the coils around the node for three phase measurement is depicted in Fig. 4.17. The PD fault can occur along any of the three phases of line. Therefore, a coil is needed to be installed around each phase. Three coils on each side of the node T_1 are represented by the respective subscripts. The subscript representation is as follow:

T_1: The node location MV/LV transformer,

R_{11}: Sensor installed at node T_1 towards the upstream (left) side of the node T_1,

R_{12}: Sensor installed at node T_1 towards the downstream (right) side of the node T_1,

$V_{T1,\ 1a}$: Voltage output of the coil $V_{(\text{node1}),\ (\text{upstream side})(\ \text{phase a})}$, and so on for phase *b* and *c*.

$V_{T1,\ 2a}$: Voltage output of the coil $V_{(\text{node1}),\ (\text{downstream side})(\ \text{phase a})}$, and so on for phase *b* and *c*.

The scenario illustrated in Fig. 4.17 describes the presence of PD source *S* along the phase *a*. Depending upon the construction of the line, the PD current flowing in a phase of origin may induce PD current in the other two phases and can be measured by respective coils (see Fig. 4.18). A positive polarity PD pulse captured during real measurement is used in this simulation. The PD sensor signal measured at phase *a* is the strongest (0.9 mV). However, the signals captured at phase *b* and *c* are very weak (0.02 mV). The PD signals at phase *b* and *c* are induced due to electromagnetic coupling between the neighboring phases and reflection of PD signals from common ground of three phases. Such small magnitude of PD signal induced in the neighboring phases reveals that the amplitude of PD signal occurring in one phase is significantly greater than the other two phases. On the other hand, a strong PD signal measured by a certain sensor provides clear information of the respective faulty phase. This also provides a simplified diagnostics information which eliminates an ambiguity when detecting the faulty phase.

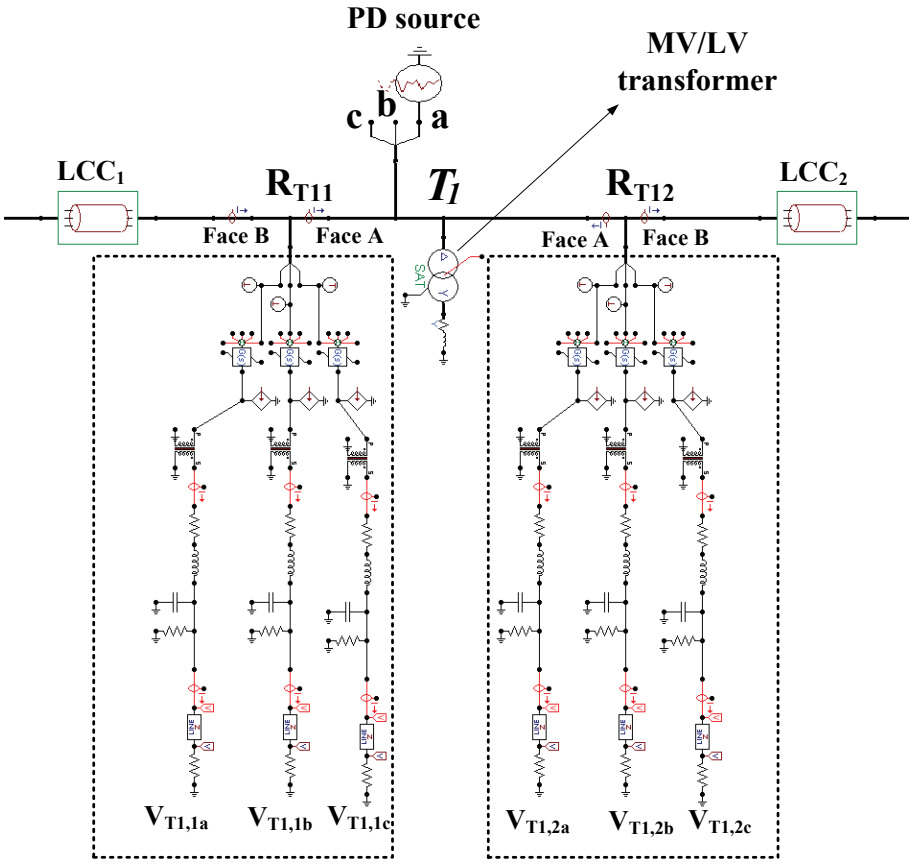

Fig. 4.17. ATP-EMTP schematic for three phase installation scheme of the sensors around node T_I.

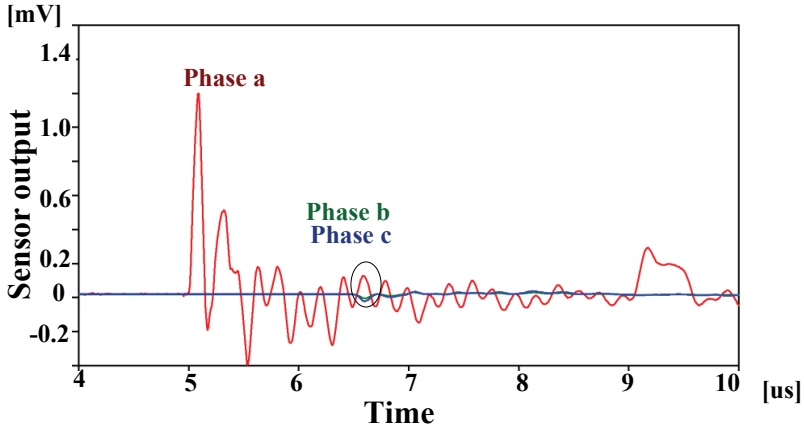

Fig. 4.18. Signals measured at location R_{T11}.

4.5. Proposed Location of PD Sensors in Cable Distribution Network

An MV/LV distribution transformer is the major component of the final link from the cable feeder in the electricity supply chain between distribution substation and the customers. These components are sensitive to insulation defects and also provide a possibility of installation of the Rogowski coil sensor for monitoring of PDs.

Figure 4.19 describes the layout of a distribution network having four cable feeders F_1, F_2, F_3 and F_4, which are connected to the MV bus bar. The feeder F_1 is feeding the load points T_i= *1, 2, 3, ... n*. Similarly, the other feeders (F_2, F_3, and F_4) are feeding the customers in their own areas. The distance between two consecutive load points depends on the number of customers and their location in vicinity. Joints and connections are needed along the cable routes due to practical limitations of cable lengths during manufacturing and transportation. Branched or T-joints are needed to tap the power towards different areas. All the components and equipment described above can experience the insulation defects and initiate PDs. However, cables, cable joints, cable terminations and transformers are the most vulnerable targets of this activity. Main stages of the implementation of the diagnostic scheme are explained in the flow chart diagram shown in Fig. 4.20. The actions mentioned in the flow chart have been described in this paper. However, de-noising of measured PD signals has already been explained by the authors in [54] and is not discussed here.

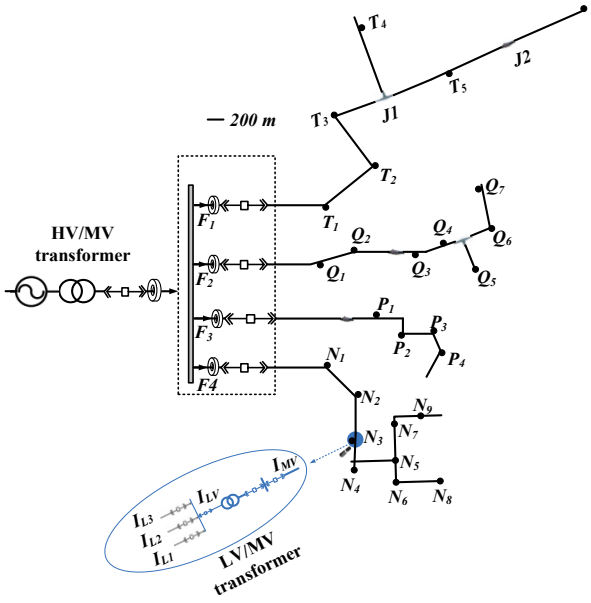

Fig. 4.19. Proposed location of PD sensors installation in a typical underground cable distribution network.

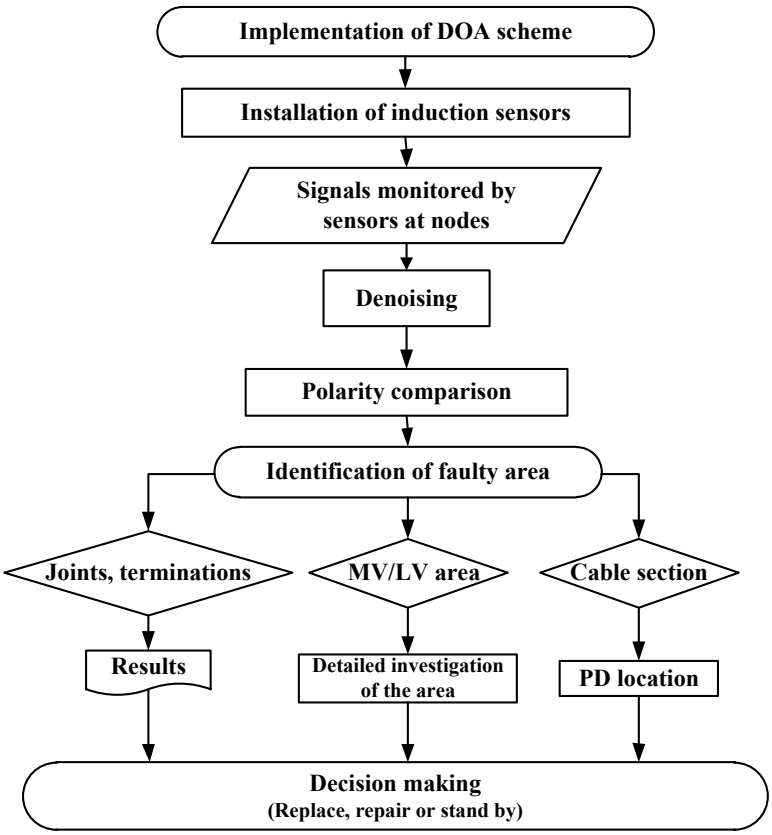

Fig. 4.20. Flow chart for implementation of DOA technique for PD diagnostic system integrated over MV network (T*- transformer).

4.6. Evaluation of Integrated Performance of DOA Technique Using ATP-EMTP

For the distribution network presented in Fig. 4.19, the feeder F_1 is considered for integration of the proposed DOA technique. The sensors are installed at each node i.e., around the HV/MV substation transformer, bus bar, MV/LV transformers, and joints. Each node is designated as priority *A* while the cable/line connecting the two adjacent nodes is designated as priority *B* as shown in Fig. 4.21. In other words, the component for which installed coils are facing through face *A* is called *A* Priority component whereas the component facing the coils through face *B* is termed as *B* Priority. A pair of sensors is installed around their dedicated *A* Priority components. This pair of sensors not only monitors their *A* Priority component but also the *B* Priority which is the cable sections between the focused *A* Priority and the next *A* Priority components along either side. The sensors R_{11} and R_{12} are installed around node T_1. Here T_1 is the *A* Priority component for these sensors while sections T_1F_1 and T_1T_2 are *B* Priority

components. The section T_1F_1 is the cable between node T_1 and F_1 whereas section T_1T_2 is the cable section between node T_1 and T_2. Similarly, in addition to A Priority component T_2, the sensors R_{21} and R_{22} take care of their B Priority sections T_2T_1 and T_2T_3 as well, respectively.

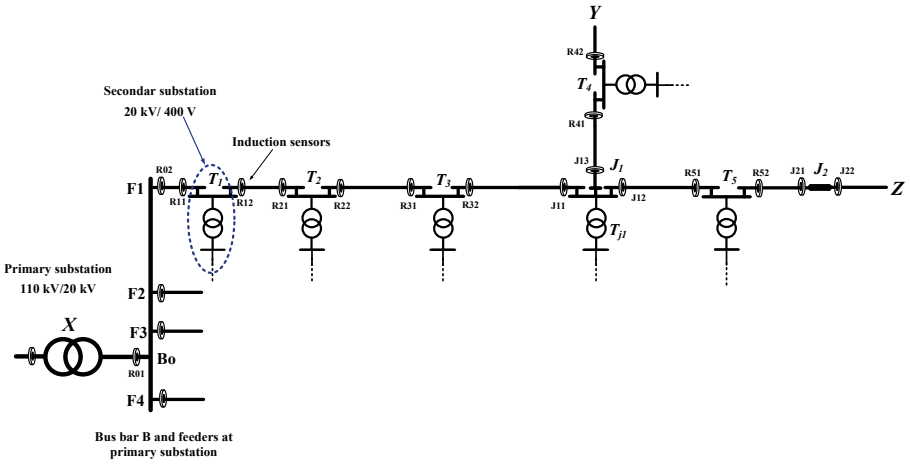

Fig. 4.21. Installation scenario of Rogowski sensors along the feeder F_1.

The cable feeder network described above is simulated in ATP-EMTP environment as shown in Fig. 4.22. The schematic of the Rogowski coil is not shown in the figure. The outgoing cable feeder of 20 kV consists of different nodes; T_1, T_2, T_3, T_4, T_5, joint J_1, and J_2 leading to feeder branches Y and Z. The Rogowski coils are installed around each node such that the face A of each Rogowski coil is towards their respective node. In order to describe the DOA sensing technique, in CC line test (Fig. 4.9), the face A of every coil was directed towards the source (upstream) side. However, in multi-node and complex line network, face A-towards-node scheme is recommended to develop symmetry for interpretation of the signals. Similarly, directional sensing and detected polarities should be assessed accordingly.

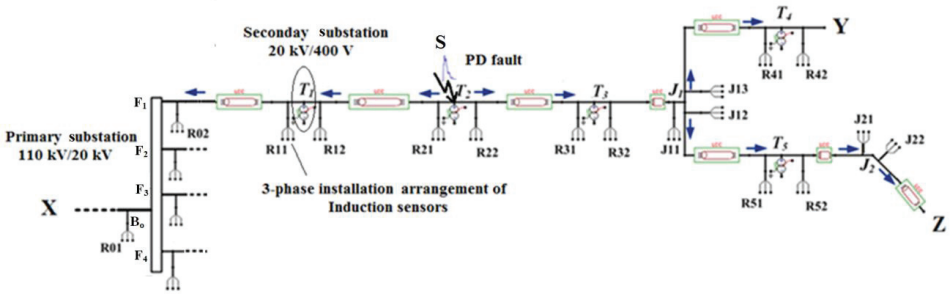

Fig. 4.22. ATP-EMTP model for performance evaluation of the DOA technique for feeder F_1.

4.6.1. Measurement Results

During PD monitoring along the feeder F_1, the signals measured by Rogowski coils around respective nodes are shown in Fig. 4.23. The phase *a* has been identified as faulty phase. Therefore, further evaluation is made only for sensors of phase *a* (at each node) while the measurements of other phases is not taken into account. Each figure represents the plot of output from the pair or set of sensors around individual nodes. Corresponding to the substation bus bar (Fig. 4.22), *X* represents the line section from secondary of HV/MV transformer to bus bar B_o. Here B_o is the *A* priority for sensor pair positioned as R_{01} and R_{02}. Due to not being the (direct) part of feeder F_1, the measured signals at this pair of sensor has not been included in Fig. 4.23.

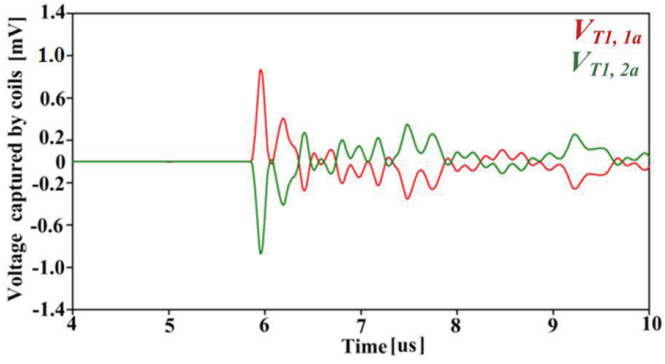

(a) Voltage signals measured by sensors installed at node T_1.

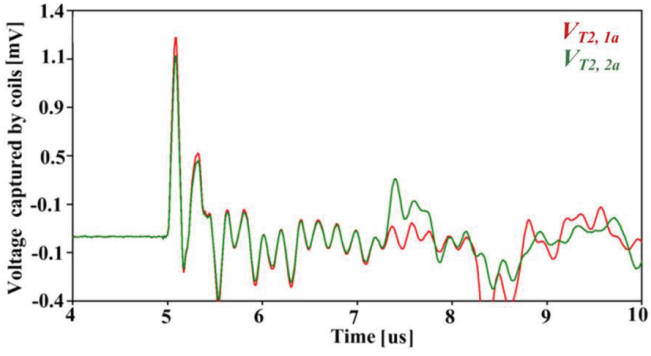

(b) Voltage signals measured by sensors installed at node T_2.

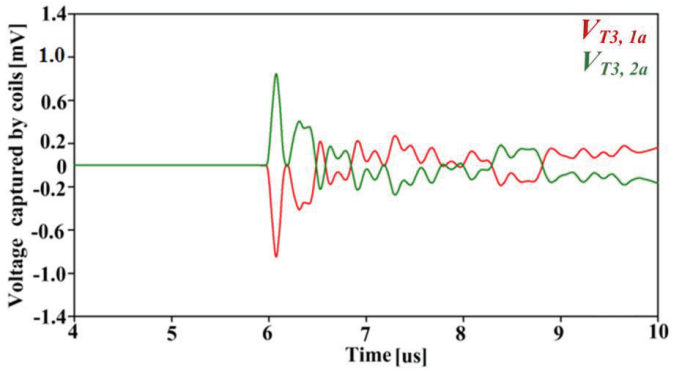

(c) Voltage signals measured by sensors installed at node T_3.

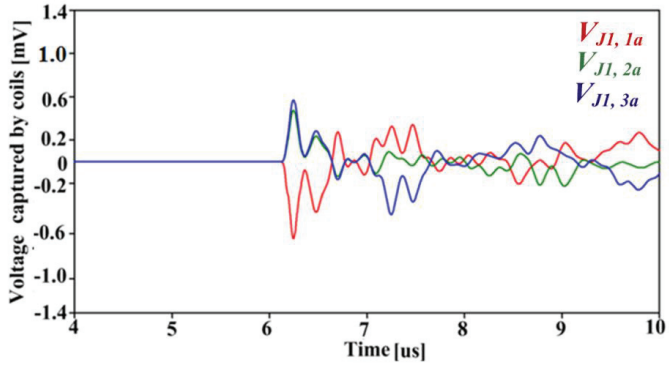

(d) Voltage signals measured by sensors installed at node J_1.

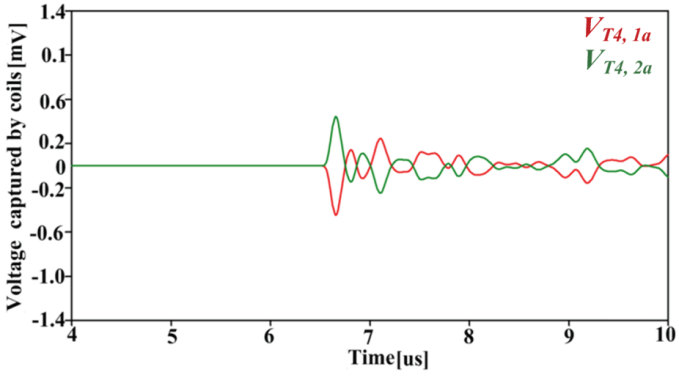

(e) Voltage signals measured by sensors installed at node T_4.

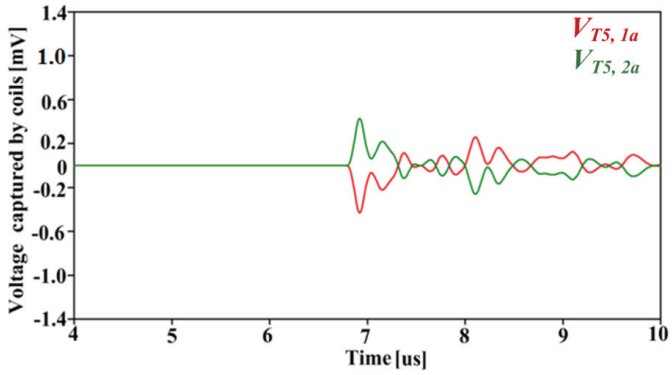

(f) Voltage signals measured by sensors installed at node T_5.

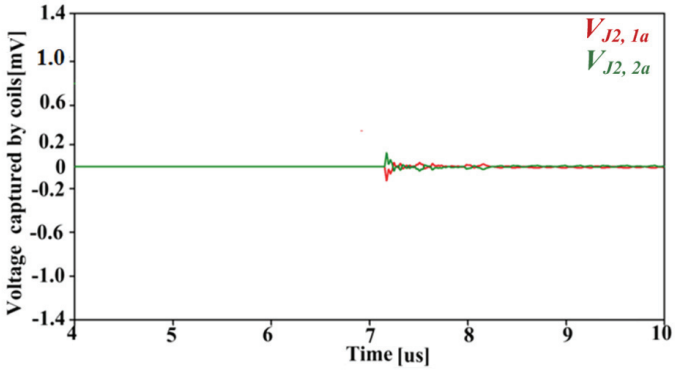

(g) Voltage signals measured by sensors installed at node J_2.

Fig. 4.23. Sensors' data measured at each node of feeder F_1.

4.6.2. Fault Identification

Table 4.1 presents the basic idea to develop an algorithm-oriented database for the observed feeder of the network. This database would include the substation transformers, cable sections, joints, and sensors, with accordingly assigned subscripts. The *A* Priority components are described in column *P_A*. Column S_1 sensor and S_2 sensor reports the sensors at each *P_A* component. The P_B_1 and P_B_2 are the cable sections immediate to sensor S_1 and S_2 respectively, as their *B* Priority. The arrows in each row describe the DOA of the PD current signal at the respective sensors. The positive and negative polarity voltage $V_{T1,1a}$ and $V_{T1,2a}$ respectively (Fig. 4.23(a)) measured by coils ($R_{1,1a}$ and $RC_{1,2a}$) at node 1, shows that PD pulse arrives at sensor $R_{1,1a}$ through face *A* and at sensor $R_{1,2a}$ through face *B*, hence suspecting the presence of PD source along downstream direction. At the same time, Fig. 4.23(b) and 4.23(c) show signal measured by $R_{2,1a}$, $R_{2,2a}$, $R_{3,1a}$ and $R_{3,2a}$, their measurements are given by the entries

of rows 2 and 3 respectively. Similarly, the entries of the rest of the rows account the record of PD measurements at relevant nodes. The measured signals at $R_{2,1a}$ and $R_{2,2a}$ present an alarming data. Same polarities detected by this pair of sensors and opposite DOA providing a caution about their A Priority component. This pair of sensors conveys the information of presence of PD origin between these sensors. Therefore, T_2 is identified as the faulty component. It can also be concluded that, based on installed configuration of sensors i.e., face A towards the node, the set of pair that have the same polarity of captured signals, will be declared as the faulty section or component.

Table 4.1 PD fault location algorithm development

No	P_B_1	S_1 (upstream) sensor	P_A	S_2 (downstream) sensor	P_B_2
1	B_oX	$R_{0,1a}$ (0.02 mV) 0	B_0	$R_{0,2a}$ (-0.02 mV) 0	B_oF_1
2	T_1F_1	$R_{1,1a}$ (+0.9 mV) ⟵	T_1	$R_{1,2a}$ (-0.9 mv) ⟵	T_1T_2
3	T_2T_1	$R_{2,11}$ (+1.3 mV) ⟵	T_2	$R_{2,2a}$ (+1.3 mV) ⟶	T_2T_3
4	T_3T_2	$R_{3,1a}$ (-0.80 mV)⟶	T_3	$R_{3,2a}$ (+0.80 mV) ⟶	T_3J_1
5	J_1T_3	$R_{j1,1a}$ (-0.67 mV) ⟶	J_1	$R_{j1,2a}$ (+0.6 mV) ⟶ $R_{j1,3a}$ (+0.57 mV) ⟶	J_1T_4 $J_1T_5(P\_B3)$
6	T_4J_1	$R_{4,1a}$ (-0.4 mV) ⟶	T_4	$R_{4,2a}$ (+0.4 mV) ⟶	T_4Y
7	T_5J_1	$R_{5,1a}$ (-0.04 mV) 0	T_5	$R_{5,2a}$ (+0.04 mV) 0	T_5J_2
8	J_2T_5	$R_{j2,1a}$ (-0.01 mV) 0	J_2	$RC_{J2,2a}$ (+0.01 mV) 0	J_2Z

B_o represents bus bar s

J_{13} (+) is S_3 at J_1.

Point X, Y, Z represents the continuation on the network

The sensors with '0' output do not detect any PD activity as given in rows 1, 7, and 8. The '0' output is the result of relatively small amplitude of measured signal which is considered less than the set threshold. The threshold was defined so that the sensors' output less than 0.1 mV is logically set to '0'. Amplitude of the generated PD current pulse determines the intensity

of the PD defect to assess how severe it is. Threshold value of a sensor is adjusted based on the sensitivity of the sensor and amplitude of the PD signal. In this case the PD is emitted from T_2, therefore larger amplitude (1.3 mV) of PD signal is measured by the immediate surrounding sensors $R_{2,1a}$ and $R_{2,2a}$. As the PD propagates along the line, dispersion and attenuation decrease the energy of the PD signal which results in decreased amplitude of the PD pulse [50]-[51]. During propagation, if the magnitude of the PD pulse is still significant enough as compared to the threshold set in the algorithm, it will also be detected by the neighboring sensors, otherwise indicating '0'.

4.7. Automated Fault Identification

A logic rule based system is presented in Table 4.1, whose display can be seen in specific colors. A conventional traffic indication scheme consisting of green, yellow, and red color is adopted to indicate the condition of network sections. The rows (1, 7, and 8) with green color indicate that the respective sections are clear from the fault. These sensors measure '0' PD activity as mentioned above. The row 3 appearing in red color declares the faulty region. The identified region encloses the PD source whose location can be determined (discussed in section 4.8). The rows (2, 4, 5, and 6) appearing in yellow color show that PD activity has been measured by the relevant sensors. The corresponding (yellow color) sections may not contain the PD source, instead, a PD signal is detected which is propagating from a PD source lying in the neighboring sections. The more simplified on-screen interface for normal maintenance crew to monitor the networks condition is described as Table 4.2, shown in Fig. 4.24. This type of user friendly interface does not require a continuous interaction of the specialized experts which reduces the decision time and service cost.

An overall layout of the system is presented in Fig. 4.24. Such intelligent system can be developed by using well known computational techniques such as: logic rules, fuzzy logic, neural networks etc. Knowledge of sensors at designated location, their calibration, set threshold and propagation characteristics of PDs, play an important role during development of this system. Starting from the HV/MV-110 kV substation, a hypertext system can be created to access the information about different parts of the distribution network. Following the hypertext of feeder 1, the information about feeder 1 such as; components of this feeder, monitored activity, and other measuring or metering tasks can be observed. Condition monitoring blocks are proposed to be appeared like Table 4.2 so that it could be easily interpretable by simply trained shift crew. The processed data by all the sensors of feeder 1 is showing the present state of its components. Each entry of Table 4.2 brings out the further information using hyperlinks from these entries. For example 'clicking' T_2 in row 3, presents the signal measured by both

sensors (S_1 and S_2) around it which provide visual insight of PD activity. Similarly, 'clicking' sensors S_1 and S_2 for each component, can provide individual wave forms as well, in order to observe the wave-shapes, polarity, and amplitude of captured PD signals. The simplified display presented as Table 4.2 enhances the capability of on-line monitoring and diagnostics by eliminating the time gap between the instantaneous data of PD faults and its analysis by an expert. Recorded data over a time span can be used later by the experts to analyze the ongoing behavior of the fault.

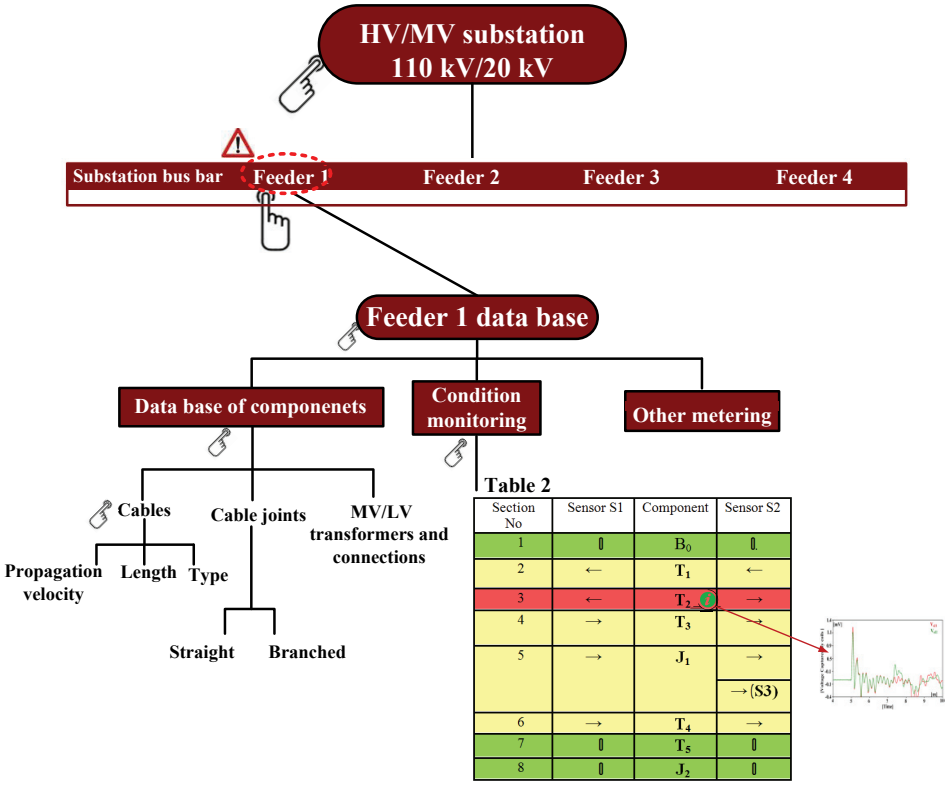

Fig. 4.24. Proposed system (interface) scheme for an on-line PD diagnostics.

4.8. Location of PD Faults

The possible PD sites can be described as follows.

I. MV/LV transformers (load points)

II. Cable joints or terminations

III. Cable sections.

The detailed PD investigation in the above three components is based on the two stage analysis, i.e., identification of the faulty component and detected fault location. The identification has been demonstrated above. For a location further analysis is required based on the type, out of the above three, of the components. In an MV/LV power transformer insulation system, PDs generate high-frequency electromagnetic transients that travel along the windings, bushings, and the cable feeding the transformers [102]. The coil sensors can be installed e.g. at the interface of the MV/LV transformer or neutral terminations to detect the PD transients. The PD activity detected around the transformer can be investigated further by using known techniques like acoustical measurements (as shown in Fig. 4.25) or DGA to find out the location and cause of the insulation defect [103]-[106].

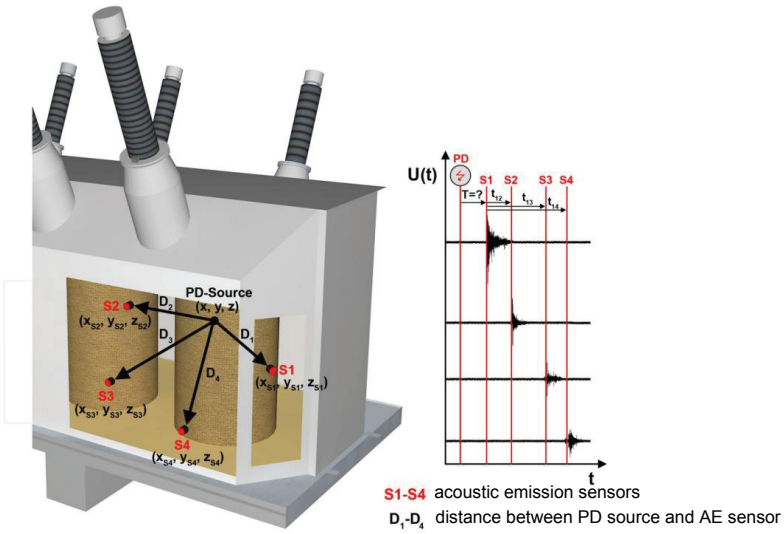

Fig. 4.25. Schematic diagram of Time of Arrival (TOA) technique using Acoustic Emission Method for PD location in a power transformer [103].

The joints and terminations in the cables are the most prone locations to the PD defects [107]. Identified joints or terminations are further investigated to quantify the extent of fault in order to make a decision: replace, repair, or stand by. Figure 4.26 shows a faulty MV cable joint to visualize its damaged form. In case a cable section is declared as faulty, the exact PD location can be determined by using TDR or TDA techniques as illustrated in Section 2.5. In Fig. 4.27 a cable is shown where the copper wire earth screen of the XLPE insulated cable was burned away. Quantification will be the final stage to assess the condition of the located fault [Publication I].

Fig. 4.26. A damaged MV cable joint [108].

Fig. 4.27. A damaged part of the XLPE cable [109].

4.9. Discussion

It is described previously in this chapter and [Publication VII] that TDR, TOA or FAA techniques cannot be alone used for PD source location in longer single or branched route lines. The non-suitability of these techniques in the later case is obvious, because generally these techniques rely on two-end measurement for comparison of the pulse travelling towards the two ends of the line. The long single route line means the CC lines or cables going across several kilometers. For example in case of a CC line (shown in Fig. 4.28) going through a forest area of 10 km, two sensors are applied at the ends (*A* and *B*) of the line to find the location of a PD fault due to a leaning tree. Trees can lean on or touch the line anywhere along this 10 km long line. In a worst case if the tree is leaning somewhere in the middle (at a point P), what could be the expected scenario of measurement from the sensors installed at the ends? First it should be realized that PD signals are high frequency (several MHz) and low amplitude signals in the

range of few mA to few tens mA. The line causes attenuation and dispersion to the PD signal during propagation. The signal gets very week (due to attenuation) and pulse width may increase significantly (due to dispersion). The noise is an added problem here which can be solved (by denoising techniques) if the signal to noise ratio is high. However, denoising may not be effective for low signal to noise ratio. Therefore, after travelling such a long distance of 5 km (from the fault location to line end), it is impracticable to detect or measure the PD signal reliably. Considering the most optimistic situation, if the PD fault occurs near to one end, sensor *A* can capture it reliably, nonetheless the signal propagating toward end *B* has to travel 9 km which will result in an extremely unreliable measurement. Such measurement scheme will lead to missed faulty event and breakdown may occur without early information.

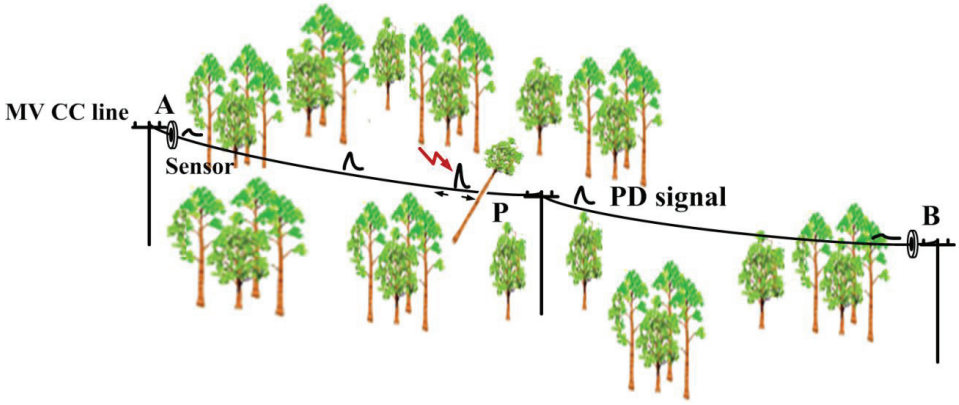

Fig. 4.28. Two Rogowski coils installed for a long length of CC line *AB*.

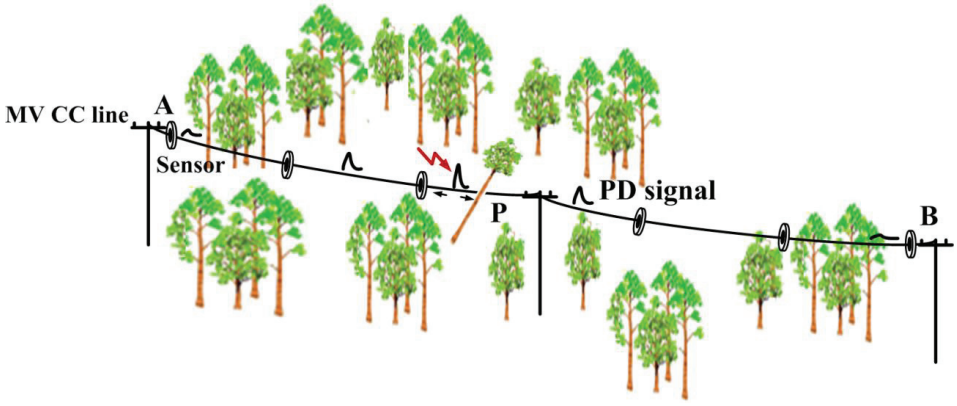

Fig. 4.29. Multiple Rogowski coils are installed at distributed locations along CC line *AB*.

The efficient option is to divide the long single route line into smaller parts termed as sections. A sensor should be installed for each section as depicted in Fig. 4.29. The length of

section should be selected by keeping in view the attenuation constant of the line and the sensitivity of the sensor. It is preferred to keep the length of each section same which makes it simple to analyze the captured data. However, the length of section can be varied according to the variation of the density of trees where the probability of leaning tree event is higher. Similar explanation is valid for a cable network.

For integrated application of the on-line monitoring system, periodic and continuous data collection system can be employed. The system can be selected based on the type of components, geographical location of the components, age specific risk level, and economy of the system versus components. The data collected from the field sensors will be transferred to the centralized system at the substation and can be processed for fault diagnostics as demonstrated in Table 4.1. The sensors can be installed permanently around the nodes. In case of periodic monitoring system, the data can be stored using data logger system for single cycles of supply at specified intervals of time [110]. The stored data can be transported 'manually' to the center for processing. For continuous monitoring, the wireless sensor technology is a preferred solution. Considering wired links, the overall cost of installing and wiring a sensor exceeds the cost of the sensor by more than ten times. However, application of wireless communication significantly reduces installation costs [111]-[112]. In addition, with wireless technology, integrated instrumentation is possible in applications where wiring is unfeasible [113]. The unique code assigned to each node and its sensors can be used to recognize its data. The large scale wireless sensor network on a number of feeders between a primary (HV/MV) substation to a secondary (MV/LV) substations can be divided into several local communication clusters which further transmit the data to superior cluster area and then finally to control room [114]. The concept of distributed wireless sensors [115] can be analyzed in more detail to envision its real implementation.

5. Summary of the Publications

Publication I

On-line Condition Monitoring System for Medium Voltage Distribution Networks

An organized framework of insulation condition assessment system for power line has been described. Condition assessment system consists of monitoring and diagnostics tasks. Design and implementation of the sensors, and data collection are the functions of monitoring task whereas diagnostic consists of essential and sequential composite of detection, location, and quantization functions. PD activity is monitored by induction sensors. Captured PD signals are used to accomplish diagnostics task. Signal signature recognition is used for detection purpose. Direction of Arrival (DOA) technique along with Time Difference of Arrival (TDA) method is used for location purpose. For quantization, determination of line attenuation constant is considered as the significant parameter. In the end, a detailed flow chart is presented for integrated implementation of the proposed PD diagnostic system.

Publication II

Parameters Identification and Modeling of High Frequency Current Transducer for Partial Discharge Measurements

High frequency current measurement is an important aspect of PD monitoring. Accuracy of the captured PD signal data depends on the performance of the measuring sensor. Rogowski coil is used as high frequency electromagnetic sensor. A suitable geometrical design is presented for PD measurements. An improved method for identification of electrical parameters of Rogowski coil is suggested which provides an accurate electrical model of the Rogowski coil measuring system. Integration of the signals sensed by Rogowski coil winding is an imperative feature to obtain the actual measured signal. In this work, a digital integration technique is used in order to avoid complex and expensive analogue integrators. The performance of the Rogowski coil is validated in comparison with the commercial PD sensor during real PD measurements in the laboratory.

Publication III

Effect of terminating resistance on high frequency behavior of Rogowski coil for transient measurements

In this paper, Rogowski coil sensor has been recognized and developed as a cascaded combination of the three components, Rogowski coil head, damping resistor, and integrator. The detailed investigation of the behavior of the damping (terminating) resistor is presented. The PD signal sensed by Rogowski coil head is overlapped by the oscillation caused by electrical the coil. The frequency of the oscillation depends upon the electrical parameters of the coil. A suitable terminating resistance is necessary to damp these oscillations in order to get the original signal. Effect of the terminating resistance and its selection for proper damping is presented using laboratory experimentation. The Rogowski coil is simulated in ATP-EMTP to observe the behavior of non physical electrical parameters (self-resistance, self-capacitance. and self-inductance) of the coil which is not possible to do experimentally. The analysis of Rogowski coil is based on theoretical, experimental, and simulation studies, which provide a deeper insight of the high frequency behavior of induction sensors.

Publication IV

Air-Core Sensors Operation Modes for Partial Discharge Detection and On-line Diagnostics in Medium Voltage Networks

Partial discharges produce extremely short duration electromagnetic signals having bandwidth ranging from few hundred kHz to several tens of MHz. In this paper, resonant frequency of air core induction sensors has been identified as the decisive parameter to determine their high frequency pulse measurement capability. The resonance phenomenon is present due to inherent electrical properties which are dependent on the selected geometrical parameters of the induction sensors. Resonant modes of operation: un-damped, critically-damped, and over-damped, have been investigated. Measuring performance of the coil sensor is compared for each mode of operation in time and frequency domain considering most important operating factors i.e., sensitivity and upper bandwidth of coil. Frequency response analysis has provided a clear understanding to recommend the critically damped-integrated mode as an optimum selection of coil's operation for measurement of PD signals.

Publication V

Effect of Geometrical Parameters on High Frequency Performance of Rogowski Coil for Partial discharge Measurements

The resonant frequency and sensitivity of the Rogowski coil are the significant performance parameters to determine its suitability for measurement. These parameters depend upon the geometrical parameters of Rogowski coil. Selection of suitable geometrical parameters has been identified as an important aspect regarding proper operation and installation of the coil around the power component under test. In this publication, the effect of variation in the major parameters of the coil such as, core and coil diameter, diameter of the wire used for coil winding, and number of turns, have been experimentally analyzed. The return winding, as a non-conventional method of creating return loop for the Rogowski coil, is compared with the conventionally used return wire to analyze sensor's performance regarding cancellation of external magnetic fields. The comparison of various designs of coil provides a guideline to develop an optimum design of the coil to obtain suitable sensitivity and bandwidth for PD measurements.

Publication VI

Directional Calibration of Rogowski Coil for Localization of Partial Discharges in Smart Distribution Networks

Location of PD defects is the most important function of a PD diagnostic system. In this work, Rogowski coil is used for location purpose. Directional sensing feature of Rogowski coil is explored to determine the direction of arrival (DOA) of PD signals. The coil is calibrated such that, the polarity of incoming PD pulse, polarity of the half cycle of operating voltage, and the output terminal connection of the Rogowski coil, provide the DOA of PD signals. The calibration is done experimentally by using a PD calibrator for single route and branched route line. For real PD defects, the performance of DOA technique is experimentally evaluated with the possibility of PD defects at different locations, on an overhead CC line. The technique is proved to be efficient for identification of faulty line sections in medium voltage distribution networks.

Publication VII

On-line Partial Discharge Diagnostics in Medium Voltage Branched Cable Networks

The commonly used location techniques such as, time domain reflectrometry (TDM), time of arrival (TOA), and frequency amplitude analysis (FAA) are usually implemented on single section of the cable. However, it is not possible to use these techniques for multi-section or branched line networks for reliable diagnostics. This is due to interconnected composite cable system of different (or same) types having discontinuities in impedances and different propagation characteristics for the travelling PD signals. Therefore, it is required to identify the faulty cable section before implementation of the conventional techniques. In this paper, three medium voltage cables are connected to develop a branched joint. Induction sensors are employed by using direction of arrival (DOA) technique. Polarity based comparison is made to determine the direction of fault point. The technique has been successfully implemented for on-line identification of the faulty cable branch.

Publication VIII

An Improved Technique to Determine the Wave Propagation Velocity of Medium Voltage Cables for PD Diagnostics

Wave propagation characteristics of the medium voltage cables plays a key role during location of PD faults on the cables. Time domain reflectrometry (TDR) and time of arrival (TOA) techniques have been frequently used to determine the wave propagation velocity (WPV) of the cables. These techniques use the time difference of arrival of the pulse captured by the employed PD sensors. It has been identified that dispersion and attenuation effects of the cables can cause an error in calculating the WPV. This paper provides an alternate technique in frequency domain termed as quarter wave length (QWL), to determine the WPV. This technique is based on transmission line theory and eliminates the practical limitations faced by TDR and TOA techniques. The improved performance of the QWL technique has been evaluated in the laboratory. The QWL technique can be used to enhance the accuracy of PD diagnostics in distribution lines.

Publication IX

Integration of On-line Proactive Diagnostic Scheme for Partial Discharge Detection in Distribution Networks

This publication presents the extension of the developed DOA technique. Due to the very nature of DOA technique, it is equally applicable to detect the PDs in the cables, CC lines, and

in the vicinity of the components such as power transformers and switchgear. In this work, the DOA technique is integrated over a medium voltage cable network which includes straight and branched route lines. An intelligent algorithm is proposed for practical implementation of DOA technique for PD monitoring. Proposed scheme can be adopted in distribution automation system to improve proactive diagnostic capabilities of the network.

6. Conclusions and Future Work

6.1. Conclusions

High frequency measurement is an important aspect of PD investigation in power components. Accurate measurement and interpretation of measured PD signal depends on the understanding of the electrical model of the measuring sensor. In this work, Rogowski coil induction sensors have been presented with various attributes such as: simplicity in design, flexibility of installation, compatibility of using for multiple diagnostic solutions, and possibility of integrating into the supply network. Under the umbrella of online condition assessment, the monitoring and diagnostics tasks have been explored.

A Rogowski coil was designed, analyzed, modeled, and simulated for PD current measurements. The parameters of its electrical model were determined by using a measurement based method which takes into account all the main and stray elements contributing to the equivalent value of each parameter. During the design of the coil, the stages of signal processing between signal sensing, and signal output are accomplish by applying the intrinsic rules of RLC circuit theory. The final component (integrator) of the Rogowski coil sensor was implemented using digital integration employed by data acquisitions system. For all types of sensors in PD applications, the presence of DAS is the integral part of the measuring system. The use of digital integrator is not only a simple methodology of integration but also avoids the need of additional and expensive analogue components. A quantified approach was presented to configure the comparative effectiveness of different geometrical designs of the Rogowski coil on its electrical behavior. The comparison of various geometrical designs was presented with simplest approach which can be used to set tradeoffs of benefits for better mechanical and electrical design of the Rogowski coil.

Induction sensors (Rogowski coil and HFCT) were used for PD diagnostics. The polarity of the PD signals with respect to the polarity of the supply voltage was considered for detection and location purpose. The DOA technique was developed to enhance the locating capabilities of the conventional location techniques. The important feature of the DOA technique is its ability to integrate the induction sensors in the distribution network. The developed diagnostic scheme is equally applicable to both CC lines and cables. ATP-EMTP program was used to evaluate the integrated implementation of the DOA technique to describe its operation. Based on ATP-EMTP simulation results, the basic structure of the algorithm was proposed for automated

identification of faulty section of the line. The correct value wave propagation velocity is necessary for accurate location of PD faults on a line. An alternate (QWL) technique was presented to determine the wave propagation velocity of the cables. The propagation velocity was measured with the help of frequency response of the impedance of the cable. The technique is simpler in methodology as the required measurements are needed to be done at single end of the line only.

The use of CC lines has been increasing in MV networks in densely forested countries like Finland. On the other hand, most of the developed countries have adopted the underground cable supply system especially in the urban areas and this trend is becoming increasingly popular in under developed countries as well. On-line automated detection of PD threats reduces the workload in finding the problematic locations and improves reliability of the network.

6.2. Future work

During analysis of the geometrical features of the coil, a hypothetical assessment from the mathematical expression was based on the geometry of the coil regarding cancellation of external magnetic fields of conventional 'return wire' and non-conventional 'return winding' design of coil [Publication V]. The experimental investigation of both designs in the noisy environment will provide valuable results to conclude if return winding design has better performance than the return wire.

In this work, the Rogowski coil was used for calibrated and real PD pulses in the laboratory. It is intended to make measurements in the real field (in the presence of real noise) to evaluate the performance regarding polarity based identification features for implementation of DOA technique. The next step is to develop shielding of the coil. Due to shielding additional capacitance is expected which will affect the sensitivity and bandwidth of the coil. The selection of optimized geometrical design to compensate the effect of shielding keeping in view the comparison of the shielded coil with the unshielded coil will provide interesting results.

It can be seen in the plots given in Fig. 13 and Fig. 15 of [Publication VI], that for branched joint, the PD signal emitted at one branch propagates towards the joint and is split into connected branches according the proportion of the impedances of the each branch line. In this work the identification of the faulty branch is made by comparing the polarity of the PD pulses at each branch line. An alternative to identify the faulty branch is to compare the amplitudes of the PD signals at each cable. The basic idea of this phenomenon is described in [Publication VI], however detailed quantitative analysis will help to develop an alternative technique to identify the faulty section. This approach may not be very useful for a single route line, however

it is supposed to have equal diagnostic capability in case of a branched route line.

In this work, single PD source has been considered and polarity is used as the major index for the comparison and analysis. Continuation of this work will focus on implementation of the presented techniques for multiple PD sources in the vicinity. In a real scenario, multiple PD sources can be present at different locations simultaneously. The PD signal generated at a faulty site travels away along both directions on the lines. If multiple PD sources are active in the vicinity, any specific sensor will measure a "sum" of PD signals. Therefore, the polarity of PD signal alone, may not give accurate information of the PD sources' locations. In this case, DOA of PD signals, amplitude of the PD signals along the power lines and phase difference due to time delay during propagation has to be taken into account. Therefore, three dimensional analysis in terms of polarity, amplitude, and phase would be required for location of multiple PD sources. In this work QWL technique [Publication VIII] is used to determine the wave propagation velocity of the cables. The required calculation is extracted from the plot presenting frequency response of the impedance of the cable. Impedance of the cable is composed of its line parameters. Further analysis by QWL technique can be done to derive the data which can be helpful to improve the accuracy of model parameters of the cable.

Developing technologies have improved the reliability of communication between sensors installed over a wide geographical area. For this reason, increased numbers of sensors for enhanced distribution automation is not a big challenge. When integrating the scheme over the distribution network, a centralized processing of sensors' data can be accomplished for the coverage of the network by constructing wired or wireless links using various communication technology solutions [116]. The architectures of wireless sensor networks integrated over electrical distribution systems have been described in [117]. There is need for practical implementation of these sensor networks.

Research on the wireless sensor network is getting a momentum, the work is going on to improve the data management and hardware of wireless sensors. A practical limitation for adopting wireless technology is a huge amount of data. Due to high frequency phenomenon, if the data is captured for 20 ms at a sampling rate of few hundred picoseconds (400 ps is used in this work) there might be some limitations regarding continuous transmission of this data. This issue has been addressed in [118]. The significance of wireless sensor technology has been agreed, economical advantages have been proved and the necessary operational components dealing with the wireless communication part are developing [116], [119]. The next specific step is to couple the PD sensor with the communication system and to analyze the characteristics of the original and measured signal for assessment of its reliability. Such development will be a leap toward practical implementation and utilization of the integrated on-line condition monitoring concept.

Automated detection and location of PD activity not only minimizes the time and man-hours to find the incipient fault locations compared to visual inspection but also provides alert/alarm to the maintenance crew to take corrective actions timely. Implementation of the proposed technique can be efficiently implemented with the help of sophisticated information technology (IT) and communication solutions. Presented diagnostic scheme can effectively enhance the distribution automation features of the modern grids.

References

[1] M. Firozian, S. Soleymani, and M. A. Kamarposhti, "Causes of Unplanned Interruption of 20 kV Feeders and Provide Solutions to Reduce them in Order to Promote Quality of Electrical Goods", in International Conference on Innovations in Electrical and Electronics Engineering (ICIEE'2012), Dubai UAE, Oct. 2012.

[2] T. Kostic, "Asset Management in Electrical Utilities: How Many Facets it actually has", in IEEE Power Engineering Society General Meeting, Baden, Switzerland, Vol. 1, pp. 275-281, Jul. 2003.

[3] D. B. Rhopoint, "Voltage Dips Predictive Maintenance – The Key to Power Quality Systems Copper Development Association", March 2001.

[4] K. L.Butler, "An Expert System Based Framework for an Incipient Failure Detection and Predictive Maintenance System", in International Conference on Intelligent Systems Applications to Power Systems (ISAP, 96), Orlando, Florida, pp. 321-326, Feb. 1996.

[5] R. C. M. Yam, P.W. Tse, L. Li, and P. Tu, "Intelligent Predictive Decision Support System for Condition-Based Maintenane", The International Journal of Advanced Manufacturing Technology, Vol. 17, Issue 5, pp. 383-391, 2001.

[6] W. J. (Bill) Bergman, "Equipment Monitoring Selection as a Part of Substation Automation Circuit Breaker Monitoring", in IEEE Switchgear Meeting Pittsburgh, Alberta, Canada, Nov. 1999.

[7] A. M. Wagle, A. M. Lobo, A. S. Kumar, S. Patil, and A. Venkatasami, "Real Time Web Based Condition Monitoring System for Power Transformers - Case Study", in IEEE International Conference on Condition Monitoring and Diagnosis, Beijing, China, Apr. 2008.

[8] C. Kane and A. Golubev, "Advantages of Continuous Monitoring of Partial Discharges in Rotating Equipment and Switchgear", in IEEE Pulp and Paper Industry Conference, Charleston, USA, Jun. 2003.

[9] P. Mulroy, I. Gilbert, and A. Hurtado, "Continuous Online Monitoring of PD Activity in the Medium Voltage Distribution Network", in 22nd International Conference on Electricity Distribution CIRED 2013, Stockholm, Jun. 2013.

[10] E. Gulski. F.J. Wester, W. Boone, N. V Schaik, E.F. Steennis, E.R.S. Groot, and J. Pellis, "Knowledge Rules Support for CBM of Power Cable Circuits", in CIGRE Paris, 2002.

[11] G. C. Stone, "Partial Discharge Diagnostics and Electrical Equipment Insulation Condition Assessment", IEEE Transactions on Dielectrics and Electrical Insulation Vol. 12, No. 5, pp. 891-903, Oct. 2005.

[12] L. Bertling, R. Eriksson, R. N. Allan, and L. G. M. Ahlen, "Survey of Causes of Failures Based on Statistics and Practice for Improvements of Preventive Maintenance Plans", in 14th Power Systems Computation Conference, Seville, Spain, Jun. 2002.

[13] S. K. Watkins, "Electrical Insulation System Degradation Sensors: Improving Reliability of Power Generation and Distribution", in 6th International Conference on Nuclear Engineering, Paper No. ICONE16-48130, Florida, USA, pp. 35-39, May 2008.

[14] Integrated Partial Discharge Testing and Monitoring Solutions, [online]. Available: http://www.hvmcorp.com/wp-content/uploads/2012/12/HVM_Partial-Discharge-Testing-and-Monitoring_R06-11.pdf.

[15] S. I. Cho, "On-line Partial Discharge Monitoring of Power System Components", Master's Thesis, School of Electrical Engineering, Aalto University Espoo, Sep. 2011.

[16] C. Xiao, L. Zhao, T. Asada, W. G. Odendaal, and J. D. V Wyk, "An Overview of Integratable Current Sensor Technologies", in 38th Industry Applications Conference Annual Meeting (IAS 2003), Salt Lake City, USA, Vol. 2, pp. 1251-1258, Oct. 2003.

[17] P. N. Murgatroyd and D. N. Woodland, "Geometrical Properties of Rogowski Sensors", in IEE Colloquium on Low Frequency Power Measurement and Analysis (Digest No. 1994/203), London, UK, Nov. 1994.

[18] R. Hlavacek, R. Prochazka, K. Draxler, and V. Kvasnicka, "The Rogowski Coil software", in 16th Symposium on Exploring New Frontiers of Instrumentation and Methods for Electrical and Electronic Measurements, Florence, Italy, Sep. 2008.

[19] W. F. Ray and R. M. Davis, "High Frequency Improvements in Wide Bandwidth Rogowski Transducers", in Conference Proceedings- European Power Electronics and Drives Association, Lausanne, Switzerland, 1999.

[20] I. A. Metwally, "Self-Integrating Rogowski Coil for High-Impulse Current Measurement"', IEEE Transactions on Instrumentation and Measurement, Vol. 59, No. 2, pp. 353-360, 2010.

[21] M. Faifer and R. Ottoboni, "An Electronic Current Transformer Based on Rogowski Coil", in IEEE Instrumentation and Measurement Technology Conference Proceedings (IMTC 2008), Victoria, Canada, pp.1554-1559, May 2008.

[22] J. D. McDonald, B. Wojszczyk, B. Flynn, and Ilia Voloh, "Distribution Systems, Substations, and Integration of Distributed Generation", Chapter of the book, Electrical Transmission Systems and Smart Grids, Springer, New York, pp. 7-68, 2013.

[23] EATON, "Power distribution system", Sheet Number. 01008, Aug. 2013, [online]. Available: www.eaton.com (14.03.2014).

[24] M. S. Mashikian, R. Bansal, and R. B. Northrop, "Location and Characterization of Partial Discharge Sites in Shielded Power Cables", IEEE Transactions on Power Delivery Vol. 5, Issue 2, pp. 833-839, Apr. 1990.

[25] P.C.J.M. Van Der Wielen, "On-Line Detection and Location of Partial Discharges in Medium Voltage Cables", Doctoral dissertation Eindhoven Technische Universiteit Eindhoven, Netherlands, Apr. 2005.

[26] G. Katsuta, A. Toya, K. Muraoka, T. Endoh, Y. Sekii, and C. Ikeda, "Development of a Method of Partial Discharge Detection in Extra-High Voltage Cross-Linked Polyethylene Insulated Cable Lines", IEEE Transactions on Power Delivery, Vol. 7, No. 3, pp. 1068-1074, 1992.

[27] A. Contin, A. Cavallini, G.C. Montanari, G. Pasini, and F. Puletti, "Digital Detection and Fuzzy Classification of Partial Discharge Signals", IEEE Transactions on Dielectrics and Electrical Insulation, Vol. 9, No. 3, pp. 335-348, Jun. 2002.

[28] J. Anatory, N. Theethayi, M. M. Kissaka, N. H. Mvungi, and R.Thottappillil, "The Effects of Load Impedance, Line Length, and Branches in the BPLC—Transmission-Lines Analysis for Medium-Voltage Channel", IEEE Transactions on Power Delivery, Vol: 22, Issue: 4, pp. 2156 – 2162, Oct. 2007.

[29] J. Anatory, N. Theethayi, R. Thottappillil, C. Mwase, and N. H. Mvungi, "The Effects of Multipath on OFDM Systems for Broadband Power-Line Communications a Case of Medium Voltage Channel", World Academy of Science, Engineering and Technology Vol. 30, pp. 177-180, 2009.

[30] W. Boone, "Branched Cable Circuits Testing: Meeting a New Challenge", in IEEE 9th International Conference Transmission and Distribution Construction, Operation and Live-Line Maintenance Proceedings, Montreal, Canada, pp. 70-77, Oct. 2000.

[31] S. Bahadoorsingh and S. Rowland, "A Framework Linking Knowledge of Insulation Aging to Asset Management-[Feature Article]", IEEE Electrical Insulation Magazine, Vol. 23, No. 3, pp. 38-46, Jun. 2008.

[32] J. Densley, "Ageing Mechanisms and Diagnostics for Power Cables - An Overview", IEEE Electrical Insulation Magazine, Vol.17, No.1, pp.14-22, 2001.

[33] R. Bartnikas, "Partial discharges. Their Mechanism, Detection and Measurement", IEEE Transactions on Dielectrics and Electrical Insulation, Vol.9, No.5, pp.763-808, Oct. 2002.

[34] M. reading, X. Zhiqiang, V. Alun and L. Paul, "The Effect of Sample Thickness on the Relative Breakdown Strength of Epoxy Systems", in Conference on Dielectrics-2011, The University of Kent, Canterbury, UK, Apr. 2011.

[35] P. Pakonen, "Detection of Incipient Tree Faults on High Voltage Covered Conductor Lines", Doctoral dissertation, Tampere University of Technology (TUT), Tampere, Finland, Nov. 2007.

[36] G. J. Paoletti and A. Golubev, "Partial Discharge Theory and Technologies Related to Medium-Voltage Electrical Equipment", IEEE Transactions on Industry Applications, Vol.37, No.1, pp.90-103, Jan. 2001.

[37] F. H. Kreuger, “Detection and Location of Discharges in Particular in Plastlc-Insulated High-Voltage Cables”, Thesis, Elektrotechnisch Ingenieur Geboren Te Amsterdam, Netherlands, 1961, [online]. Available: 132225190.Pdf – Repository.

[38] R. J. V. Brunt, “Physics and Chemistry of Partial Discharge and Corona. Recent Advances and Future Challenges”, IEEE Transactions on Dielectrics and Electrical Insulation, Vol. 1, No. 5, pp. 761-784, Oct. 1994.

[39] S. A. Boggs, “Partial Discharge. III. Cavity-induced PD in Solid Dielectrics”, IEEE Electrical Insulation Magazine, Vol. 6, No. 6, pp. 11-16, Nov. 1990.

[40] Dr. C. Smith,“Partial Discharge and Insulation Failure”, IPEC Ltd. 2005.

[41] G. M. Hashmi, “Partial Discharge Detection for Condition Monitoring of Covered-Conductor Overhead Distribution Networks Using Rogowski Coil”, Doctoral dissertation, Helsinki University of Technology, Espoo, Finland, 2008.

[42] A. Pedersen, G. C. Crichton, and I. W. McAllister, “PD Related Field Enhancement in the Bulk Medium”, Journal of Gaseous Dielectrics VII, Springer US, pp. 223-229, 1994.

[43] A. Pedersen, G. C. Crichton, and I.W. Mcallister, “The Theory and Measurement of Partial Dscharge Transients”, IEEE Transactions on Electrical Insulation, Vol. 26, No.3, pp. 487-497, Jun. 1991.

[44] C. G. Crichton, P. W. Karlsson, and A. Pedersen, “Partial Discharges in Ellipsoidal and Spheroidal Voids”, IEEE Transactions on Electrical Insulation, Vol. 24, No. 2, pp. 335-342, 1989.

[45] B. Ramachandra and R. S. Nema, “Characterisaticin of Partial Disc Pulsics in Artificial Voids in Polyp Films used in Capacitors”, in IEEE International Symposium on Electrical Insulation, Montreal, Canada, Jun. 1996.

[46] T. Seghier, D. Mahi, T. Lebey, and D. Malec, “The Effect of Space Charge on Partial Discharges Inception Voltage in Air Gaps Within High Density Polyethylene” Courrier Du Savoir – N°10, Université Mohamed Khider – Biskra, Algériepp, pp. 35-41, April 2010.

[47] M. Fenger, “Sensitivity Assessment Procedure for Partial Discharge Measurements on Transmission Class Cables”, in IEEE International Symposium on Electrical Insulation (ISEI 2008), Toronto, Canada, pp. 667-671, Jun. 2008.

[48] X. Wang, “Partial discharge analysis at arbitrary voltage waveform stimulus”, Doctoral dissertation, KTH, Sweden, Dec. 2012.

[49] Power diagnostics system, [Online]. Available: http://www.pd-systems.com (25.03.2014).

[50] E. W. Shu and S. A. Boggs, “Effect of Dispersion on PD Pulse Propagation in Shielded Power Cable”, in Annual Report Conference on Electrical Insulation and Dielectric Phenomena (CEIDP 2008), Quebec, Canada, pp. 427-430, Oct. 2008.

[51] E. W. Shu and S. A. Boggs, “Dispersion and PD Detection in Shielded Power Cable [Feature Article] ”, IEEE Electrical Insulation Magazine, Vol. 24, No. 1, pp. 25-29, 2008.

[52] J. R. Gyorki (Ed), "Signal Conditioning & PC-based Data Acquisition Handbook: A Reference for Analog & Digital Signal Conditioners & PC-based Data Acquisition Systems**",** Measurement Computing Corporation, Third Edition, USA, published 2004-2012.

[53] L. Satish and B. Nazneen, "Wavelet-Based Denoising of Partial Discharge Signals Buried in Excessive Noise and Interference", IEEE Transactions on Dielectrics and Electrical Insulation, Vol. 10, No. 2, pp. 354-367, April 2003.

[54] G. A. Hussain, L. Kumpulainen, M. Lehtonen, M. Hashmi, and M. Shafiq, "Signal Processing of PD Measurements to Predict Arcing Faults in MV Switchgears", in IEEE International Conference on Industrial Technology (ICIT 2013), Cape Town, South Africa, pp. 916-921, Feb. 2013.

[55] L. Kutt, "Analysis and Development of Inductive Current Sensor for Power Line On-Line Measurements of Fast Transients", Doctoral dissertation, Tallinn University of Technology, Estonia, June 2012

[56] P. Wagenaars, P. A. A. F. Wouters, and P. V. D. Wielen, and E. F. Steennis, "Approximation of Transmission Line Parameters of Single-Core XLPE Cables", in IEEE conference record for International Symposium on Electrical Insulation (ISEI 2008), pp. 20-23, Jun. 2008.

[57] Transmission Lines, [online]. Available: http://www.ece.mcmaster.ca/faculty/georgieva/4FJ4_downloads/lectures/L06_TLs.pdf.

[58] G. Mugala and R. Eriksson, "High Frequency Characteristics of a Shielded Medium Voltage XLPE Cable", in Conference on Electrical Insulation and Dielectric Phenomena, Kitchener, Canada, pp. 132-136, Oct. 2001.

[59] G. M. Hashmi and M. Lehtonen, "Covered-Conductor Overhead Distribution Line Modeling and Experimental Verification for Determining its Line Characteristics", in IEEE Conference and Exposition in Africa Power Engineering Society (PowerAfrica 07), Johannesburg, South Africa, pp. 1-7, Jul. 2007.

[60] A. Cavallini, G. C. Montanari, and M. Tozzi, "Partial Discharge Measurement and Cable Length: Meaning and Limits", in Conference Record of the IEEE International Symposium on Electrical Insulation (ISEI 2008), Vancouver, Canada, pp. 616-619, June 2008.

[61] A. Ametani, Y. Miyamoto, and N. Nagaoka, "Semiconducting Layer Impedance and its Effect on Cable Wave-Propagation and Transient Characteristics", IEEE Transactions on Power Delivery, Vol. 19, No. 4, pp.1523-1531, Oct. 2004.

[62] G. M. Hashmi, M. Lehtonen, and M. Nordman, "Calibration of On-Line Partial Discharge Measuring System Using Rogowski Coil in Covered-Conductor Overhead Distribution Networks", IET Science, Measurement & Technology, Vol. 5, No. 1, pp. 5-13, Jan. 2011.

[63] M. D. Judd, "Radiometric Partial Discharge Detection", in International Conference on Condition Monitoring and Diagnosis (CMD 2008), Beijing, China, pp. 1025-1030**,** Apr. 2008.

[64] P. J. Moore, I. E. Portugues, and I. A. Glover, "Radiometric Location of Partial Discharge Sources on Energized High-Voltage Plant", IEEE Transactions on Power Delivery, Vol. 20, No. 3, pp. 2264-2272, Jul. 2005.

[65] R. Schwarz, M. Muhr, and S. Pack, "Evaluation of Partial Discharge Impulses with Optical and Conventional Detection Systems", in Proceedings of the 24th International Symposium on High Voltage Engineering, Tsinghua University, Beijing, China, Aug. 2005.

[66] R. Schwarz and M. Muhr, "Modern Technologies in Optical Partial Discharge Detection", in Annual Report - Conference on Electrical Insulation and Dielectric Phenomena (CEIDP 2007), Vancouver, Canada, pp. 163-166, Oct. 2007.

[67] S. Ahmadi, M. R. Naghashan, and M. Shadmand, "Partial Discharge Detection During Electrical Aging Of Generator Bar Using Acoustic Technique", in Conference Record of the IEEE International Symposium on Electrical Insulation (ISEI 2012), San Juan, Puerto Rico, pp.576-578, Jun. 2012.

[68] L. E. Lundgaard, "Partial Discharge. XIV. Acoustic Partial Discharge Detection-Practical Application", IEEE Electrical Insulation Magazine, Vol.8, No.5, pp.34-43, Sep. 1992.

[69] D. M. Hepburn, I. J. Kemp, A. J. Shields, and J. Cooper, "Degradation of Epoxy Resin by Partial Discharges", in IEE Proceedings Science, Measurement and Technology, Vol. 147, No. 3, pp. 97-104, May 2000.

[70] R. Samsudin, A. Q. Ramli, A. Berhanuddin, and Y. Zaidey, "Field Experience of Transformer Untanking to Identify Electrical Faults and Comparison with Dissolved Gas Analysis", 3rd International Conference on Energy and Environment (ICEE 2009), Malacca Malaysia, pp. 299-305, Dec. 2009.

[71] G. C. Stone, "Partial Discharge Diagnostics and Electrical Equipment Insulation Condition Assessment", IEEE Transactions on Dielectrics and Electrical Insulation, Vol. 12, No.5, pp. 891-904, Oct. 2005.

[72] IEC 60270, International Standard for High-voltage test techniques – Partial discharge measurements, Third Edition, 2000-12.

[73] M. Muhr, T. Strehl, E. Gulski, K. Feser, E. Gockenbach, W. Hauschild, and E. Lemke, "Sensors and Sensing used for Non-Conventional PD Detection", in 21 Rue D'artois CIGRE, F-75008 Paris, D1-102, Paris, France, pp. 1-7, 2006.

[74] D. A. Ward, J. La. T. Exon, "Using Rogowski Coil for Transient Current Measurements", Engineering Science and Education Journal, Volume: 2, Issue: 3, pp.105-13, 1993.

[75] C. R. Hewson, W. F. Ray, and R. M. Davis, "Verification of Rogowski Current Transducer's Ability to Measure Fast Switching Transients", in 21st Annual IEEE Applied Power Electronics Conference and Exposition (APEC), Dallas, USA, Mar. 2006.

[76] P. Mähönen and V. Virtanen, "The Rogowski Coil and the Voltage Divider in Power System Protection and Monitoring", in Internationale des Grandes Reseaux Electriques a Haute Tension, CIGRE, 1996.

[77] G. Robles, M. Argueso, J. Sanz, R. Giannetti, and B. Tellini, "Identification of Parameters in a Rogowski Coil Used for the Measurement of Partial Discharges", in IEEE Conference Proceedings on Instrumentation and Measurement Technology (IMTC 2007), Warsaw Poland, pp. 1-4, May 2007.

[78] G. M. Hashmi, M. Lehtonen, and M. Nordman, "Modeling and Experimental Verification of On-line PD Detection in MV Covered-conductor Overhead Networks", IEEE Transactions on Dielectrics and Electrical Insulation, Vol. 17, No. 1, pp. 167-180, 2010.

[79] D. G. Pellinen, M. S. D. Capua, S. E. Sampayan, H. Gerbracht and M. Wang, "Rogowski Coil for Measuring Fast, High Level Pulsed Currents", Review of Scientific instruments Vol. 51, pp. 1535 – 1540, 1980, current version 2009.

[80] J. D. Ramboz, "Machinable Rogowski Coil, Design, and Calibration", IEEE Transactions on Instrumentation and Measurement, Vol. 45, No.2, pp. 511-515, April 1996.

[81] Q. Zhang, J. Zhu, J. Jia, F. Tao, and L. Yang, "Design of a Current Transducer with a Magnetic Core for use in Measurements of Nanosecond Current Pulses", Measurement Science and Technology, Vol. 17, pp. 825-900, 2006.

[82] I. A. Metwally, "Novel Designs of Wideband Rogowski Coils for High Pulsed Current Measurement", IET Science, Measurement & Technology, Vol.8, No.1, pp. 9-16, Jan. 2014.

[83] A. Marta, G. Robles, and J. Sanz, "Implementation of a Rogowski Coil for the Measurement of Partial Discharges", Review of scientific instruments 76.6, 065107, (2005).

[84] S. T. Karris, "Circuit Analysis II: With MATLAB Applications", Vol. 2. Orchard publications, California, USA, 2003.

[85] M. R. Boelkins, J. L. Goldberg, M. C. Potter, "Differential Equations with Linear Algebra", Oxford University Press, USA, 2009.

[86] L. D Slifka,"An Accelerometer Based Approach to Measuring Displacement of a Vehicle Body", University of Michigan, Dearborn, Michigan, 2004.

[87] M. Shafiq, L. Kutt, M. Isa, M. Lehtonen, "Design, Implementation and Simulation of Non-Intrusive Sensor for On-line Condition Monitoring of MV Electrical Components", accepted for publication in Engineering (ENG) journal, Scientific Research Publishing, 2014.

[88] L. Kütt, M. Shafiq, M. Lehtonen, H. Mõlder, and J. Järvik, "Sensor Resonance and its Influence on the. Measurement Results of Fast Transients", in International Conference on Power Systems Transients, IPST-2013, Vancouver, Canada, Jul. 2013.

[89] L. Kutt and M. Shafiq, "Magnetic Sensor Coil Shape Geometry and Bandwidth Assessment", in IEEE 7th International Conference-Workshop on Compatibility and Power Electronics (CPE 2011), Tallinn, pp. 470 -473, Jun. 2011.

[90] N. G. James and R. G. Wilson, "Control and Automation of Electrical Power Distribution Systems", Taylor & Francis CRC press, 2007.

[91] M. S. Mashikian and A. Szarkowski, "Medium voltage cable defects revealed by off-line partial discharge testing at power frequency", IEEE Electrical Insulation Magazine, Vol. 22, No. 4, pp. 24-32, Jul. 2006.

[92] C. H. Lee, L. Y. Chih; M. Y. Chiu, H. C. Hsien, S. S. Yen, and C. Haeng, "Recognition of Partial Discharge Defects in Cable Terminations", in IEEE International Conference on Condition Monitoring and Diagnosis (CMD 2008), Beijing, China, pp. 1242-1245, Apr. 2008.

[93] P. Wagenaars, "Integration of Online Partial Discharge Monitoring and Defect Location in Medium-Voltage Cable Networks", Doctoral dissertation, Technische Universiteit Eindhoven, Netherlands, Mar. 2010.

[94] Covered Conductor is Reliable Solution for Electricity Distribution, 2013, [online]. Available: www.ensto.com (03.01.2014).

[95] T. Leskinen, "Design of Medium Voltage and High Voltage Covered Conductor Overhead Lines", in International Conference on Electricity Distribution (CIRED), Barcelona, Spain, May 2003.

[96] M. Isa, G. M. Hashmi, and M. Lehtonen, "Comparative Study of On-Line Three Phase PD Monitoring Systems for Overhead Covered Conductor Distribution Lines", in Proceedings of the 44th International Universities Power Engineering Conference (UPEC 2009), Glasgow, Scotland, UK, pp. 1-5, Sept. 2009.

[97] A report by Nexans, "60-500 kV High Voltage Underground Power Cables XLPE insulated cables", Nexans France, 2004.

[98] T. Sandri, "Cable Testing and Fault Locating at Wind Farms...Part IV", Aug. 2011, [online]. Available: www.protecequip.com (10.03.2014).

[99] W. Weissenberg, F. Farid , R. Plath, K. Rethmeier, and W. Kalkner, "On-Site PD Detection At Cross-Bonding Links of HV Cables", in CIGRÉ 21, Rue D'artois, F-75008 Paris, 2004.

[100] J. R. Marti, "Accurate Modeling of Frequency-Dependent Transmission Lines in Electromagnetic Transients Simulations", IEEE Transactions on Power Apparatus and Systems, Vol. 101, No.1, pp. 147-157, Jan. 1982.

[101] M. Isa, "Partial Discharge Location Technique for Covered-Conductor Overhead Distribution Lines", doctoral dissertation, Aalto University, Finland, 2013.

[102] N. H. Ahmed and N. N. Srinivas, "On-Line Partial Discharge Detection in Transformer", in Conference Record of the IEEE International Symposium on Electrical Insulation, Arlington, Virginia, pp. 39-42, Vol. 1, Jun. 1998.

[103] W. Sikorski and K. Walczak, "Power Transformer Diagnostics Based on Acoustic Emission Method, Acoustic Emission", Chpater 5 published in book Research and Applications published by InTech, pp. 91-116, Mar. 2013.

[104] S. M Markalous, M. Boltze, A. Bolliger, and A. Wilson, "On-Line Partial Discharge Diagnosis at Power Transformers", in Proceedings of the 76th Annual International Doble Client Conference, Boston, USA, Apr. 2009.

[105] J. Fuhr, M. Haessig, and P. Boss, D. Tschudi, and R. A. King, "Detection and Location of Internal Defects in the Insulation of Power Transformers", IEEE Transactions on Electrical Insulation, Vol.28, No.6, pp.1057-1067, Dec. 1993.

[106] Guide for Partial Discharge Measurements in Compliance to IEC 60270 by CIGRE (WG D1.33), 2008.

[107] C. Mazzetti, F. M. F. Mascioli, F. Baldini, M. Panella, R. Risica, and R. Bartnikas, "Partial Discharge Pattern Recognition by Neuro-Fuzzy Networks in Heat-Shrinkable Joints and Terminations of XLPE Insulated Distribution Cables", IEEE Transactions on Power Delivery, Vol. 21, No.3, pp.1035-1044, 2006.

[108] [Online]. Available: http://www.cablejoints.co.uk/blog/article/earthing-of-single-core-cables (26.03.2014).

[109] A. N. Cuppen, E. F. Steennis, and P. C. J. M. V. der Wielen, "Partial Discharge Trends in Medium Voltage Cables Measured while In-Service with PDOL", IEEE Transmission and Distribution Conference and Exposition, New Orleans, USA, pp.1-5, April 2010.

[110] M. Shafiq, M. Lehtonen, G. A. Hussain, L. Kutt, "Performance evaluation of PD monitoring technique integrated into medium voltage cable network for smart condition assessment", IEEE International Conference on Electric Power Quality and Supply Reliability Conference (PQ), Rakvere, Estonia, pp.351-357, Jun. 2014.

[111] G. Scheible, J. Schutz, and C. Apneseth, "Novel Wireless Power Supply System for Wireless communication Devices in Industrial Automation Systems", in IEEE Annual Conference of the Industrial Electronics Society (IECON02), Sevilla, Spain, Nov. 2002.

[112] T. Brooks, "Wireless Technology for Industrial Sensor and Control Networks", Sensors for Industry Conference, Sicon'01, Rosemount, USA, 2001.

[113] Siemens AG Infrastructure & Cities Sector Smart Grid Division, "Communications Network Solutions for Smart Grids", Germany, 2011, [online]. Available: www.siemens.com (12.01.2014).

[114] Z. Zi-Nan and G. Wei-Feng, "Research on Monitoring Power System Faults by Wireless Sensor Network", in Proceedings of the 3rd International Symposium on Electronic Commerce and Security Workshops (ISECS 10), Guangzhou, P. R. China, pp. 354-357. Jul. 2010,

[115] M. Nordman and M. Lehtonen, "A Wireless Sensor Concept for Managing Electrical Distribution Networks", in IEEE Power Systems Conference and Exposition (PES 2004), New York, USA, Vol. 2, pp.1198-1206, Oct. 2004.

[116] K. Sohraby, D. Minoli, and T. Znati, "Wireless Sensor Networks: Technology, Protocols, and Applications". John Wiley & Sons, New Jersey, USA, 2007.

[117] M. Nordman, "An Architecture for Wireless Sensors in Distributed Management of Electrical Distribution Systems", Doctoral Dissertation, Helsinki University of Technology, Espoo, Finland, 2004.

[118] B. Greenstein, "Capturing High-Frequency Phenomena Using a Bandwidth-Limited Sensor Network", in Proceedings of the 4th International Conference on Embedded Networked Sensor Systems, Colorado, USA, Nov. 2006.

[119] Y. Jennifer, M. Biswanath, and G. Dipak, "Wireless Sensor Network Survey Computer Networks", Computer Networks Elsevier, Vol. 52, Issue 12, pp. 2292–2330, Aug. 2008.

In this work partial discharge (PD) measurements have been considered for insulation condition assessment of distribution system components using non-intrusive induction sensors. Rogowski coil sensors have been designed and modeled for high frequency PD measurements in order to detect and locate the insulation defects in the MV power lines (cables and overhead CC lines). The conventional techniques of fault location are used for individual sections of the MV cables, however this work presents fault location technique for a wider part of the network. An online integrated monitoring system is proposed for the MV network consisting of multi-section and multi-branch cable network taking into account the PD diagnostics for the cable accessories (joints and terminations). PD fault location algorithm is presented for automated fault identification. The proposed monitoring system can be adopted in distribution automation system to improve the proactive diagnostic capabilities of the network.

Aalto-DD 152/2014

ISBN 978-952-60-5892-4
ISBN 978-952-60-5893-1 (pdf)
ISSN-L 1799-4934
ISSN 1799-4934
ISSN 1799-4942 (pdf)

Aalto University
School of Electrical Engineering
Department of Electrical Engineering and Automation
www.aalto.fi

BUSINESS + ECONOMY

ART + DESIGN + ARCHITECTURE

SCIENCE + TECHNOLOGY

CROSSOVER

DOCTORAL DISSERTATIONS